D I S R U P T I O N S I N T O K A M A K S

by

KEITH IAIN HOPCRAFT

IMPERIAL COLLEGE
LONDON

Thesis submitted for the degree of Doctor of Philosophy
of the University of London and for the Diploma
of Membership of the Imperial College.

December 1983

For My Parents

All things are in a flux.

(Heraclitus, 504-480 BC)

Island in the Sun.

(Song by Harry Belafonte, b.1927)

ABSTRACT

The disruptive instability in tokamak devices is investigated. The experimental features of disruptions are briefly discussed and they support the currently held consensus that disruptions are caused by resistive magnetohydrodynamic activity.

We briefly summarise the theory of resistive tearing modes in both the linear and non-linear regimes before reviewing applications of this theory to disruptions.

Certain problems arising from the standard 'mode coupling' disruption model advanced by the Oak-Ridge group are discussed. The Oak-Ridge calculations are repeated using an alternative quasi-linear model, which explains disruptions in terms of evolution towards a bifurcation catastrophe. The results show no evidence of a disruption having occurred.

The change in the stability properties of the plasma caused by removing a conducting wall from the plasma boundary are discussed and shown to be crucial. When placed at the boundary, the wall suppresses tearing mode activity in the outer regions.

An investigation into the numerical properties of the Oak-Ridge computer code RSF shows that the previously published results have been performed close to a numerically unstable regime, where the accuracy of the results is uncertain. A new numerical stability criterion is described and used in a multi-helicity calculation at moderate magnetic Reynolds' number ($S \sim 10^4$). The results conform to those obtained from the quasi-linear calculation. The effects of

increased magnetic Reynolds number are discussed. We conclude that mode-coupling has a role in the dynamics of the disruption, however, the salient features of how the disruption is triggered and its subsequent evolution may be adequately described by quasi-linear theory.

Time-dependent calculations are performed for a plasma undergoing an increasing current phase. A model explaining the resulting sequence of soft disruptions is explained and compared with experiment. The conditions under which major and minor disruptions occur in the model are delineated.

The concept of current restriction on axis being instrumental in triggering the disruption is broadened to the case when there is no $q=1$ surface in the plasma.

CONTENTS

LIST OF SYMBOLS

a	minor radius
b	radius of conducting shell
B	magnetic flux density
γ	growth rate
Δ'	discontinuity of the logarithmic derivative of ϕ
Δ^*	non-linear Δ'
d/dt	convective derivative
E	electric field
ϵ	inverse aspect ratio
ζ	toroidal angle
η	resistivity
θ	poloidal angle
I	current
j	current density
k	wave number
K	finite difference approximation of wave number
κ	thermal conductivity
λ	eigenvalue of amplification matrix
Λ	amplification matrix
m	poloidal mode number
n	toroidal mode number
n	number density
ξ	fluid displacement
$\perp$	perpendicularity to the ζ-axis
q	safety factor

r	radial coordinate
R	major radius
$\mathscr{L}$	radiation loss function
t	time
τ_A	Alfvén transit time
τ_R	resistive diffusion (skin) time
T	temperature
u	vorticity
v	velocity
φ	velocity stream function
w	magnetic island width
δW	change in potential energy
x	slab coordinate (= poloidal)
y	slab coordinate (= radial)
ψ	magnetic flux function
z	slab coordinate (= toroidal)

LIST OF FIGURES

ACKNOWLEDGEMENTS

The work contained in this thesis was performed whilst a member of the Plasma Physics Group at Imperial College and latterly whilst attached to the Theory Division at Culham Laboratory. My thanks extend to both institutions for the facilities and hospitality provided. In particular I would like to thank my supervisor, Professor Malcolm Haines for his support, encouragement and comments, especially in preparation of this thesis. I would like to acknowledge Dr Jim Eastwood, with whom I have collaborated in some of the work on RSF. I am grateful to Mrs Marion Turner for her patience and general help in using the Culham computer system. My thanks also go to Ainslee Rutledge for making such a professional job of the typing. I am especially grateful to Dr John Wesson for his encouragement, support and inspiration; it has been both a pleasure and a privilege to work with him. Finally, a word for the inmates of room 734 and 1010. It is thanks to them that I have retained my insanity.

CHAPTER I

1.1 DISRUPTIONS IN THE TOKAMAK

If nuclear fusion reactors, based upon the principle of magnetically confining a hot plasma, are to become a viable future source of power, many outstanding problems must be tackled and solved. These questions are quite distinct from the engineering difficulties allied to reactor design and maintenance which must ultimately be considered. Indeed it is the limitations of engineering that will govern whether or not a fusion reactor is economically competitive, even if the outstanding physics problems are eventually solved. The various physical processes experienced by a plasma in the tokamak are particularly rich and in this thesis we address a problem which plagues most modern devices; the *disruption*. It will become apparent that a thorough understanding of this particular instability is required considering both the magnitude and violence of its effect. This is especially true at the present stage of the world fusion effort, when large and expensive machines are just coming into operation.

We shall have cause to refer to two types of disruption which have been variously labelled *major* and *minor* or *hard* and *soft*. A certain degree of confusion may result over this terminology which is primarily of historical origin. Many experimentalists refer to *sawtooth* relaxation oscillations[1] as being minor disruptions or 'internal' disruptions. So as to avoid any misunderstanding, we shall ascribe these oscillations to be 'sawteeth' throughout.

The major disruption is a sudden, dramatic loss of plasma confinement, always preceded by a violent burst of magnetic activity. Such activity is often observed after a lengthy period of quiescence and is apparently triggered without perceptible change to the global plasma parameters. The conditions under which disruptions occur are therefore poorly understood. However, experiment shows that disruptions repeatedly occur if a current or number density threshold is exceeded.[2] This provides a vital clue in discovering one of the basic causes of the disruption.

During the disruptive phase, the plasma is lost either to the limiter or directly to the wall of the containing vessel. This causes the plasma current (of order 10^6A in the new generation of machine) to collapse on a timescale of milli-seconds. The rate at which the current falls appears to be constant for a particular device.[3] The potential for a vast amount of damage to the torus and its constituent parts is self evident.

The soft disruption is a less vigorous version of the major disruption from which the plasma is able to recover. Often a sequence of soft disruptions precedes the terminating major disruption.

Figure (1.1) shows an oscillogram of the total plasma current during a TFR tokamak discharge. The machine runs in a steady state for a lengthy period before the disruption causes the current to fall abruptly.

Figure (1.2) shows an expanded view of the current, soft X-ray emission from the centre of the plasma and signals from the Mirnov oscillation pickup coils prior to the disruption. The Mirnov coils measure a component of the perturbed radial magnetic field.

Fig.(1.1) *The current in the TFR tokamak showing the collapse at the time of the disruption (scale is 20 ms/division).*

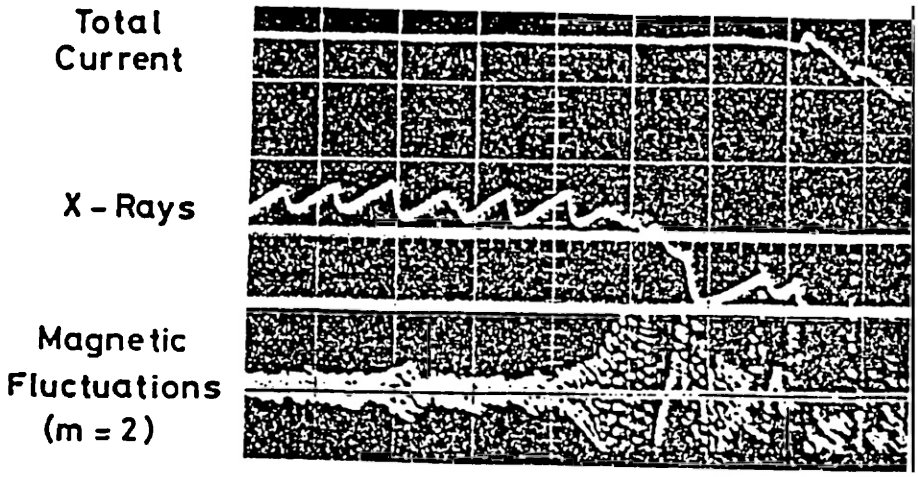

Fig.(1.2) *Expanded view of the current, X-ray emission and m=2 Mirnov oscillations up to the time of the disruption.*

The X-ray emission is a measure of the axial temperature, which undergoes repeated sawtooth relaxation oscillations. The timescale for an individual sawtooth is $\sim$ 1 ms, the relaxation time a fraction of this. Note that the fall of the temperature precedes the fall of the current. It is clear that the first precursor of the disruption is the sudden increase in the amplitude of the m = 2 Mirnov oscillations.

That m = 2 oscillations act as first precursor to the disruption appears to be common to all tokamaks but they are not the only oscillations present at any time. A whole spectrum of modes appears during the disruption itself, indicating that the plasma is probably turbulent.

Another characteristic signature of disruptions is the negative pulse observed in the toroidal electric field as measured by the loop volts. It is likely that the rapid expansion of the plasma column forces the inductance to change, thereby producing the voltage spike. A more dramatic observation is the rise of the toroidal electric field close to the minor axis of the device; the amplitude increasing to some ten times greater than the quiescent value.[4] This indicates that the current is being strongly inhibited close to the axis, a concept which will prove to be of great importance in the following work.

We have given a brief account of the effects of disruptions and listed the precursors and signatures that usually accompany them. The first precursor is always the growth of activity measured by the Mirnov coils. Since in tokamaks, m $\sim$ 0(1), the perturbations causing the oscillations on the coils are gross structures within the plasma. This indicates that the macroscopic theory of magneto-

hydrodynamics (MHD) is adequate to explain the oscillations.

Since disruptions manifestly affect the plasma interior and the precursors may be interpreted as gross perturbations of the plasma it is obvious to concentrate upon resistive MHD in the hope of shedding light on the basic causes.

For the remainder of this chapter, we shall review the theory of resistive MHD in both linear and non-linear regimes before seeing, in Chapter II, how this theory has been applied to model disruptions in tokamaks.

1.2 INTRODUCTION TO RESISTIVE MHD

The inclusion of a finite but small amount of resistivity in the equations of MHD relaxes the constraints imposed upon the plasma by Alfvén's theorem[5] and allows the otherwise 'frozen in' magnetic field and fluid to decouple. In such circumstances it is possible, depending upon the initial configuration, for the fluid to relax to a state of lower magnetic energy. Such a state is topologically inaccessible in the ideal case. The release of this free energy drives certain instabilities.

There are three main types of resistive instability. The first, the *g-mode*, is the resistive analogue of the classical Rayleigh-Taylor interchange instability.[6] The driving force of the latter is an inverted mass density gradient in a gravitational field. The g-mode analogue of this is a large pressure gradient in the presence of a magnetic field with strong curvature. The effect of the instability is to exchange regions of high pressure with regions of low pressure thereby reducing the destabilising force. This instability occurs at short wavelengths[7] and is stabilised by

good field curvature and the effects of shear. It is known that tokamaks are stable to g-modes[8] and therefore require no further consideration.

The second, the *rippling mode* is also interchange in character. The instability is driven by a gradient in the resistivity profile, along which the fluid is convected. Perturbed currents flow preferentially along channels or 'ripples' where the conductivity is higher. These currents cross with the zero-order magnetic field and generate a motor force which increases the convection, hence the instability grows. Like the g-mode, the rippling mode is short wavelength[7] and normally located near the plasma edge where the temperature is low (the threshold for the instability to grow is that the temperature $T \lesssim 30$ eV[10]). Since the temperature in tokamaks is much greater than the threshold, we may discount the rippling mode as a candidate to explain the disruption.

The third instability, the *tearing mode* differs from the previous instabilities since it is long wavelength in nature and causes a gross deformation to the magnetic field topology. The mode is driven by the global properties of the configuration and in particular by the presence of a gradient in the zero-order toroidal current density. Hence in a tokamak, the potential energy reservoir which the instability taps derives from the poloidal magnetic field. The instability is able to appear anywhere across the minor axis of the device, though the size of the perturbation and precisely where a given mode grows depends upon the distribution of the current. Therefore, within the context of resistive MHD, the tearing mode is the only candidate able to explain the disruption and discussion shall

henceforth be limited exclusively to this mode.

That the topology of an initial configuration may change due to the inclusion of resistivity may initially seem puzzling. A wave equation containing irreversible viscous or resistive terms has dissipative solutions, the diffusion being most rapid where spatial gradients are steepest. After sufficient time has elapsed, the wave like solutions become broadened and smoothed. It may, at first sight, appear that the only effect resistivity has, is to cause the magnetic field to decay. This was shown not to be the case in a seminal paper on resistive MHD[9], where the concept of magnetic field line reconnection was introduced. A full and rigorous analysis of sheet pinch was performed thereafter.[10] It was shown[10] that though the field does diffuse across the entire plasma cross-section, the diffusion has a dominant effect at only a finite number of surface within the plasma. The surfaces are located where the helicity of the zero order field matches the wavelength of the instability. At these surfaces the plasma is able to move without causing the field lines to bend. These surfaces are known as *resonant* surfaces, though the term *mode-rational* surface is often used for reasons which shall become apparent later. At the resonant surfaces, the resistive diffusion changing the field, is of comparable magnitude to the changes caused by advection. Therefore, the field and fluid may decouple, i.e. diffuse with respect to each other, thereby altering the topology of the field.

To see quantitatively how this arises, we examine the incompressible resistive MHD equations[11], which are as follows :

$$\rho\frac{d\underline{v}}{dt} = \underline{j} \wedge \underline{B} - \nabla p + \rho\underline{g} \qquad (1.2.1)$$

$$\frac{\partial \underline{B}}{\partial t} = - \nabla \Lambda \underline{E} \qquad (1.2.2)$$

$$\mu_o \underline{j} = \nabla \Lambda \underline{B} \qquad (1.2.3)$$

$$\underline{E} = \eta \underline{j} - \underline{v} \Lambda \underline{B} \qquad (1.2.4)$$

$$\nabla . \underline{B} = 0 \qquad (1.2.5)$$

together with

$$\nabla . \underline{v} = 0 \qquad (1.2.6)$$

ρ is the mass density which is taken to be constant, $\underline{v}$ the fluid velocity, p the fluid pressure, $\underline{g}$ the gravitational force, $\underline{B}$ the magnetic field, $\underline{E}$ the electric field, $\underline{j}$ the current density and η the resistivity of the fluid. The last equation, expressing the incompressibility of the fluid is chosen for simplicity and as a convenient closure to the set. We could, instead include as energy equation, giving the temperature of the fluid as a function of space and time, but would then require an equation of state in order to obtain closure. The equations of resistive MHD are simply the equations of fluid mechanics and electromagnetism joined together through Ohms Law (1.2.4).

Combining (1.2.2) and (1.2.3) with (1.2.4) and using (1.2.5) gives the well known full induction equation

$$\frac{\partial \underline{B}}{\partial t} = \nabla \Lambda (\underline{v} \Lambda \underline{B}) + \frac{\eta}{\mu_o} \nabla^2 \underline{B} \qquad (1.2.7)$$

The first term of the right hand side of (1.2.7) represents the coupling of the field to the plasma, the second term gives the diffusion of the field. The diffusion has a characteristic timescale associated with it

$$\tau_R = \mu_o a^2/\eta$$

known as the diffusion time. Ideal MHD instabilities have growth times characterised by the Alfvén speed, as may be seen from (1.2.1),

$$\tau_A = a/V_A$$

where $V_A^2 = B_o^2/\mu_o\rho$. The ratio of these timescales,

$$S = \tau_R/\tau_A$$

is traditionally called the magnetic Reynolds' number. Inserting values of the parameters found in contemporary tokamaks gives $S \sim 10^4 - 10^8$, the latter figure being appropriate to a reactor plasma. Hence the diffusion time is many orders of magnitude greater than the inertial time.

Let us consider a simple case in slab geometry, of a plasma embedded in a magnetic field $\underline{B}_o$. The field is perpendicular to the direction across the slab (the y-direction) but varies with y such that is has a null at y = 0. Hence $\underline{B}_o = b_o y/L\hat{\underline{x}}$ where L is a suitable scale length and $\hat{\underline{x}}$ a unit vector along the line y = 0, as in Fig.(1.3).

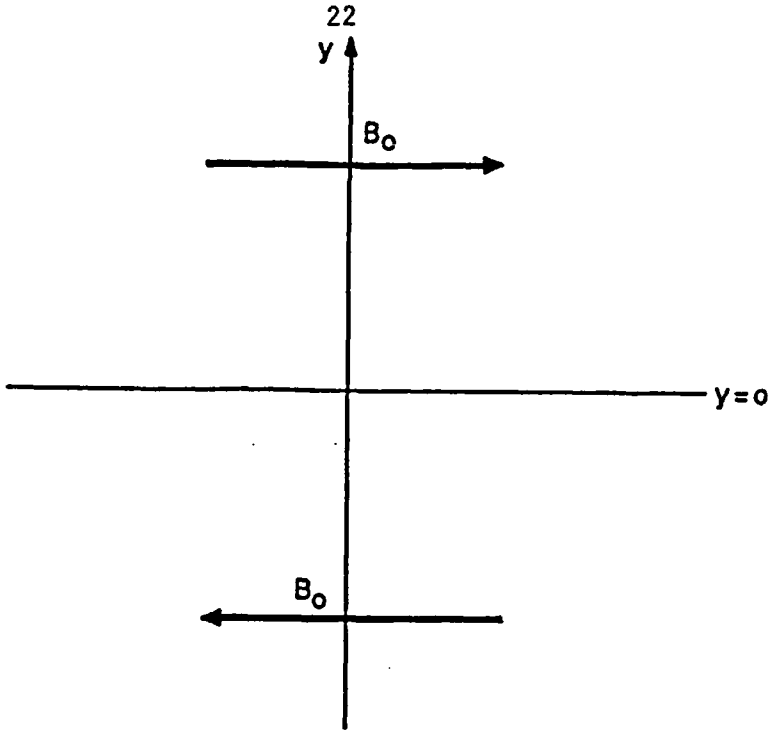

Fig.(1.3) Magnetic field configuration for the tearing mode in slab geometry.

Consider perturbations to the magnetic field and velocity flow across the slab of the form

$$r_y(x,y,z,t) = r_y(y)\exp(ik_x x + ik_y y + \gamma t)$$

and insert this into the linearised form of (1.2.7); then

$$B_y = (\underline{k}.\underline{B}_o)\underline{\xi} + \frac{\eta}{\mu_o \gamma}\left(\frac{d^2 B_y}{dy^2} - k^2 B_y\right) \qquad (1.2.8)$$

where $\xi = \int^t v_y dt'$ is the fluid displacement and $k^2 = k_x^2 + k_z^2$.

The second term on the RHS of (1.2.8) is generally of the order 1/S times the first and may therefore be neglected, since S is large. Note however, when $\underline{k}$ is perpendicular to $\underline{B}_o$, the first term vanishes and the equation becomes purely diffusive. Away from those surfaces where $\underline{k}.\underline{B}_o = 0$, the plasma may be thought as being a perfectly

conducting fluid and the ideal MHD equations can be employed. However, near the resonant surfaces, diffusion of the field with respect to the fluid occurs and therefore within a diffusive or 'tearing layer', the full equation (1.2.8) must be solved.

To summarise, we have seen that even though $\tau_R >> \tau_A$, the field diffusion must be included due to the fact that the scalelength appearing in τ_R is different from the scalelength appearing in τ_A. Rather, it is the length over which $(\underline{k}.\underline{B}_o)\xi \lesssim \frac{\eta}{\mu_o \gamma} \nabla^2 B_y$.

In the next section we estimate the width of the diffusive or tearing layer.

1.3 SIZE OF THE TEARING LAYER

In order to obtain a solution to equation (1.2.8), another relationship between the linear variables B_y and ξ is required. The linearised version of the momentum equation (1.2.1) provides such a relationship.

By substituting for $\underline{j}$ using Ampere's Law and then taking the curl of the resulting momentum equation in order to eliminate the pressure gives

$$\gamma^2 \rho \left(\frac{d^2\xi}{dy^2} - k^2 \xi\right) = \frac{\underline{k}.\underline{B}_o}{\mu_o}\left\{\frac{d^2 B_y}{dy^2} - k^2 B_y - \frac{B_y}{(\underline{k}.\underline{B}_o)} \frac{d^2(\underline{k}.\underline{B}_o)}{dy^2}\right\} \tag{1.3.1}$$

In obtaining (1.3.1) the density was assumed constant and the gravitational force neglected.

Equations (1.2.8) and (1.3.1) are a pair of second order differential equations in two unknowns and may therefore be solved,

subject to a suitable choice of boundary conditions.

Using (1.2.8) and (1.3.1), it is possible to estimate the size of the tearhing layer δ, over which the resistive diffusion term in (1.2.8) is of comparable magnitude to the ideal MHD term, i.e.

$$(\underline{k}.\underline{B}_o)\xi \sim \frac{\eta}{\mu_o \gamma} \frac{d^2 B_y}{dy^2} \tag{1.3.2}$$

Equating the inertial force with the magnetic force terms in (1.3.1) gives another estimate for $d^2 B_y/dy^2$:

$$\gamma^2 \rho \frac{d^2 \xi}{dy^2} \sim \frac{\underline{k}.\underline{B}_o}{\mu_o} \frac{d^2 B_y}{dy^2} \tag{1.3.3}$$

Combining (1.3.2) and (1.3.3) gives

$$\frac{d^2 \xi}{dy^2} \sim \frac{(\underline{k}.\underline{B}_o)^2 \xi}{\eta \gamma \rho}$$

Putting $d^2\xi/dy^2 \sim \xi/\delta^2$, expanding $(\underline{k}.\underline{B}_o)$ about the resonant surface so that $(\underline{k}.\underline{B}_o) \sim d(\underline{k}.\underline{B}_o)\delta/dy$ gives on solving for δ,

$$\delta \sim \left\{ \frac{\gamma \rho \eta}{(\underline{k}.\underline{B}_o)'^2} \right\}^{\frac{1}{4}} \tag{1.3.4}$$

where the prime denotes differentiation with respect to y.

Note that the tearing layer width is a function of the growth rate γ of the instability. In the next section a description of how γ is calculated is given.

1.4 GROWTH RATE OF THE TEARING MODE

We have seen that outside the tearing layer, the ideal equations of MHD are valid so that the governing equations are (1.2.8) and (1.3.1) with $\eta = 0$. Within the layer, resistivity is important and so the full versions of (1.2.8) and (1.3.1) must be solved.

Hence, inside the layer, the magnetic field is found by solving a fourth order differential equation and matching the solution at the layer boundary to the solution calculated from the second order ideal equation.

The eigenvalue for the growth rate is found by calculating from the outer solution, the jump in the logarithmic derivative of B_y across the layer. This is equated to the logarithmic derivative of B_y as calculated from the inner solution.

Let Δ' and Δ'_i denote the jump of the logarithmic derivative of B_y in the outer and inner regions respectively. Δ'_i is a function of γ, and so the required eigenvalue is found by solving the dispersion equation

$$\Delta' = \Delta'_i(\gamma) \qquad (1.4.1)$$

Thus, the eigenvalue is affected by the global field structure outside the layer.

The growth of a mode will occur if $\Delta' > 0$, marginal stability occurs if $\Delta' = 0$ and linear stability for $\Delta' < 0$. This result will be verified in section 1.6, by consideration of the energy.

For the slab configuration shown in Fig.(1.3), the dispersion equation has an analytical[10] solution

$$\gamma \sim \frac{(\Delta' a)^{4/5} (ka)^{2/5}}{\tau_R^{3/5} \tau_A^{2/5}} \qquad (1.4.2)$$

Using (1.4.2) to substitute for γ into (1.3.4) gives the size of the tearing layer. It can be seen that the layer scales with $S^{-2/5}$ or equivalently, with $\eta^{2/5}$.

Equation (1.4.2) shows that the inverse linear growth-rate is between the resistive and ideal MHD timescales and typically of order milliseconds. Hence the linear growth time is a fraction of the total discharge time. For this reason it will be necessary to see how the growth of the tearing mode changes, once the non-linear regime is entered.

Before proceeding however, we shall pause to derive the stability equation in a geometry suited to modelling a tokamak. We have already seen this equation ((1.3.1) evaluated at marginal stability) but it is considered a worthy effort to re-derive it since it is this form of the equation that will be subsequently used.

1.5 DERIVATION OF THE STABILITY EQUATION IN THE CYLINDER

The tearing mode has been considered only in simple slab geometry so far. The geometry plays a crucial role in determining both the strength of the instability and its location within the plasma. Consideration will be given to the class of tokamak which can be approximated by a circular cross-section and small inverse aspect ratio ϵ (ratio of the minor radius a to the major radius R of the torus). This approximation enables the torus to be modelled as a straight but periodic cylinder with coordinates (r,θ,z). Here r is the radial coordinate, θ the poloidal angle and z the length

along the cylinder, with periodicity length $2\pi R$. This approximation rules out direct applicability to machines like JET which has a large inverse aspect ratio and D-shaped cross-section, though the basic principles still apply.

We shall assume standard tokamak ordering throughout.[8] The toroidal magnetic field is constant both in space and time. The magnitudes of the field components are such that

$$B_\perp \sim \varepsilon B_{zo}$$

$\perp$ denoting perpendicularity to the z-axis, i.e. the (r,θ) plane. The total field may be expressed in the form

$$\underline{B}(r,\theta,z,t) = \underline{B}_\perp(r,\theta,z,t) + B_{zo}\,\hat{\underline{z}}$$

Since the divergence of $\underline{B}_\perp$ is zero, the field can be derived from a stream function, or flux function ϕ such that

$$B_r = -\frac{1}{r}\frac{\partial\phi}{\partial\theta}(r,\theta,z,t)$$

$$B_\theta = \frac{\partial\phi}{\partial r}(r,\theta,z,t)$$

Note that ϕ is equivalent to the z-component of the magnetic vector potential,

$$\underline{B}_\perp = \hat{\underline{z}} \wedge \nabla\phi \qquad (1.5.1)$$

From Ampere's Law :

$$j_z = \frac{1}{\mu_o} \nabla_\perp^2 \phi \qquad (1.5.2)$$

and

$$\underline{j}_\perp = \frac{1}{\mu_o} \frac{\partial}{\partial z} \underline{\nabla}\phi$$

Consider an axisymmetric equilibrium state, derived from an equilibrium flux function $\phi_o = \phi_o(r)$, to which is added a perturbation of the form

$$\tilde{\phi}(r,\theta,z,t) = \tilde{\Phi}(r)\exp(im\theta - in\zeta + \gamma t)$$

where ζ is the 'toroidal' angle z/R. The perturbed perpendicular magnetic field has the form

$$\underline{\tilde{B}}_\perp = \left(-\frac{im\tilde{\Phi}}{r}, \frac{\partial\tilde{\Phi}}{\partial r}, 0\right)$$

and the perturbed toroidal current density is

$$\mu_o \tilde{j}_z = \frac{1}{r}\frac{\partial}{\partial r}\left(r\frac{\partial\tilde{\Phi}}{\partial r}\right) - \frac{m^2}{r^2}\tilde{\Phi}$$

Linearising the momentum equation (1.2.1) about the equilibrium, and taking the curl to remove the pressure gives an equation for the vorticity

$$\rho \frac{d}{dt} \nabla\Lambda\underline{v} = (\underline{j}_o.\nabla)\underline{\tilde{B}}_\perp - (\underline{\tilde{B}}_\perp.\nabla)j_o + (\underline{\tilde{j}}.\nabla)\underline{B}_o - (\underline{B}_o.\nabla)\underline{\tilde{j}}$$

which on projecting into the z-direction gives

$$\rho \frac{d}{dt} (\nabla \Lambda \underline{v})_z = - (\underline{B}_\perp . \nabla) j_{zo} - (\underline{B}_o . \nabla) j_z \qquad (1.5.3).$$

We assume that the flow is incompressible, a reasonable assumption on the timescales of interest. This assumption enables the velocity to be written in terms of a potential $\tilde{\varphi}$

$$\underline{v} = \hat{\underline{z}} \Lambda \nabla \tilde{\varphi} \qquad (1.5.4)$$

then, the z-component of the vorticity becomes

$$(\nabla \Lambda \underline{v})_z = \nabla_\perp^2 \varphi$$

Assuming that $\tilde{\varphi}$ varies like $\tilde{\varphi}(r,\theta,z)e^{\gamma t}$, (1.5.3) becomes on writing out each component explicitly

$$\gamma \rho \nabla_\perp^2 \tilde{\varphi} = - \tilde{B}_r \frac{dj_{zo}}{dr} - \frac{iB_{\theta o}}{r} (m - nq)\, j_z \qquad (1.5.5)$$

where $q(r) = rB_{zo}/RB_{\theta o}(r)$ is the inverse rotational transform or <u>safety factor</u>. Evaluating (1.5.5) at the point of marginal stability gives

$$\tilde{B}_r \frac{dj_{zo}}{dr} + \frac{iB_{\theta o}}{r} (m - nq) j_z = 0$$

Now, $\tilde{B}_r = - \frac{im}{r} \tilde{\Psi}(r)$, so on writing $\tilde{j}_z$ explicitly in terms of the flux

$$\frac{1}{r} \frac{d}{dr} \left(r \frac{d\tilde{\Psi}}{dr} \right) - \frac{m^2}{r^2} \tilde{\Psi} - \frac{\mu_o m\, dj_{zo}/dr\, \tilde{\Psi}}{B_{\theta o}(m-nq)} = 0 \qquad (1.5.6)$$

This is the stability equation from which the amplitude of the perturbed radial field $\tilde{B}_r = m\tilde{\Phi}/r$ may be calculated. This equation is the cylindrical version of the RHS of (1.3.1). Note that (1.5.6) has a singularity whenever $q(r) = m/n$, i.e. when $\underline{k}.\underline{B}_o = 0$ which is the condition for the helicity of the zero-order magnetic field to match the wavelength of the perturbed field. It is at these surfaces where the fluid and field decouple, and about these surfaces that the instability grows.

The safety factor measures the pitch of a field line, so that a field line with $q = m/n$ winds n times in the poloidal direction for each m transits in the toroidal direction before joining upon itself. A surface at which q is an irrational number has a field line at that surface which covers the surface densely.

Equation (1.5.6) is valid everywhere, excepting those surfaces where the flow is decoupled. At these surfaces, a fourth order equation must be solved within the tearing layer in order to resolve the singularity.

The solution of (1.5.6) requires solving the equation as a boundary value problem from the external boundary at $r = a$ inwards to the singularity at $r = r_s+\delta$ and from the origin outwards from $r = 0$ to $r_s-\delta$. Clearly, $B_r(r_s)$ must be continuous for the solution to be physical. Such a stipulation will, in general, force the first derivative of B_r to be discontinuous. Hence

$$\Delta' = \lim_{\delta \to o} \left[\frac{d}{dr} B_r(r_s+\delta) - \frac{d}{dr} B_r (r_s-\delta)\right] / B_r(r_s) \qquad (1.5.7)$$

will in general be non-zero.

The 'driving term' of (1.5.6) is that involving dj_{zo}/dr, hence

Δ' is determined by the global plasma profiles, away from the tearing layer.

1.6 RELATION BETWEEN Δ' AND ENERGY

It was stated in section 1.2 that the tearing mode draws energy from that stored in the poloidal magnetic field. In this section it is shown how Δ' is related to energy available to drive the instability by the method used in ref.(12).

Using the energy principle for a low β-tokamak, the potential energy of the plasma is[13]

$$\delta W = \pi^2 R_o \int_o^a \left\{ \left(\frac{d\tilde{\Psi}}{dr}\right)^2 + \frac{m^2}{r^2}\tilde{\Psi}^2 + \frac{m\, dj_o/dr}{B_{\theta o}(m-nq)}\tilde{\Psi}^2 \right\} rdr$$

where a is the plasma boundary.

Since the first two terms on the RHS are positive definite, only the last term is able to provide a destabilising effect. Since dj_{zo}/dr is usually negative, the last term is destabilising if $q < m/n$. Tokamaks generally have q-profiles that increase radially with r, so the destabilising region lies within the resonant surface. A negative current gradient outside the resonant surface has a stabilising effect on the mode.

Writing

$$\int_o^a \left(\frac{d\tilde{\Psi}}{dr}\right)^2 rdr = -\int_o^a \left\{\frac{d}{dr}\left(r\frac{d\tilde{\Psi}}{dr}\right)\tilde{\Psi}\right\} dr + \left[r\tilde{\Psi}\frac{d\tilde{\Psi}}{dr}\right]_o^a$$

enables the energy equation to be cast into the form

$$\delta W = -\pi^2 R_o \int_o^a \left\{ \frac{1}{r}\frac{d}{dr}\left\{ r\frac{d\tilde{\psi}}{dr}\right\} - \frac{m^2}{r^2}\tilde{\psi} - \frac{m dj_{zo}/dr\tilde{\psi}}{B_{\theta o}(m-nq)} \right\} \tilde{\psi} r dr +$$

$$+ \pi^2 R_o \left[r\frac{d\tilde{\psi}}{dr}\tilde{\psi}\right]_o^a$$

where square brackets denote the difference of the variable evaluated at the two limits. Divide the range of integration into two $0 < r < r_s - \delta$ and $r_s + \delta < r < a$, where r_s is the resonant surface, then

$$\delta W = -\pi^2 R_o \int_o^{r_s-\delta} \left\{ \frac{1}{r}\frac{d}{dr}\left(r\frac{d\tilde{\psi}}{dr}\right) - \frac{m^2}{r^2}\tilde{\psi} - \frac{m dj_{zo}/dr\tilde{\psi}}{B_{\theta o}(m-nq)} \right\} \tilde{\psi} r dr +$$

$$- \pi^2 R_o \int_{r_s+\delta}^a \left\{ \frac{1}{r}\frac{d}{dr}\left(r\frac{d\tilde{\psi}}{dr}\right) - \frac{m^2}{r^2}\tilde{\psi} - \frac{m dj_{zo}/dr\tilde{\psi}}{B_{\theta o}(m-nq)} \right\} \tilde{\psi} r dr +$$

$$\pi^2 R_o \left[r\frac{d\tilde{\psi}}{dr}\tilde{\psi}\right]_o^{r_s-\delta} + \pi^2 R_o \left[r\frac{d\tilde{\psi}}{dr}\tilde{\psi}\right]_{r_s+\delta}^a$$

The integral appearing in the first two terms of δW is precisely the stability equation (1.5.6), which is identically zero for tearing mode eigenfunctions $\tilde{\psi}$, hence the energy reduces to

$$\delta W = \pi^2 R_o \left[r\frac{d\tilde{\psi}}{dr}\psi\right]_o^{r_s-\delta} + \pi^2 R_o \left[r\frac{d\tilde{\psi}}{dr}\tilde{\psi}\right]_{r_s-\delta}^a$$

Let us assume a perfectly conducting wall placed at the plasma boundary $r = a$, then $\psi(a) = 0$ and

$$\delta W = -\pi^2 R_o \left\{ (r_s+\delta)\tilde{\psi}(r_s+\delta)\frac{d\tilde{\psi}}{dr}(r_s+\delta) - (r_s-\delta)\psi(r_s-\delta)\frac{d\tilde{\psi}}{dr}(r_s-\delta)\right\}$$

So,

$$\lim_{\delta \to 0} \delta W = -\pi^2 R_o r_s \tilde{\phi}^2(r_s)\Delta' \qquad (1.6.1)$$

For the potential energy to decrease, $\Delta' > 0$ which again gives the condition for instability. The contribution to the energy from the inner range of integrations $[r_s-\epsilon, r_s+\epsilon]$ is negligible for antisymmetric displacement ξ which characterise the tearing mode.[12]

In ref.(8), the effect of removing a conducting wall at r = a is illustrated. The perturbed flux $\tilde{\psi}(a)$ is no longer zero and the solution must be matched on to a vacuum solution for $\tilde{\psi}$. The removal of the wall allows surface tearing modes, which are the resistive analogue of ideal kink modes driven by a large value of Δ' at the plasma surface. The wall on plasma case is therefore more stable than if the wall is removed from the plasma edge.

In this section, we have seen from energy considerations, that the tearing mode will be unstable, provided the criterion $\Delta' > 0$ is satisfied. So far, consideration has been given to states of marginal stability. Having discovered what determines the linear marginal stability properties, we proceed to investigate how the tearing mode behaves in the non-linear regime.

1.7 NON-LINEAR BEHAVIOUR OF THE TEARING MODE

We have established that tearing modes grow as a consequence of the plasma lowering its magnetic potential energy. This is achieved by the field altering its topology about the resonant surface where $q(r_s) = m/n$. The topology change manifests itself by the formation of magnetic islands. Islands are regions within the plasma having a separate magnetic axis from the axisymmetric component of

the field.

Consider a uniform poloidal field $B_\theta(r)$ to which is added a perturbed radial field $B_r(r)\cos(m\theta+n\zeta)$. The perturbed field is the solution to equation (1.5.6). Figure (1.4) shows the magnetic surfaces before and after the radial field perturbation has been applied; the helicity of the mode m/n = 2/1. The m = 2 islands are clearly visible and the 'torn' state has three distinct magnetic axes.

The magnetic islands cover an appreciable fraction of the minor radius and therefore significantly perturb the system. It is the aim of non-linear theory to calculate the perturbation and see how the subsequent growth of the island changes.

In section 1.5, the stability equation for the tearing mode was derived by consideration of the linearised vorticity equation. In deriving this equation, the inertia in the outer region was neglected. At first sight this could appear to be a rather drastic measure, however we shall see that once the size of a magnetic island exceeds the tearing layer width, the inertia is indeed negligible.

The approximations used are the same as in section 1.5; these approximations allow the magnetic and velocity fields to be derived in terms of flux and stream functions respectively. Integration of Faraday's Law, and the subsequent projection into the z-direction gives

$$\frac{\partial \psi}{\partial t} + (\nabla\varphi \Lambda \nabla\psi).\hat{\underline{z}} = \eta j_z - \frac{\partial \chi}{\partial z} - E_{zo} \qquad (1.7.1)$$

where the gauge potential χ can be identified with the velocity stream function φ.[14] The constant of integration E_{zo} is the toroidal

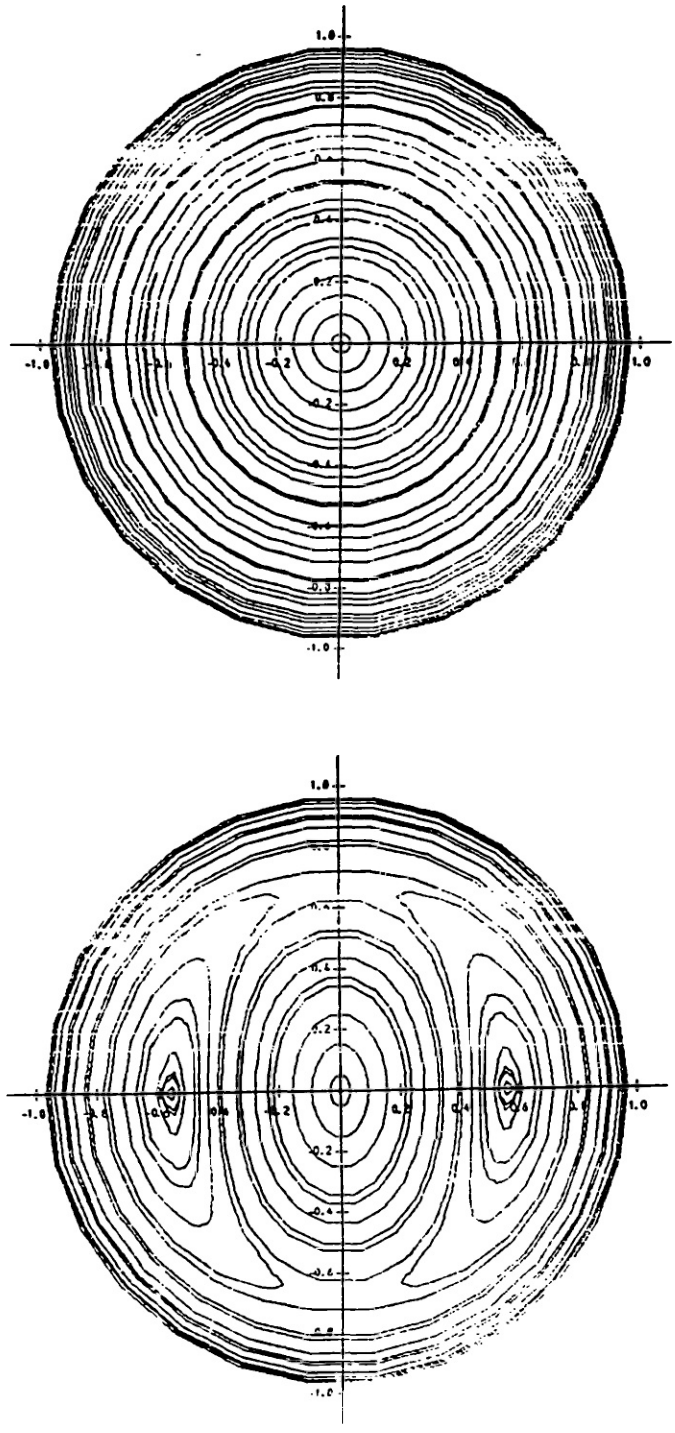

Fig.(1.4) *Helical magnetic flux function showing the change in topology due to tearing modes.*

electric field, which maintains the initial resistive equilibrium in the absence of a perturbation to ϕ, i.e. $E_{zo} = \eta j_{zo}$, where $j_{zo} = \nabla_\perp^2 \psi_o$.

Taking the curl of the momentum equation and projecting into the z-direction gives the vorticity equation,

$$\rho \frac{\partial \nabla_\perp^2 \varphi}{\partial t} + \rho(\nabla\varphi \Lambda \nabla \nabla_\perp^2 \varphi).\hat{\underline{z}} = (\nabla\psi \Lambda \nabla j_z).\underline{z} \qquad (1.7.2)$$

The linear terms on the RHS of (1.7.2) reduce to the stability equation (1.5.6). The full term on the RHS of (1.7.2) represents the non-linear destabilising torque on the plasma.

Equations (1.7.1) and (1.7.2), together with Ampere's Law (1.5.2),

$$j_z = \frac{1}{\mu_o} \nabla_\perp^2 \psi \qquad (1.7.3)$$

form the basis of Rutherford's analysis of the non-linear tearing mode.[15]

The crux of Rutherford's analysis is in calculating the quasi-linear change in the current due to the presence of an island of finite width W. The quasi-linear toroidal currents cross with the radial perturbation magnetic field (which cause the island to grow in the first place). The resulting motor force opposes the vortex flow of plasma within the island, making the effect of inertia negligible. The exponential growth of the linear phase (which is a function of the MHD timescale τ_A) is halted. Subsequent algebraic growth occurs on the slower resistive timescale.

We shall now give a simple derivation for the condition that

the non-linear $\underline{j} \Lambda \underline{B}$ force be of comparable magnitude with the inertial force within the tearing layer.

We shall assume a simple sheet pinch configuration, as in section 1.2, though the analysis is similar for cylindrical geometry.[16] A sheared equilibrium field has the structure $B_x = B_x'y$ near the singularity at $y = 0$. For a perfectly conducting and incompressible plasma, the area within a surface of constant flux $\psi_o = \frac{1}{2} B_x'y$ is invariant. The addition of a perturbation $\tilde{\psi}$ to the flux gives a total flux ϕ where

$$\phi(x,y,t) = \phi_o(y) + \tilde{\psi}(y,t)\cos kx,$$

the perturbed velocity stream function is

$$\varphi(x,y,t) = \tilde{\varphi}(y,t)\sin kx$$

The perturbed magnetic flux gives rise to a x-independent component of the current δj_{zo} within the tearing layer.[15] Hence, the current is given by

$$j(x,y,t) = j_{zo}(y) + \tilde{j}(y,t)\cos kx + \delta j_{zo}$$

where the second order zero-harmonic of the current δj_{zo} is calculated from the second-order zero-harmonic of eqn(1.7.1)

$$\frac{\partial \delta\phi_o}{\partial t} + (\nabla\tilde{\varphi} \Lambda \nabla\tilde{\psi}).\underline{\hat{z}} = \eta \delta j_{zo} \qquad (1.7.4)$$

Within the tearing layer of width δ, the characteristic resistive time

$\tau_R^L \sim \delta^2/\eta$. From section 1.4, the layer width scales with $\eta^{2/5}$ and hence

$$\tau_R^L \sim \eta^{-1/5}$$

Contrasting τ_R^L with the linear growth time $\gamma^{-1} \sim \eta^{-3/5}$, we see that

$$\gamma^{-1} \gg \tau_R^L$$

Hence, the current distribution resistively relaxes within a linear growth time; consequently the term $\partial\delta\phi_o/\partial t$ in (1.7.1) can be neglected so that :

$$\eta\delta j_{zo} = \langle(\nabla\tilde{\varphi}\wedge\nabla\tilde{\phi}).\hat{z}\rangle \qquad (1.7.5)$$

where

$$\langle f\rangle \equiv \int_0^{2\pi/k} \frac{k}{2\pi} f\, dx$$

Inserting $\tilde{\varphi}$ and $\tilde{\phi}$ into (1.7.5) gives :

$$\eta\delta j_{zo} = \tfrac{1}{2}k\tilde{\phi}\frac{d\tilde{\varphi}}{dy} \qquad (1.7.6)$$

Substituting (1.7.6) in (1.7.3) and approximating $\nabla_\perp^2 \approx d^2/dy^2$, we obtain

$$\rho\frac{\partial}{\partial t}\left(\frac{d^2\tilde{\varphi}}{dy^2}\right) = k\left(\frac{d\psi_o}{dy}\tilde{j}_z - \tilde{\phi}\frac{dj_{zo}}{dy}\right) - \tilde{\phi}\frac{d\delta j_{zo}}{dy} \qquad (1.7.7)$$

$$\text{or} \qquad (\rho\frac{\partial}{\partial t} + \frac{k^2\tilde{\psi}^2}{2\eta})\frac{d^2\tilde{\psi}}{dy^2} = k(\frac{d\psi_o}{dy}\tilde{j}_z - \tilde{\psi}\frac{dj_{zo}}{dy}) \qquad (1.7.7)$$

Now, assuming that the island width w ($w = 4(\tilde{\psi}/B_o')^{\frac{1}{2}}$) is of comparable size with the tearing layer width δ, we can proceed to estimate the terms on the LHS of (1.7.7). So,

$$w \sim \delta$$

$$\frac{\tilde{\psi}^2}{B_o'^2} \sim \frac{\gamma\rho\eta}{k^2B_o'^2}$$

i.e. that

$$\gamma\rho \sim \frac{k^2\tilde{\psi}^2}{\eta}$$

Hence, when the island is of the same size as the tearing layer width, the quasi-linear current δj_{zo} gives rise to a force of comparable magnitude to the inertia. The tearing instability therefore changes its character at a small amplitude $w \sim \delta$. Rutherford calculates that for islands with width $w \gtrsim \delta$, the growth of the perturbed flux scales with (t/τ_R) i.e. the growth is algebraic rather than the exponential growth of the linear regime. Specifically, the non-linear growth of an island is given by[15]

$$\frac{\partial w}{\partial t} = \frac{1.66\ \eta(r_s)}{\mu_o}\Delta' \qquad (1.7.8)$$

where η is evaluated at the resonant surface r_s, and t is measured in units of τ_R. Thus a magnetic island grows linearly with time in the

non-linear regime.

The work of Rutherford was extended in ref.(16). By considering the self-consistent change in the resistivity due to the island, the equation for island growth becomes

$$\frac{\partial w}{\partial t} = \frac{1.66\ \eta(r_s)}{\mu_o} (\Delta'(w) - \alpha w) \qquad (1.7.9)$$

Here, Δ' is written explicitly as a function of w, i.e.

$$\Delta'(w) = (\frac{d\tilde{\Phi}}{dy} (r_s + \tfrac{1}{2}w) - \frac{d\tilde{\Phi}}{dy} (r_s - \tfrac{1}{2}w))/\tilde{\Phi}(r_s)$$

The island will attain its saturation width when

$$\Delta'(w) = \alpha w$$

In practice, α is small and so the approximation

$$\Delta'(w) = 0$$

is usually sufficiently accurate to calculate the saturation width.

The main stabilising effect of the non-linear tearing mode arises from the decrease in Δ' with growing island width. This represents the decrease in the free magnetic energy which drives the instability. For typical current profiles, the saturation width is attained in a fraction of the resistive time.[16] After saturation, the evolution adiabatically follows the changing current profile. As the current profile alters (for whatever reason one chooses), the value of Δ' will change, and consequently W will change in order to

maintain $\Delta'(W) \approx 0$. Therefore the non-linear evolution of the tearing mode is a sequence of equilibrium states characterised by a diffusive growth (or decay) of magnetic islands.

1.8 SUMMARY

In this chapter, the experimental effects of disruptions together with the signatures associated with them, have been briefly described. The experimental evidence supports the view that disruptions occur as a consequence of MHD activity.

A brief introduction to resistive MHD has been given and we have found that the tearing mode is unstable to sheared equilibrium field structures, such as those found in tokamaks. The linear growth of the tearing mode occurs on a timescale between the resistive and ideal MHD times, but is short compared with the overall duration of a typical experiment. For this reason it is necessary to consider the behaviour of the tearing mode once the non-linear regime has been entered.

The non-linear evolution of the mode is radically different from the linear growth phase, the growth being algebraic rather than exponential in time. A mode will reach its saturated amplitude in a fraction of the resistive time, and thereafter the evolution will be characterised by a resistive decay, or growth, of magnetic islands.

In the next chapter we shall see how the ideas described in this chapter, have been applied to model disruptions in the tokamak.

CHAPTER II

2.1 INTRODUCTION

We have considered the resistive tearing mode in the linear and non-linear regimes. In this chapter we shall see how this theory has been extended and applied to explaining disruptions. An extension to the theory is required since, as was stated in section 1.7, the non-linear tearing mode is self-stabilising for a wide class of conditions. Much of the work done in this area had been directed to finding conditions for which the growth of tearing modes is destabilising.

We shall describe two theories which purport to explain disruptions as a consequence of tearing mode activity. This does not exhaust all the currently available models[17,18,19], one of which (Ref.19) does not resort to an MHD description at all! The model described in Ref.17 is, however, a variation on the 'Oak-Ridge Model', which is currently favoured by the plasma physics community as being the most likely model for the disruption.[3] We shall describe the Oak-Ridge model in section 2.2, and then progress to describe the 'catastrophe' model of Wesson et al in section 2.3. In section 2.4 we conclude the chapter with a critical review of both models. In particular, certain details of the Oak-Ridge model appear to be at variance with physical intuition. We list three (what we consider to be) major criticisms of the model and it is the resolution of these criticisms that forms the bulk of the work in this thesis.

2.2 DISRUPTIONS CAUSED BY THE NON-LINEAR INTERACTION OF TEARING MODES OF DIFFERENT HELICITY : THE OAK-RIDGE MODEL

In this section, we describe the currently held consensus view of the cause of tokamak disruptions, the Oak-Ridge Model.

The theory outlined in the previous chapter described the consequences of the non-linear growth of a single tearing mode. In general, a plasma can be unstable to more than one tearing mode at any time. Magnetic islands of different helicity (pitch) will grow about their respective resonant surfaces. If the surfaces are close or if the islands are large, the islands will be able to overlap each other. Magnetic flux surfaces are destroyed in the overlap region and hence field lines can wander stochastically or ergodically within a volume. This provides an efficient thermal short circuit across the minor radius of the plasma, connecting the hot core with the cold exterior. There then follows an energy quench, i.e. a disruption.

The model is inferred from numerically solving the reduced MHD equations.[14] The geometry is cylindrical and therefore applicable to small inverse aspect ratio ($\epsilon = a/R_o << 1$) tokamaks, with standard tokamak ordering.[8] The reduced formalism is particularly suited to modelling tokamaks by virtue of the strength of the toroidal component of magnetic field ($B_{zo} \sim \epsilon B_\perp$). The consequence of this is that the fastest timescale within the full set of MHD equations does not occur within the reduced set. The fastest timescale within the reduced formalism is the 'slow' Alfvén time, the time for Alfvén waves to propagate in the toroidal direction, along the magnetic field lines. Since the fastest characteristic time is longer for the reduced equations than for the full set, the reduced equations afford

an easier numerical solution.

Originally, the reduced equations were solved in helical geometry, suitable for modelling a single helicity perturbation.[20] The results of these calculations verified Rutherford's theory; clearly illustrating that a magnetic island grew linearly in time, attaining its saturation width when $\Delta'(W) = 0$.

A larger computer code, RS3, was able to solve the reduced equations in 3-D, thereby affording the possibility for studying the interaction of modes with different helicity.[21] The results were radically different from the single helicity calculations; the conclusion being that the m = 2, n = 1 tearing mode non-linearly destablisied the m = 3, n = 2 mode, thereby initiating a cascade to other modes. The work in this area culminated in the development and use of a sophisticated 3-D spectral computer code RSF.[22] This was capable of solving the reduced equations at very large values of S ($\sim 10^6$), the magnetic Reynolds number.[23] The results obtained with RSF[23] were similar to those obtained with RS3[21], although the computational efficiency and accuracy was claimed[22] to be much improved.

The reduced MHD equations, when cast into a dimensionless form, are[21] :

$$\frac{d\Psi}{dt} = \eta j_z - E_z^W - \frac{\partial \Phi}{\partial z} \qquad (2.2.1)$$

$$\frac{dU}{dt} = S^2 \quad (\nabla\Psi \wedge \nabla j_z).\hat{z} - \frac{\partial j_z}{\partial z} \qquad (2.2.1)$$

$$\underline{B} = (\epsilon\, \hat{z} \wedge \nabla\, \Psi + \hat{z})\, B_{zQ} \qquad (2.2.3)$$

$$j_z = \nabla_\perp^2 \Psi \tag{2.2.4}$$

$$\underline{v}_\perp = \nabla\Phi \wedge \underline{\hat{z}} \tag{2.2.5}$$

$$u = \nabla_\perp^2 \Phi \tag{2.2.6}$$

where the radial length is normalised to the minor radius a, η to its value on axis ($\eta(o) = 1$), time to the resistive diffusion time τ_R, $a^2\mu_o/\eta$, Ψ to $a^2 B_{zo}$, Φ to $a^2 B_{zo}/\tau_R$, j_z to $B_{zo}/(\mu_o R_o)$ and $v_\perp$ to a/τ_R. The toroidal Alfvén time τ_A is $R_o(\mu_o\rho)^{\frac{1}{2}}/B_{zo}$ and $S = \tau_R/\tau_A$.

Equations (2.2.1) - (2.2.6) are similar to the equations of section 1.5 and section 1.7. Equation (2.2.1) is derived by integrating the combined Faraday's and Ohm's Laws (1.2.2) and (1.2.4) and projecting the equation into the z-direction. Equation (2.2.2) is the curl of the momentum equation, projected into the z-direction where the assumption of constant density is used. The form of the magnetic field (2.2.3) is a result of tokamak ordering and div $B_\perp$ = 0. Equation (2.2.4) is Ampere's Law and (2.2.5) a consequence of incompressible flow. Equation (2.2.6) expresses the vorticity u in terms of the stream function Φ. As usual, the convective derivative

$$\frac{d}{dt} = \frac{\partial}{\partial t} + \underline{v}.\nabla$$

The reduced equations possess non-trivial, velocity free solutions so that initially

$$\Phi(r,\theta,z,t = 0) = 0$$

can be assumed without loss of generality.

The field and velocity potentials are expanded in terms of a Fourier series in the angle-like variables θ and $\zeta = z/R_o$:

$$\Psi(r,\theta,\zeta,t) = \sum_{mn} \psi_{mn}(r,t)\cos(m\theta + n\zeta)$$

and

$$\Phi(r,\theta,\zeta,t) = \sum_{mn} \varphi_{mn}(r,t)\sin(m\theta + n\zeta)$$

The equilibrium, axisymmetric component of the flux is determined from the initial current distribution, or alternatively by defining the q-profile, then :

$$\psi_{oo}(r,t = 0) = \int_r^1 \frac{r'dr'}{q(r')}$$

and the initial q-profile is parametrised by

$$q(r) = q(o)\left[1 + \left(\left\{\frac{q(1)}{q(o)}\right\}^{\lambda} - 1\right) r^{2\lambda}\right]^{1/\lambda} \qquad (2.2.7)$$

where q(o) is the value of q on axis, q(1) the value at the wall and λ a shaping parameter. The larger λ, the flatter the current becomes close to the axis.

The resistivity is a specified function of space which does not evolve in time :

$$\eta(r) = E_{zo}^{W}/j_z(r,t = 0)$$

This choice of resistivity profile ensures that, in the absence of tearing mode activity, the flux is constant in time.

The reduced equations are numerically advanced in time[22], subject to the boundary conditions

$$\varphi_{mn}(1,\theta,\zeta,t) = 0$$

and

$$\phi_{mn}(1,\theta,\zeta,t) = 0,$$

consistent with an impervious and perfectly conducting boundary at $r = 1$. Both potentials are regular at the origin.

The calculation is initiated by choosing an equilibrium profile unstable to the $m/n = 2/1$ and $m/n = 3/2$ tearing modes. The system is perturbed and magnetic islands subsequently grow about their respective resonant surfaces. Figure (2.1) shows the 2/1, 3/2 and 5/3 islands as functions of time, plotted at their respective positions within the plasma.

Initially the islands grow as for single-helicity calculations, the growth being entrenched in the Rutherford regime. When the islands overlap, the growth of the islands rapidly increases. The timescale for the evolution is no longer characterised by τ_R, but by γ_{21}^{-1} where γ_{21} is the growth-rate of the 2/1 mode.[23] This scaling is apparently independent of S.

The destabilisation results from the non-linear interaction as can be seen from Fig.(2.2) which shows the growth-rate for a non-linearly coupled and a single helicity calculation. Clearly no peak

occurs in γ_{32} when it is the only mode present.

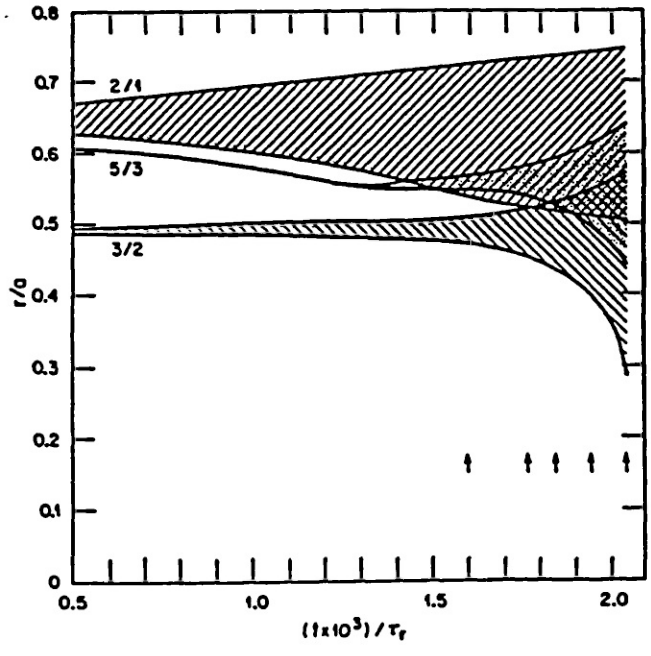

Fig.(2.1) Time evolution of magnetic islands. Note the increased growth when the 3/2 island touches the 2/1. (Taken from Phys. Fluids, 23, 1811, (1980)).

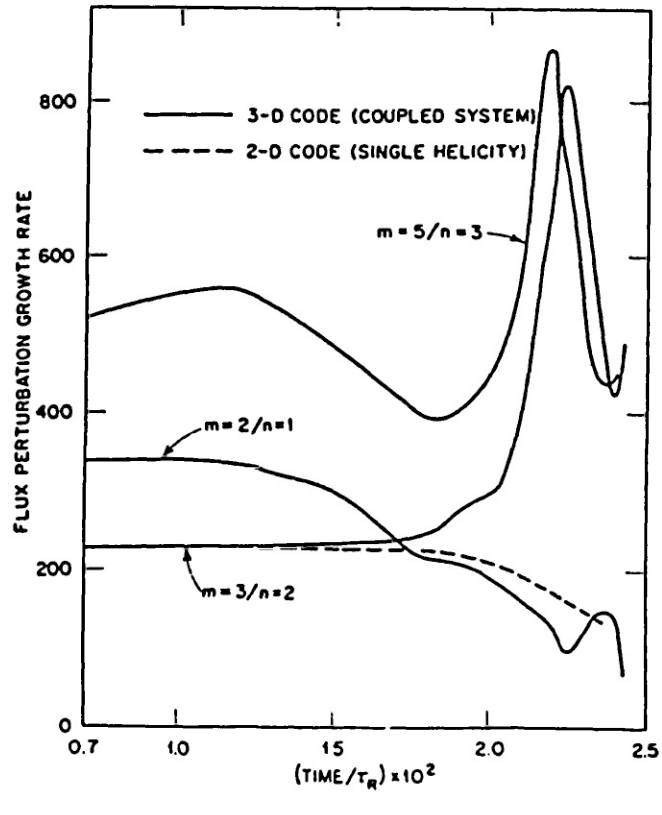

Fig.(2.2) Growth rates of the 2/1, 3/2 and 5/3 modes for coupled and uncoupled systems. The behaviour is independent of S. (Taken from Phys. Fluids, 22, 896, (1979)).

During the overlap phase, many modes of different helicity are non-linearly generated; the origin of these modes being the quadratic terms in (2.2.1) and (2.2.2). The presenceof these modes destroys the flux surfaces in the overlap region, causing the magnetic field to become ergodic. Figure (2.3) shows the intersection of a single field line with the poloidal plane at the times marked by arrows in fig.(2.1). The field at time $2.06 \times 10^{-3}/\tau_R$ is ergodic within the overlap region suggesting that the core is connected to the outer regions.

One of the most remarkable features of the calculation is the behaviour of the toroidal current density at the time of island overlap. The current profile is severely distorted by the islands and exhibits finescale filaments as may be seen in fig.(2.4).

It is assumed by Oak-Ridge that the gross distortion of the current density, together with $\sim$ 45% of the minor radius being threaded with ergodic lines are conditions similar to those experienced by a plasma during a disruption; ergo the results describe a disruption.

To summarise, the main feature of the model is the non-linear destabilisation of the 3/2 tearing mode by the 2/1. This interaction initiates a cascade to higher mode numbers m and n. The islands associated with these modes destroy the nested flux surfaces, and severely distort the toroidal current profile, thereby providing a thermal short circuit across the plasma minor radius. It is then assumed that the energy of the plasma would quench, hence a disruption.

The calculations performed with $S = 10^4$ (ref.21) showed similar behaviour as those performed with $S = 10^6$ (ref.22). Furthermore

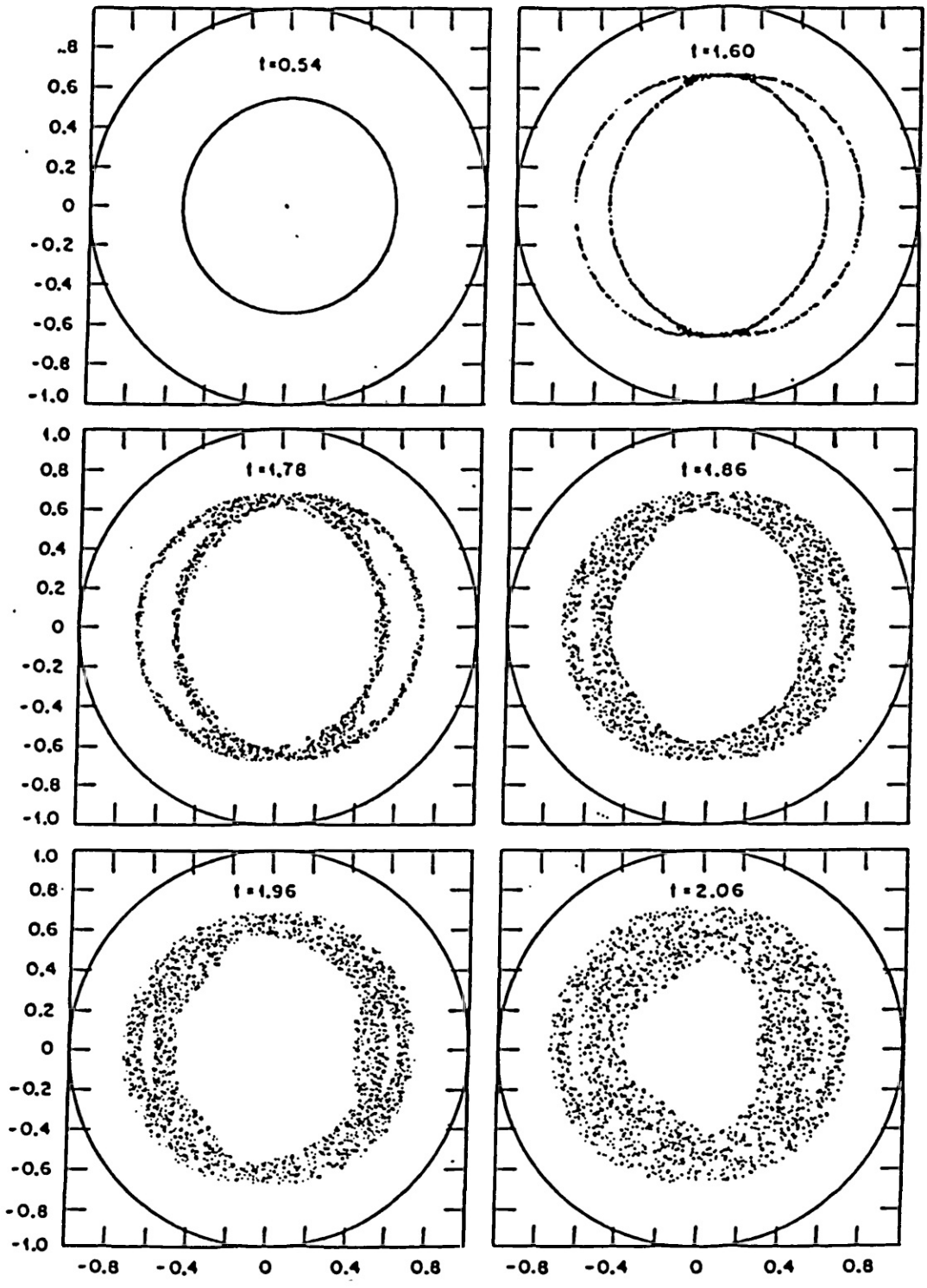

Fig.(2.3) *Intersection of a single magnetic field line with the poloidal plane $\zeta = 0$. (Taken from Phys. Fluids, 23, 1811, (1980)).*

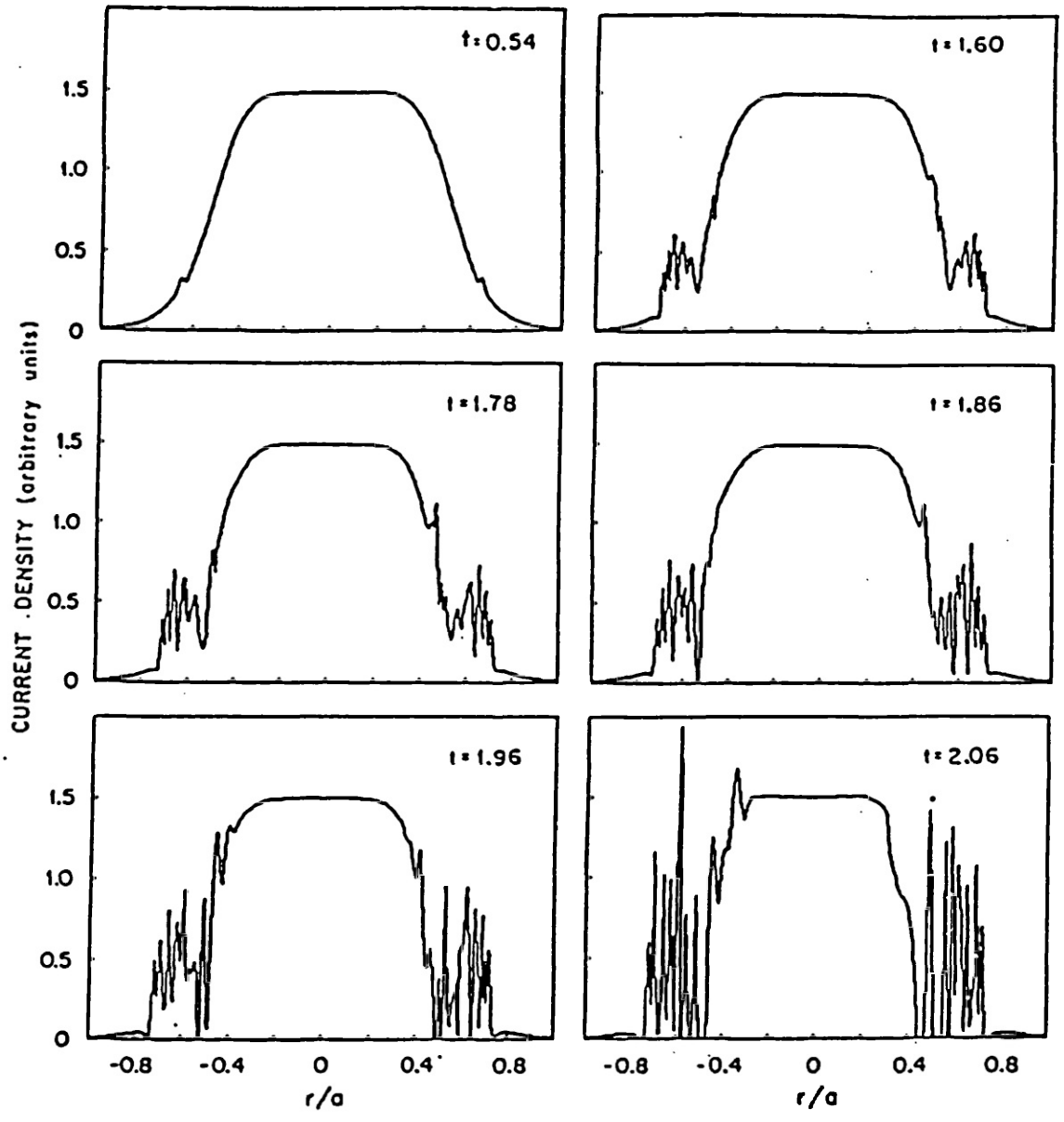

Fig.(2.4) *Toroidal current density illustrating the finescale current filamentation caused by the non-linearly generated modes. (Taken from Phys. Fluids, 23, 1811, (1980)).*

calculations where the resistivity was self-consistently evolved by virtue of solving an energy equation were no different from those where $\eta = \eta(r)$ only.

2.3 DISRUPTIONS CAUSED BY THE CATASTROPHIC GROWTH OF A SINGLE MODE : THE CATASTROPHE MODEL

The model described in this section has yet to become fully accepted by the community at large and its detailed exposition has yet to appear in the literature. For this reason, we shall discuss the model in greater detail than was the case for the Oak-Ridge model.

The model attempts to explain why a disruption occurs without perceptible change to the pre-existing conditions in the plasma rather than the fine details of how it proceeds. Strictly speaking, the catastrophe model and the Oak-Ridge model are not at variance since they are describing different aspects of the disruption.

In ref.(24), the magneto-static equations were solved in helical geometry, using standard tokamak ordering.[8] It was found that the equations admit no equilibrium solutions once a critical value of current was exceeded. In particular, by removing the conducting wall from the plasma edge, the width of the $m = 2$ island grew to large amplitude as $q(1)$ approached 2.

Further calculations were made in which the plasma profiles were self-consistently obtained, i.e. the evolution was time dependent.[25] Explicit throughout the model is the assumption that the system evolves at the resistive timescale. Once a state with a saturated magnetic island is attained, subsequent evolution will occur only in response to a change in the plasma profiles. Hence

the state of the plasma evolves through a series of diffuse equilibrium states. The evolution continues until a state is reached which is no longer arbitrarily close to a neighbouring equilibrium. A catastrophe occurs, characterised by rapid evolution of the profiles, which change in response to the explosive growth in the width of a single island (the m = 2). If this island can connect with the limiter and with an m = 1 island at the plasma core, thermal connection is made across the entire minor radius and hence confinement is lost.

The philosophy behind the model is to understand the parametric variation of the plasma behaviour rather than achieving completeness. For this reason, the model is particularly simple and 1-dimensional. The instabilities in the plasma affect the transport and in turn the transport affects the instabilities. The model calculates the interaction of transport and instability by solving the following set of equations :

$$\frac{\partial B_\theta}{\partial t}(r,t) = \frac{\partial E_z}{\partial r}(r,t) \qquad (2.3.1)$$

$$j_z(r,t) = \frac{1}{\mu_o}\frac{1}{r}\frac{\partial}{\partial r}(rB_\theta(r,t)) \qquad (2.3.2)$$

$$E_z(r,t) = \eta(T(r,t))j_z(r,t) \qquad (2.3.3)$$

$$\frac{\partial T}{\partial t}(r,t) = \frac{1}{3n}\left\{j_z E_z + \frac{1}{r}\frac{\partial}{\partial r}\left(r\kappa\frac{\partial T}{\partial r}\right)\right\} \qquad (2.3.4)$$

which are Faraday's Law, Ampere's Law, Ohm's Law and a simple energy equation. Note that Ohm's Law neglects fluid flow. This approximation

is questionable during the actual disruptive phase when the current is falling and when the effects of plasma inertia are likely to be important. The model is therefore unable to accurately describe the detailed dynamical interactions occurring during the turbulent phase of the disruption. The resistivity

$$\eta = a_s/T^{3/2} + \eta_1$$

where a_s is the Spitzer constant ($a_s = 2.8 \times 10^{-8}$ when T is measured in keV) and η_1 the effective impedance due to the presence of the m = 1 instability.

The m =1 mode is unstable when $q(o) < 1$.[26] Stability is restored whenever modification of the current density on axis causes $q(o) > 1$.[27] A simple description of this process is given[26] by assuming the poloidal flux before the instability,

$$B_{\theta i} = \frac{B_{zo} r}{R_o}\left(\frac{1}{q(o)} - \left(\frac{1}{q(o)} - 1\right)\left(\frac{r}{r_1}\right)^2\right)$$

is transformed by the instability to

$$B_{\theta f} = \frac{B_{zo} r}{R_o}\left(1 - \left\{\frac{1}{q(o)} - 1\right\}\left(\frac{r}{2r_1}\right)^2\right)$$

where r_1 is the radius of the q = 1 surface. Assuming the field redistributes in a time τ,

$$(B_{\theta f} - B_{\theta i})/\tau = \frac{\partial E_{eff}}{\partial r}$$

where E_{eff} is the effective electric field caused by the enhanced

resistivity η_1 :

$$E_{eff} = \eta_1 j_z$$

Assuming that $\eta_1 = 0$ for $r^2 > \frac{4}{3} r_1^2$,

$$\eta_1 j_z = \frac{B_{zo} r_1^2}{3R_o \tau q(o)} (1 - q(o)) \{1 - \frac{3}{4} (\frac{r}{r_1})^2\}^2$$

Averaging over the sawtooth time τ yields

$$\eta_1 = A (1 - q(o)) \{1 - \frac{3}{4} (\frac{r}{r_1})^2\}^2 \text{ for } r^2 < \frac{4}{3} r_1^2,$$

where A is chosen to keep q(o) sufficiently close to unity. This simple model of the m = 1 instability has the effect of flattening the current profile in the region where q = 1. Since q(o) is maintained at a value close to 1, the current will be restricted on axis.

The thermal conductivity in the energy equation (2.3.4) is assumed to have a constant background value κ_o except in the regions of instability where

$$\kappa = \kappa_o + \kappa_I (1 - (2x/w)^2)$$

where x is the distance from the magnetic island centre, w the width of the island and $\kappa_I >> \kappa_o$. Hence the temperature profile is flattened across the island region, consistent with the assumption that magnetic field lines are isothermal.

The combination of (2.3.1), (2.3.2) and (2.3.3) gives a parabolic equation for $B_\theta(r,t)$ which is solved by a fully implicit difference scheme. A new value of the current is calculated from (2.2.3) and used in the stability equation

$$\frac{1}{r}\frac{\partial}{\partial r}\left(r\frac{\partial \psi_{mn}}{\partial r}\right) - \frac{m^2}{r^2}\psi_{mn} - \frac{m\,\partial j_z/\partial r\;\psi_{mn}}{B_\theta(m-nq)} = 0 \qquad (2.3.5)$$

which is solved to calculate the perturbed field ψ_{mn} for each mode individually. Hence, a non-linear Δ', denoted by Δ^* can be calculated

$$\Delta^* = r_s \frac{\partial \ell n\ \psi_{mn}}{\partial r}\Bigg|_{r_s-\frac{1}{2}w}^{r_s+\frac{1}{2}w}$$

which is used to calculate the island growth rate

$$\frac{\partial w_{mn}}{\partial t} = 1.66\,\eta(r_s)\,\frac{\Delta^*(w_{mn})}{\mu_o\, r_s} \qquad (2.3.6).$$

Δ^* differs from the previously described Δ' for two reasons :

a) The position at which ψ'/ψ is calculated is at the island separatrix rather than in the limit as $w \to 0$.

b) The driving term (the third term of (2.3.5)) implicitly contains the effects that all the other unstable modes have on the axisymmetric profiles.

So,

$$J(w) = \frac{m\,\partial j_z/\partial r}{B_\theta(m-nq)}$$

is a function of w by virtue of the effect that the instability and transport have on the j_z and B_θ profiles.

It was stated in section 1.7 that Δ' was a decreasing function of w. In ref.(28) it was shown that the form of Δ^* is different from that of Δ', as can be seen by comparing figures (2.5) and (2.6).

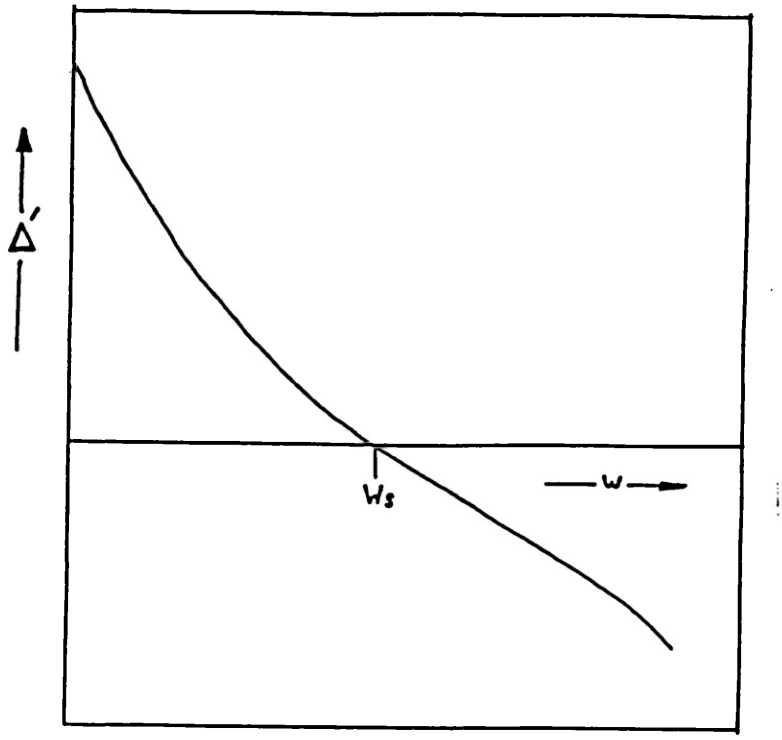

Fig.(2.5) *$\Delta'(w)$ vw. As an island grows, $\Delta'(w)$ decreases until $\Delta'(w_s) = 0$, giving the saturated island width w_s.*

Figure (2.6) shows that $\Delta^*(w) = 0$ has two solutions, w_1 and w_2. We shall see how the solutions of a simple analytic model for the form of Δ^* gives the catastrophic growth of a single mode as the plasma

conditions are slowly altered.

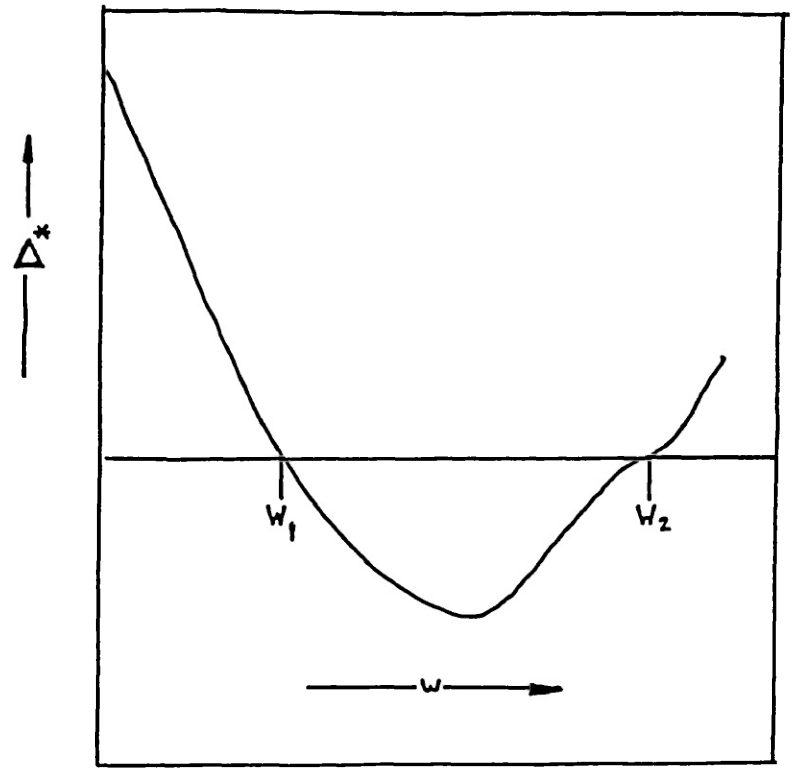

Fig.(2.6) *Δ*(w) vw. Two saturated island widths exist* w_1 *and* w_2.

Suppose, for the purpose of illustration

$$\Delta^*(w) = (w-w_1)(w-w_2)$$

Equation (2.3.6) becomes

$$\frac{1}{A}\frac{\partial w}{\partial t} = (w - B)^2 - C^2 \qquad (2.3.6)$$

where

$$A = 1.66\eta/\mu_o r_s$$

$$B = \tfrac{1}{2}(w_1 + w_2)$$

and

$$C = \tfrac{1}{2}(w_2 - w_1)$$

We have neglected the αw term in Rutherford's equation for island growth since α is small. Assuming that η = constant gives the simple solution

$$w(t) = \tfrac{1}{2}(w_1+w_2) + \tfrac{1}{2}(w_2-w_1)\,\frac{(1 + \beta \exp \gamma t)}{(1 - \beta \exp \gamma t)} \qquad (2.3.7)$$

where

$$\beta = \frac{(w_o - w_2)}{(w_o - w_1)}, \qquad \gamma = \frac{1.66\eta}{\mu_o r_s}$$

and $w_o = w(t = o)$.

Assume that $w_o < w_1 < w_2$, then $\beta > 1$ and (2.3.7) is bounded above by $w_1 \; \forall \; \gamma t > 0$. Hence,

$$\lim_{\gamma t \to \infty} w(t) = w_1$$

Consider now the case $w_1 < w_o < w_2$ for which $\beta < 0$ and (2.3.7) is bounded by $w_1 \; \forall \; \gamma t > 0$. Hence,

$$\lim_{\gamma t \to \infty} w(t) = w_1$$

The final case to consider is $w_1 < w_2 < w_o$ for which $o < \beta < 1$ and (2.3.7) is unbounded, the island attains an infinite width in a finite time, the time being

$$t = \frac{1}{\gamma} \ell n \frac{1}{\beta}$$

The evolution of the island in each of the three regimes is illustrated in fig.(2.7) clearly the state with w_1 is a stable equilibrium, whilst w_2 is unstable.

Now suppose that the global plasma conditions are slowly altered, causing the curve $\Delta^*(w)$ to move in the direction of increasing Δ^*. The stable solution w_1 will migrate towards the right in the diagram (2.6) and the unstable solution will migrate to the left. When $\Delta^*(w)$ touches the w-axis, the nature of the solution w(t) changes. Let

$$\Delta^*(w) = (w - w_c)^2 + \varepsilon^2 \qquad (2.3.8)$$

as illustrated in Fig.(2.8); w_c is the critical island width and ε a small parameter.

For the form of $\Delta^*(w)$ given by (2.3.8), the solution of (2.3.6) is

$$w(t) = w_c + (\varepsilon \tan \gamma t - w_c)/(1 + w_c/\varepsilon \tan \gamma t)$$

Hence for $\varepsilon > 0$, w(t) is unbounded. Indeed, the growth is *explosive* in the sense that the island width becomes infinite in a finite time, the

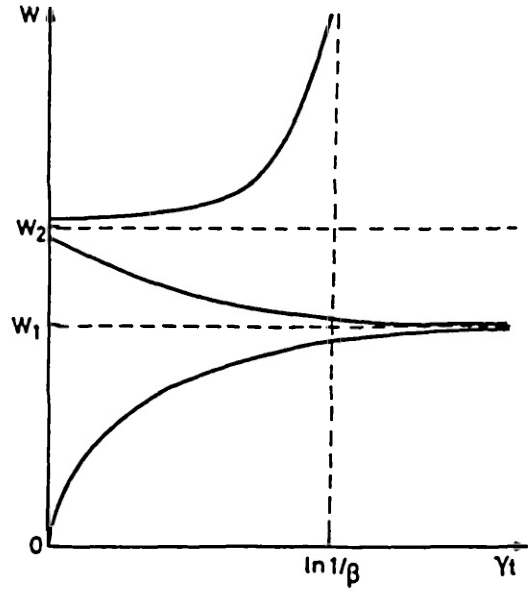

Fig.(2.7) Magnetic island width for a non-disruptive case.

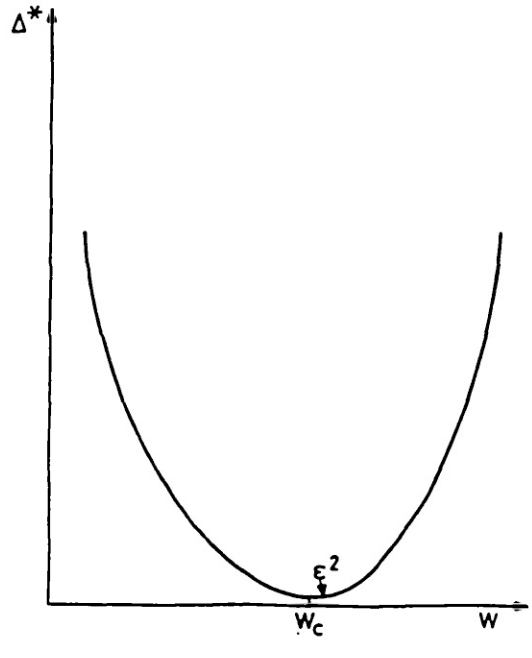

Fig.(2.8) Δ(w) v w for a disruptive case.*

time being

$$t_D = \frac{1}{\gamma}\{\pi - \tan^{-1} \epsilon/w_c\}$$

The island width as a function of time is shown in Fig.(2.9).

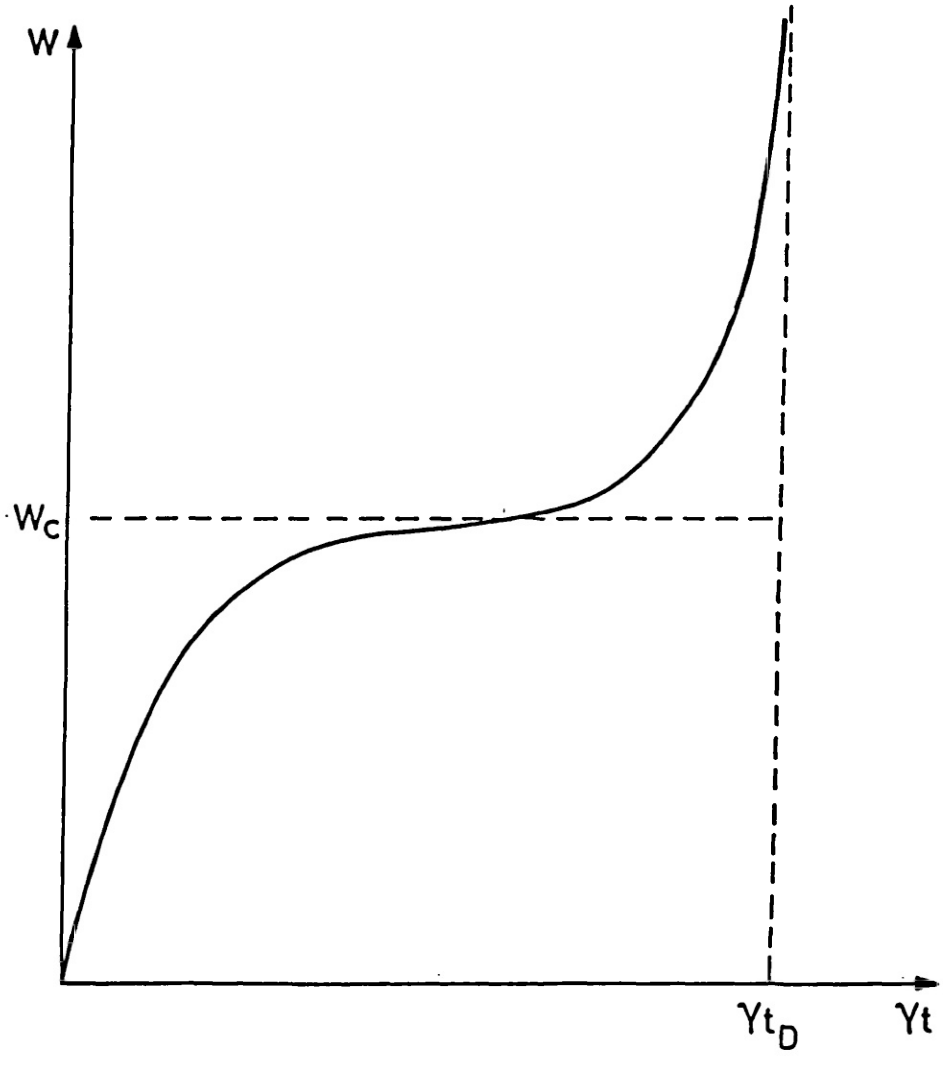

Fig.(2.9) Island width as a function time resulting from the form of Δ^* shown in Fig.(2.8).

The transition from the form of Δ^* shown in Fig.(2.6) to that in Fig.(2.8) forces the nature of the solution of (2.3.6) to change. The form of Δ^* allows the island to grow without bound; the subsequent interaction of the island with the profile and the constraints imposed on the plasma will govern precisely how the disruption will proceed. Typical constraints could be the restriction of the current on axis and a cold limiter at the plasma edge.

What the catastrophe model does not explain is how the disruption will proceed once triggered. What it does explain is why a small magnetic island can grow explosively after a lengthy period of quiescence. In this sense, it is able to describe why the $m = 2$ Mirnov oscillations undergo the transition from small to large amplitude as depicted in Fig.(1.2).

2.4 DISCUSSION

In sections 2.2 and 2.3, two models for disruptions were presented. In this section we discuss and criticise the models.

The catastrophe model shows how disruptions can occur without perceptible change to the global conditions within the plasma whilst the Oak-Ridge model describes the detailed dynamics of the disruption. Therefore the Oak-Ridge model does not describe *why* disruptions occur, but rather *how* they occur.

On one issue the two models are in conflict. Oak-Ridge demand that two tearing modes of different helicity be present in order to initiate a cascade to higher modes and thereby cause the field to become ergodic. The catastrophe model requires only one mode to be unstable, and a means of restricting (by sawtoothing) the amount

of current able to flow on axis. These conditions appear to be sufficient to cause $\Delta^*(w)$ to be concave upwards . The catastrophe model does not exclude the existence of modes other than the m = 2, rather it claims that the presence of other modes is not crucial in causing the disruption.

One of the most striking features of the Oak Ridge calculations is the finescale filaments on the current profile. It is claimed[23] that the filaments are not of numerical origin and tests have been performed using a different timestep and size of radial mesh. Each filament can be resolved over several mesh points, showing no evidence of the 'plus-minus' oscillations that characterise numerical instability.

From Fig.(2.3), it is clear that the filaments initially appear at time $t \approx 1.6 \times 10^{-3}\ \tau_R$. At time $t \approx 2.06 \times 10^{-3}\ \tau_R$ when the magnetic field is entirely ergodic within the overlap region, a typical current filament has grown such that $\Delta j/j \sim 1.6$. The spatial extent of a typical filament $\sim 1/22a$. Hence, estimating the time τ_D in which such a filament would resistively diffuse

$$\tau_D \sim (\eta k^2)^{-1} \sim (22a)^2/S \sim 0.48 \times 10^{-3}\ \tau_R$$

Note that τ_D is almost the same time as that for the growth of the filament, $\tau_g \sim (2.06\text{-}1.6) \times 10^{-3}\ \tau_R \approx 0.46 \times 10^{-3}\ \tau_R$. Therefore we could expect the filament to decay in the same time as it grew, assuming that the driving mechanism saturated at a finite amplitude after a finite time. Hence, if the calculation were to proceed for a similar length of time, the filaments could decay and the profile become smoothed. Assuming that the structures are not numerical in

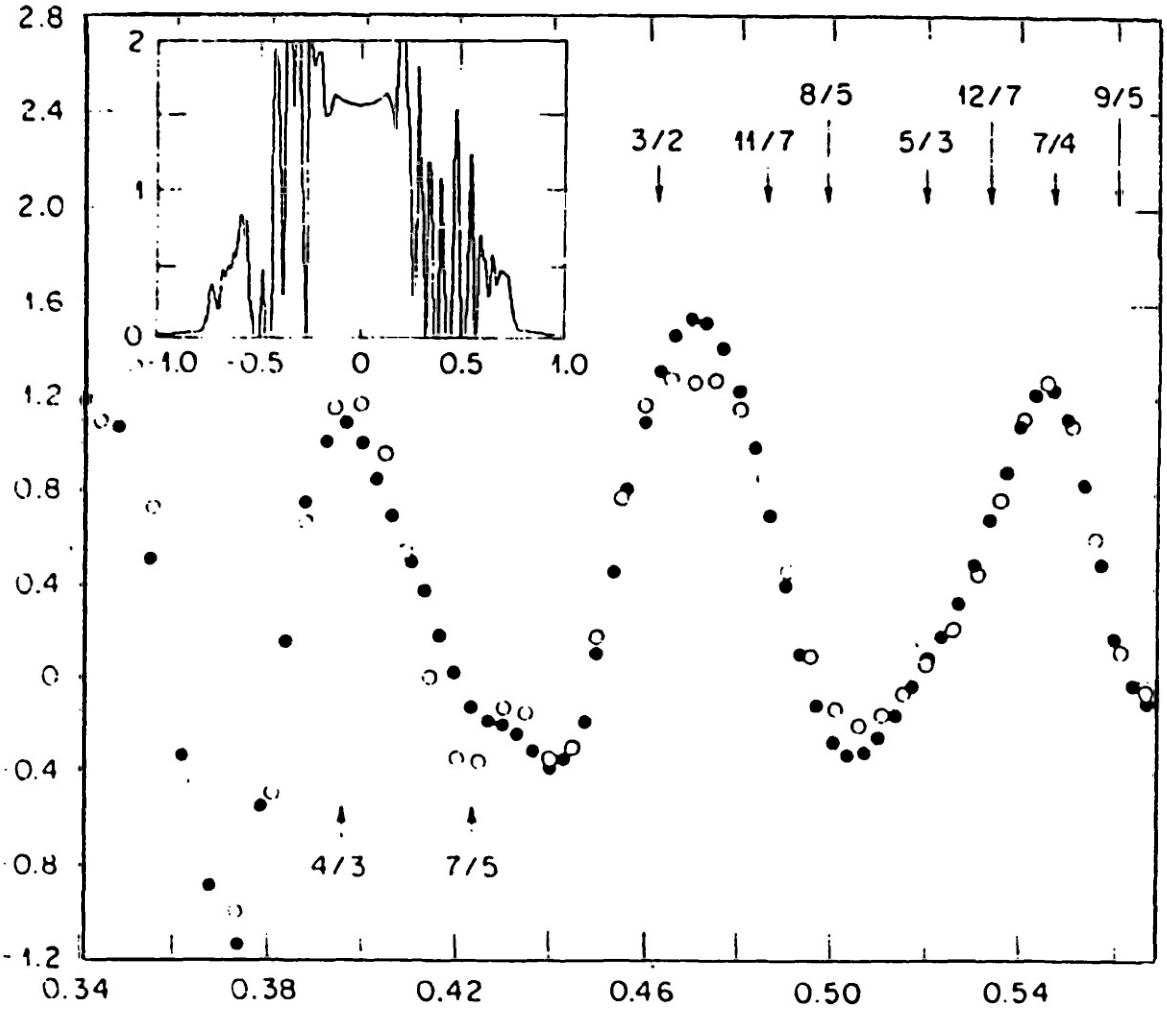

Fig.(2.10) *Expanded region showing the finescale current density oscillations.*

origin, this argument suggests that filaments could be transient. Unfortunately this hypothesis has not been tested by the Oak-Ridge group because RSF encounters numerical difficulties during the island overlap phase.[29]

It is not seriously doubted that overlapping magnetic islands destroy the flux surfaces within the overlap region, however, the fraction of the minor radius over which the field must be ergodic in order to cause a disruption is a moot point.

The Oak-Ridge calculations suggest that $\sim$ 45% of the minor radius covered with ergodic field is sufficient to cause the disruption. The catastrophe model has connection of the m = 1 and m = 2 islands across the *entire* minor radius, hence causing the central temperature to collapse. The temperature dependent calculations performed by Oak-Ridge[23], exhibit no such collapse of temperature on axis, indeed the flux surfaces within the central core (containing $\sim$ 70% of the total thermal energy) remain intact.

In section 1.6, it was stated that a perfectly conducting wall on the plasma suppresses the growth of islands in the outer regions. All the Oak-Ridge calculations have been performed with a conducting wall boundary condition $\phi(1,\theta,\zeta,t) = 0$. It is considered more realistic if the conducting wall were moved from the plasma edge, as in experiment.

We consider there to be three basic criticisms of the Oak-Ridge model :

1) the possible trans ience of the current filaments
2) the necessary degree of ergodic field line cover to constitute a disruption
3) the effect on stability of removing the conducting

wall from the plasma edge.

We shall examine each of these questions in subsequent chapters.

The catastrophe model requires two conditions appertaining to the nature of Δ^*, in order to cause a disruption :

1) Δ^* should be concave upwards

2) $\Delta^*(w) = 0$ has no solutions for real, positive values of w.

Numerical calculations[28] have vindicated both conjectures for all cases that have disrupted. Until a formal (analytical) proof is found, the model remains necessarily heuristic in nature.

CHAPTER III

3.1 INTRODUCTION

In this chapter we investigate two of the questions criticising the Oak-Ridge model in section 2.4. Specifically we shall examine points) and 3) in that discussion.

These points will be examined using the catastrophe model equations of section 2.3, thereby providing an independent test of the Oak-Ridge results. The results we present in this chapter will therefore be for a plasma where the effects of direct mode-coupling have been eliminated. The calculations should *not* be confused with the single-helicity calculations described in ref.(20) which have been compared with the directly coupled interaction results of ref.(23) (see Fig.(2.2)). Though the catastrophe model excludes direct coupling effects, a mode is able to interact with another via the deformation to the axisymmetric profiles. We shall therefore refer to the catastrophe interaction mechanism to be *quasi-linear* and the Oak-Ridge mechanism to be *non-linear* in order to differentiate between the two.

We show that many of the features ascribed to non-linear interaction are equally well explained by the quasi-linear interaction. Indeed we are able to retrieve most of the Oak-Ridge results barring one important feature; the quasi-linear calculations show none of the characteristic disruption signatures.

3.2 QUASI-LINEAR CALCULATION OF THE OAK-RIDGE DISRUPTION CASE

The calculation is initialised from a resistive equilibrium with q-profile parametrised according to (2.2.7) with $q(0) = 1.34$, $q(1) = 4.2$ and $\lambda = 3.24$. The q and current profiles are illustrated in Fig.(3.1). This profile is rather special since it is chosen by Oak-Ridge to be linearly unstable to both the 2/1 and 3/2 instabilities. Also, the resonant surfaces are close to each other, so the magnetic islands overlap after a short period of time has elapsed. Finally the current profile is flat close to the axis, even though $q(0) > 1$. The steep current gradient at the resonant surfaces implies that the free energy associated with the profile will be rapidly shed by the vigorous growth of magnetic islands.

The choice of such a profile is justified by fitting to an experimentally inferred profile in the PDX tokamak, prior to a disruption.[23] This does not imply that the particular profile is a necessary prerequisite for a disruption to ensue. Indeed, the evolution to a given profile is a function of the plasma current, transport *and* the degree of previous tearing mode activity. It is possible that the instability and transport processes required to evolve to the profile are untypical of usual plasma behaviour, and therefore the profile is pathological!

The calculation is performed using the TRINIO* computer code[30], which solves the equations of section 2.3. The values used for the various constants are typical of the DITE tokamak[31] and are listed below.

* TRansport and INstability Interaction in One dimension

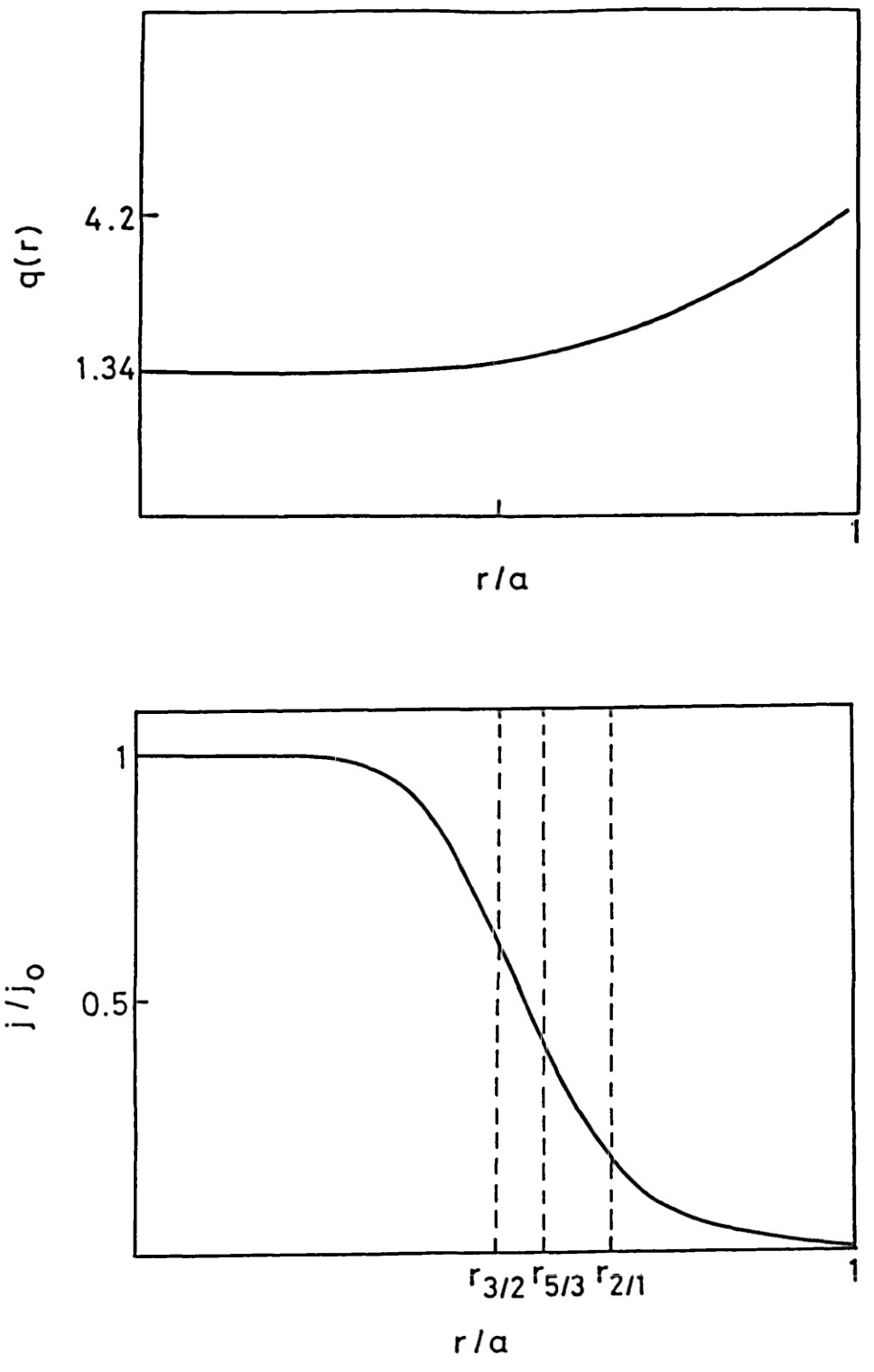

Fig.(3.1) Equilibrium current and safety-factor profiles used to initialise the calculation.

B_{zo}	1.34 T
a	0.26 m
R_o	1.17 m
n	3×10^{19} m^{-3}
Ko	$7 \times 10^{19} m^{-1} s^{-1}$
K_I	7×10^{21} $m^{-1} s^{-1}$
T(a)	10 eV

The initial resistivity profile satisfies $\eta(r) = \text{const.}/j_z(r)$ and the initial temperature profile is calculated from

$$\frac{a_s}{T^{3/2}} j^2 + \frac{K_o}{r} \frac{d}{dr} \left(r \frac{dT}{dr}\right) = 0$$

The boundary conditions used throughout the calculation are :

$$B_\theta(r=0,t) = 0, \qquad B_\theta(r=a,t) = \text{const.} \tag{3.2.1}$$

$$\frac{\partial T}{\partial r}(R=0,t) = 0, \qquad T(r=a,t) = \text{const.} \tag{3.2.2}$$

$$\frac{\partial E}{\partial r}(r=0,t) = 0 \tag{3.2.3}$$

The condition $B_\theta(r=a,t) = \text{const.}$ implies that the total plasma current is constant. The boundary conditions on the perturbed flux (radial component of magnetic field) are

$$\phi_{mn}(r=a,t) = 0 \tag{3.2.4}$$

and

$$\lim_{r\to 0} \phi_{mn}(r,t) = \text{const. } r^{m-1}, \qquad m > 1 \tag{3.2.5}$$

Boundary condition (3.2.4) implies a conducting wall on the plasma boundary, (3.2.5) is a consequence of the regularity of ψ at the magnetic axis.

The tearing modes monitored during the calculation are chosen in a rather ad hoc way, following the ordering method of ref.(22). A mode is characterised by the degree δ which it perturbs the axisymmetric component of the flux; choosing the 2/1 to be of order δ, and the 3/2 to be of order δ^2 gives the following ordering :

$0(0)$	0/0
$0(\delta)$	2/1
$0(\delta^2)$	3/2, 4/2
$0(\delta^3)$	5/3, 6/3, 1/1
$0(\delta^4)$	6/4, 8/4, 7/4, 4/3
.	
.	
.	

In general, the larger the poloidal mode number m, the more stable the mode will be. This is because the stabilising line bending term $-m^2\psi/r^2$ in (2.3.5) dominates at large values of m.

The 2/1 and 3/2 modes are linearly unstable and the 5/3 destabilised quasi-linearly. All other modes to order δ^4 inclusive are close to marginal stability/instability and do not affect the result significantly.

Fig.(3.2) shows the magnetic island widths of the 2/1, 3/2 and

5/3 modes plotted as functions of time at their respective positions within the plasma.

Note that the magnetic island evolution is remarkably similar to the RSF result (Fig.(2.1)). The rapid growth of the 5/3 mode at $t \sim 0.1$ ms and the increased growth of the 3/2 mode at $t \sim 0.2$ ms should be compared with similar events at times $t = 1.3 \times 10^{-3}\ \tau_R$ and $t = 1.9 \times 10^{-3}\ \tau_R$ in Fig.(2.1).

The final result of the two calculations is however, very different. The RSF calculation stops soon after the 5/3 and 3/2 islands touch. At this instant, the current profile exhibits the finescale filamentary structures described in section 2.2, and the complex numerics of the code prevent the calculation continuing at a realistic rate.[29] The fraction of the minor radius covered by islands is $\sim$ 46% centred about $r = 0.5a$. Therefore, within the annular region $0.3 \lesssim r/a \lesssim 0.76$, the magnetic field is expected to be ergodic. The TRINIO calculation continues after the 5/3 and 3/2 modes have touched. Indeed, the 5/3 island decays, leaving the 2/1 and 3/2 islands spanning $\sim$ 36% of the minor radius, centred about $r = 0.55a$. No characteristic disruption signatures occur and confinement within the central core is maintained. As for the temperature dependent calculations performed with a version of RSF[23], the core contains $\sim$ 70% of the total thermal energy of the plasma. Only a fraction ($\lesssim$ 5%) of the original energy within the core is transported out by the islands, indeed the central temperature increases slightly during the period of overlap!

Fig.(3.3) shows the temperature and current profiles at the time of maximum magnetic island cover ($t = 0.42$ ms). The overlap region is clearly visible by the plateau on the temperature profile.

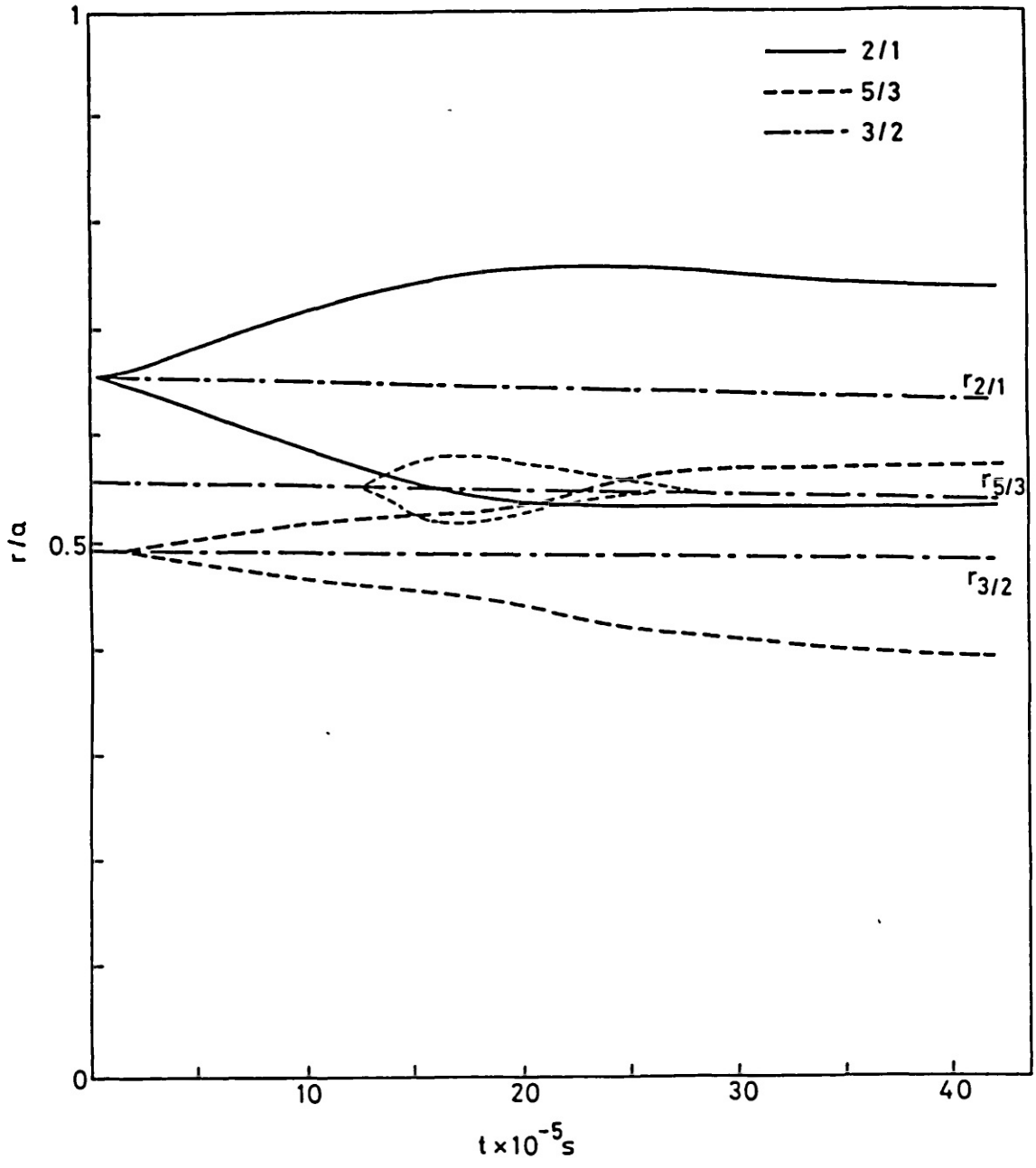

Fig.(3.2) Magnetic island widths for the 2/1, 3/2 and 5/3 modes plotted as functions of time.

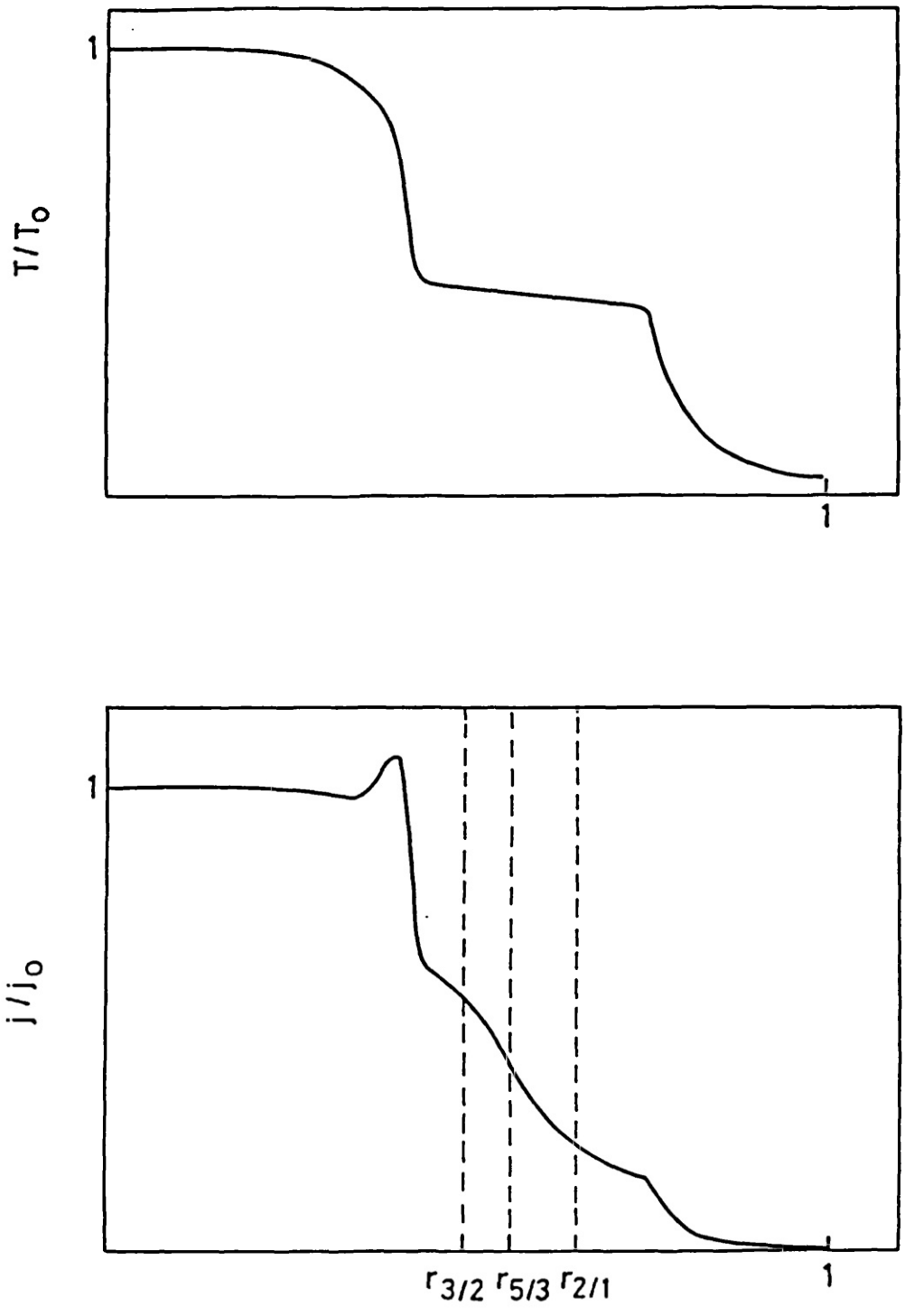

Fig.(3.3) *Quasi-linear current and temperature profiles at t = 0.4 2 ms. Island overlap region is clearly visible.*

The evolution continues further, with the 3/2 island decaying completely, leaving a small saturated 2/1 island spanning 11% of the minor radius. This state is shown in Fig.(3.4) and is an equilibrium state with Ohmic heating balanced by thermal conduction losses.

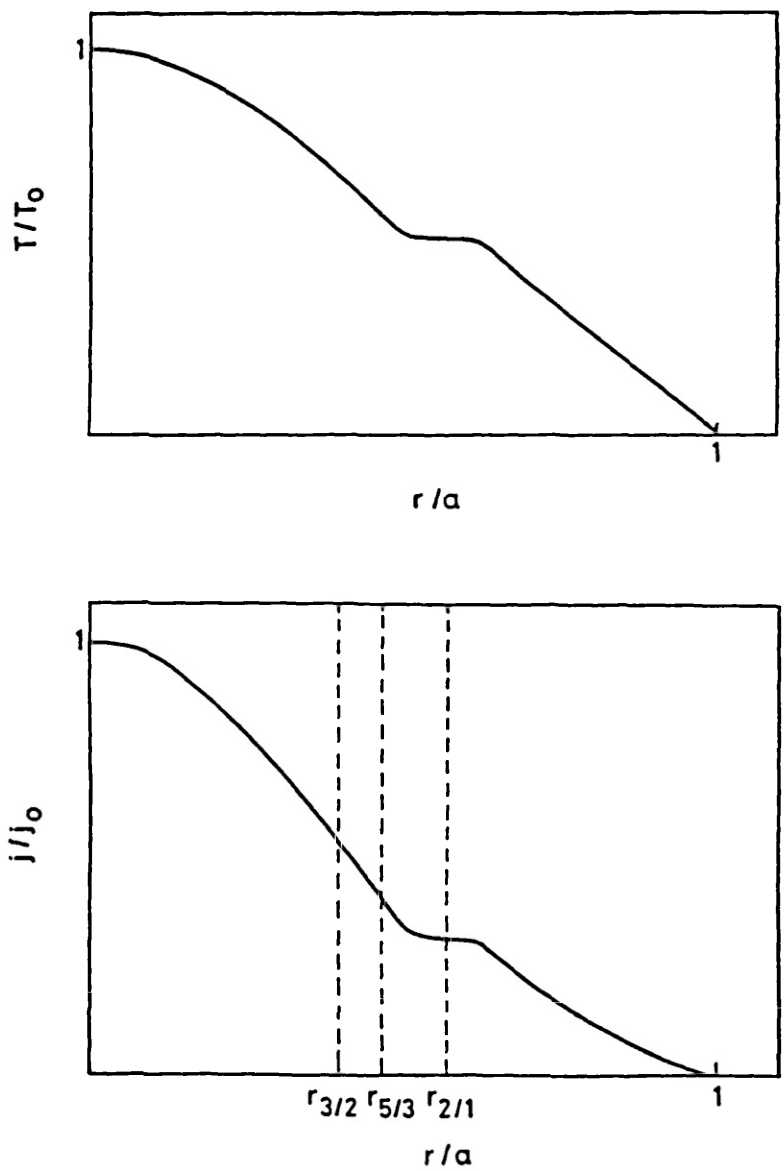

Fig.(3.4) Saturated state with Ohmic heating balanced by thermal conduction. The saturated 2/1 island covers 11% of the minor radius.

Fig.(3.5) shows the growth rates of the 5/3, 3/2 and 2/1 modes as calculated from Rutherford's work :

$$\frac{\partial w_{mn}}{\partial t} = 1.66 \frac{\eta(T(r_{mn}))\Delta^*(w_{mn})}{\mu_o r_{mn}} \qquad (3.2.6)$$

where r_{mn} is the resonant surface of the mode m/n. Note the similarity of this figure with the full, non-linear result illustrated in Fig.(2.2). The 5/3 growth rate, γ_{53} shows the same characteristic increase and the peak in γ_{32} follows that of γ_{53}; γ_{21} decreases monotonically in each calculation.

Clearly it is necessary to understand how the features in Fig.(3.5) can be understood in terms of quasi-linear theory alone and the functional dependence in (3.2.6) affords a valuable clue. The growth rate can change due to the complicated dependence of Δ^* on w, and thereby on the shape of the current profile. It can also change due to the dependence of η on T and by implication, $\dot{w}$. Finally, γ can change due to the movement of the resonant surfaces r_{mn}, however, this effect can be neglected by comparing the positions of each surface in Fig.(3.1).

When the 5/3 and 2/1 islands touch at t = 0.13 ms, the temperature across the combined width equalises, cooling r_{53} and therefore making the plasma locally more resistive. Hence the growth rate γ_{53} rises sharply.

The peak in γ_{32} is triggered by the large 2/1 island reducing the stabilising current gradient in $r_{32} < r < 1$. Consequently Δ^*_{32} increases causing γ_{32} to rise. The discontinuity in γ_{53} and γ_{21} at t = 0.15 ms is due to the combined 2/1, 5/3 island touching the 3/2.

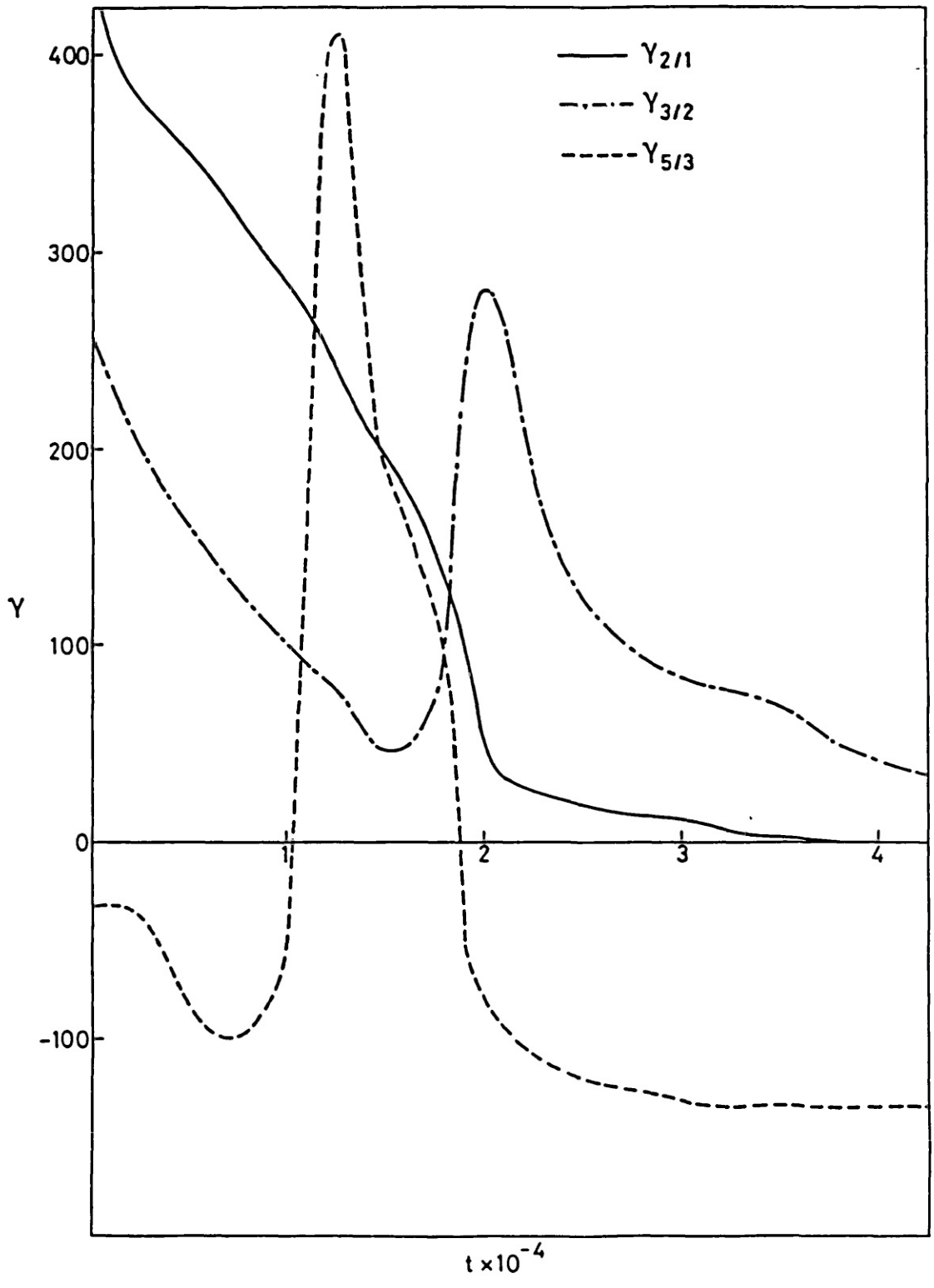

Fig.(3.5) *Growth rates of the 2/1, 3/2 and 5/3 modes as calculated from Rutherford.*

This lowers the temperature at r_{32} and hence amplifies γ_{32}, but the temperature at r_{21} and r_{53} increases slightly, thereby slowing rate at which γ_{21} and γ_{53} fall. The final temperature of the combined island is a suitably weighted mean of the temperatures before they touched, i.e.

$$T_f \approx (w_{32}\, T_{32} + w_{21}\, T_{21})/(w_{32} + w_{21})$$

Hence, by simple analysis of the interaction of magnetic islands with the temperature and current profiles, it has proved possible to explain the details of the island overlap process without appealing to the direct mode-coupling mechanism.

3.3 THE EFFECT OF REMOVING THE CONDUCTING WALL

The calculations of refs.(21) and (23) have used a plasma on wall boundary condition. In order to follow these calculations as closely as possible, the same boundary condition was used in the calculation described in section 3.2. However, from the discussion of section 1.6 and refs.(8) and (24), the position of the wall with respect to the plasma edge affects the stability.

The boundary condition on ϕ for a free boundary plasma can be found by investigating the nature of the solutions to (2.3.5) in a vacuum or cold plasma region where $j' \approx 0$. Assuming that the wall is removed to infinity so that ϕ does not match onto the fields produced by wall currents, (2.3.5) becomes

$$\frac{1}{r}\frac{\partial}{\partial r}\left(r\frac{\partial \phi}{\partial r}\right) - \frac{m^2}{r^2}\phi = 0$$

in the vacuum region.

For bounded solutions ϕ, we find

$$\phi'(a) = \frac{-m\,\phi(a)}{a} \qquad (3.3.1)$$

or

$$B_r'(a) = -(m+1)\frac{B_r(a)}{a}$$

which can be used to solve (2.3.5) for $r\in[o,a]$.

Another calculation with identical initial conditions as for those described in section 3.2 was performed with the wall radius b = 40a. The result was insignificantly different from the previous wall on plasma case. This is chiefly because r_{21} is embedded deep within the plasma (r_{21} = 0.66a) and consequently the magnitude of the perturbed field at the plasma surface is small. As the resonant surface moves toward the edge, the effect of the free boundary becomes more pronounced and the resulting magnetic island will be larger.

In order to access the importance of the wall, another case was considered using TRINIO. The initial profile used identical parametrisation, but with values :

$$\lambda = 4.0$$

$$q(0) = 1.08$$

$$q(1) = 3.0$$

for which r_{21} = 0.81a and r_{32} = 0.68a. It is claimed[23] that this

profile also disrupts, though the effects of mode coupling are weaker. First, a conducting boundary test case was performed in order to compare with the RSF result. The behaviour is similar to that described in section 3.2. The wall saturates the 2/1 island width at a smaller amplitude than before ($w_{21}^{sat} = 0.15a$). The 5/3 mode is close to marginal stability and plays an insignificant role. Again, no evidence of disruption characteristics are observed to occur.

The removal of the wall leads to a dramatically different result. The 2/1 island is able to intersect the limiter (at $r = a$), thereby cooling the outer region of the plasma. The overlapping island region spans $\sim 40\%$ of the minor radius, though confinement within the core is maintained. Again, the calculation could not be construed as being a disruption, since the central temperature did not fall, however, the results were significantly different from the wall on plasma case. For this reason, all subsequent calculations performed with TRINIO will employ the boundary condition (3.3.1).

3.4 SUMMARY AND DISCUSSION

In this chapter, results from a simple 1-D recalculation of the Oak-Ridge disruption case have been presented. Many of the features of the non-linear calculation have been retrieved by the use of quasi-linear theory alone. The two calculations differ on one crucial aspect, namely, the quasi-linear calculation shows none of the signatures of a disruption. Furthermore, the position of the conducting wall in relation to the plasma periphery is crucial. The wall on plasma boundary condition $\psi(r=a,t) = 0$ is inappropriate, not only because it is an unrealistic approximation to what occurs in experiment, but also because removal of the wall significantly

destabilises the plasma.

At the beginning of this chapter, the stated aim was to investigate two specific questions. The first was apropos the degree of ergodic field line cover necessary to constitute a disruption. Our calculation failed to disrupt, even though many of the features in the calculation were common to those obtained with RSF. Hence, we conclude that overlapping islands covering 36% of the minor radius is insufficient island cover to constitute a disruption. Increasing the island width to 46% of the minor radius decreases the thermal energy content within the core by $\lesssim$ 8% which again is insufficient to cause an energy quench.

The second question concerned the position of the conducting wall. A recalculation of the case considered in section 3.2 with the wall at (effectively) infinity gave a similar result. However, as the resonant surface of the 2/1 mode moves closer to the edge of the plasma, the island grew to a larger amplitude. We therefore conclude that a wall off plasma boundary condition serves as a useful upper bound of the stability in the outer regions.

The results of this chapter suggest that many of the effects previously ascribed as being due to direct mode-coupling mechanisms can be interpreted by quasi-linear theory alone. This does not imply that mode-coupling can be entirely discounted, rather that the effects which were exclusively attributed to mode coupling can be explained otherwise. The results also suggest that the overlap phase need not be a physical barrier, and that the evolution can continue thereafter.

One further question regarding the RSF calculations must be considered, namely the permanence of the current filaments at large

times. No solution of the reduced equations, using RSF, has been found at large times because the code encounters numerical difficulties.[29] We therefore consider it a necessary and instructive exercise to investigate the numerical stability properties of the RSF difference scheme. The results from this analysis are described in Chapter IV.

CHAPTER IV

4.1 INTRODUCTION

In this chapter, the numerical stability properties of the RSF difference scheme is analysed. We show that the numerical stability behaves in a rather subtle way once the non-linear regime has been entered. This casts doubt on the accuracy of the published solutions of the reduced equations, especially during the island overlap phase of the evolution. A new stability criterion is derived heuristically and comparisons are made between runs where this criterion has been implemented and runs where the Oak-Ridge criterion has been used.

4.2 DISCUSSION OF THE NUMERICAL STABILITY OF RSF

Before proceeding we should make clear that the finite difference algorithm used in RSF is *not* the algorithm that appears in the published literature.[22] However, since the alterations only affect the streaming properties of the system, and our stability analysis assumes no first order flows to be present, the final stability criterion remains unchanged from the published one! The *analysis for* the published algorithm is given in ref.(35).

RSF is a spectral code using direct convolution methods to represent toroidal and poloidal derivatives. A second order accurate finite difference scheme is used to represent the radial derivatives.

The algebraic equations to be solved in advancing the system from time t to t + Δt are as follows :

$$u^{t+\frac{1}{2}\Delta t} = u^t + \tfrac{1}{2}\,\Delta t\, S_u^t \tag{4.2.1}$$

$$\phi^{t+\frac{1}{2}\Delta t} = \phi^t + \tfrac{1}{2}\,\Delta t\, S_\phi^t \tag{4.2.2}$$

$$u^{t+\Delta t} = u^t + \Delta t\, S_u^{\,t+\frac{1}{2}\Delta t} \tag{4.2.3}$$

and

$$\phi^{t+\Delta t} = \phi^t + \Delta t\, S_\phi^{\,t+\frac{1}{2}\Delta t} \tag{4.2.4}$$

where

$$S_u = -\underline{v}.\nabla u + S^2\{(\nabla\phi\wedge\nabla j_z).\hat{\underline{z}} - \frac{\partial j_z}{\partial z}\} \tag{4.2.5}$$

and

$$S_\phi = -\underline{v}.\nabla\phi + \eta j_z - \frac{\partial\varphi}{\partial z} \tag{4.2.6}$$

Note that in (4.2.2), the current and advection terms are treated implicitly, while in (4.2.4) the same terms are treated explicitly. The vorticity equation is treated explicitly at each half-timestep.

The published numerical stability criterion[22] demands that

$$\Delta t < 2/S\max|m - nq(r)| \tag{4.2.7}$$

if the scheme is to be stable. The denominator is calculated over all m/n pairs and for all values of q(r). This criterion is remarkable since it is independent of the radial mesh size and therefore is far

less stringent than the corresponding CFL[33] limit. It is claimed that a particularly fine radial mesh combined with a comparatively large timestep may be used, enabling calculations with large values of $S \sim 10^6$, to be economically performed.

Due to the unique nature of the stability criterion (4.2.7), it was considered both necessary and instructive to repeat the analysis. However, we find that the criterion is valid for axisymmetric, untorn configurations i.e. for the first timestep only!

4.3 NUMERICAL STABILITY ANALYSIS OF RSF

We perform the analysis in simple slab geometry and assume that the y-direction corresponds to the radial direction, and that x and z correspond to the poloidal and toroidal directions respectively. The equilibrium magnetic flux function $\psi = \psi_o(y)$ only, to which is added a perturbation $\tilde{\psi}$, so that :

$$\psi(x,y,z,t) = \psi_o(y) + \tilde{\psi}(y,t) \exp i(k_x x + k_z z) \qquad (4.3.1)$$

where $|\tilde{\psi}| << |\psi_o|$. We assume $\psi_o'(y)$ = constant, thereby eliminating the effects of shear, but making the analysis tractable. Finally we assume that there is no zero-order flow, so the stream function is

$$\varphi(x,y,z,t) = \tilde{\varphi}(y,t) \exp i(k_x x + k_z z) \qquad (4.3.2).$$

Linearising the reduced equations (2.2.1) and (2.2.2) about the equilibrium gives

$$\frac{\partial \tilde{\psi}}{\partial t} = -\tilde{v}_x \psi_o' + \eta \tilde{j} \qquad (4.3.3)$$

$$\frac{\partial \tilde{u}}{\partial t} = - S^2(\phi_o' \frac{\partial \tilde{j}}{\partial y}) \qquad (4.3.4)$$

where primes denote differentiation w.r.t. y.

The first term of the RHS of (4.3.3) is the advection of the first-order axisymmetric component of the flux and the second term gives the resistive damping. The term on the RHS of (4.3.4) is the first order $\underline{j} \wedge \underline{B}$ term, the advection of vorticity first appears to second order.

Writing the finite-difference approximations of $\partial/\partial y$ and $\partial^2/\partial y^2$ as[34]

$$\frac{\partial}{\partial y} = \frac{i}{\Delta y} \sin k_y \Delta y$$

$$\frac{\partial^2}{\partial y^2} = - \frac{4}{\Delta y^2} \sin^2 (\frac{k_y \Delta y}{2})$$

and noting that $v_x = \tilde{\varphi}'$, (4.3.3) and (4.3.4) become

$$\frac{\partial \psi}{\partial t} = - i\alpha\varphi - \beta\psi \qquad (4.3.5)$$

and

$$\frac{\partial \varphi}{\partial t} = - i(S^2 \alpha)\psi \qquad (4.3.6)$$

where we have dropped the tildes and

$$\alpha = \frac{\phi_o'}{\Delta y} \sin k_y \Delta y = (\underline{K} . \underline{B}_o)$$

$$\beta = \frac{4\eta}{\Delta y^2} \sin^2 (\frac{k_y \Delta y}{2}) = K_\perp^2 \eta$$

The qualities K and $K_\perp^2$ are the Fourier transforms of the finite differenced $\underline{\nabla}$ and ∇^2 operators. Equation (4.3.4) integrates trivially to give (4.3.6) for the zero flow initial conditions.

We now time difference (4.3.5) and (4.3.6) according to the scheme (4.2.1) - (4.2.4) :

$$\phi^{t+\frac{1}{2}\Delta t} = \phi^t - \tfrac{1}{2}\Delta t(i\alpha\varphi^{t+\frac{1}{2}\Delta t} + \beta\phi^{t+\frac{1}{2}\Delta t})$$

$$\varphi^{t+\frac{1}{2}\Delta t} = \varphi^t - \tfrac{1}{2}\Delta t\ (iS^2\alpha)\phi^t$$

$$\phi^{t+\Delta t} = \phi^t - \Delta t(i\alpha\varphi^{t+\frac{1}{2}\Delta t} + \beta\phi^{t+\frac{1}{2}\Delta t})$$

$$\varphi^{t+\Delta t} = \varphi^t - \Delta t(iS^2\alpha)\phi^{t+\frac{1}{2}\Delta t}$$

which after a little algebra reduces to the matrix equation

$$\begin{bmatrix}\phi\\ \varphi\end{bmatrix}^{t+\Delta t} = \underline{\underline{\Lambda}}(K,k_\perp^2)\begin{bmatrix}\phi\\ \varphi\end{bmatrix}^{t}$$

where $\underline{\underline{\Lambda}}$ is the *amplification* matrix, and is given by :

$$\underline{\underline{\Lambda}}(K,k_\perp^2) = \frac{1}{(1+\frac{1}{2}\beta\Delta t)}\begin{pmatrix} 1-\frac{1}{2}\beta\Delta t-\frac{1}{2}(\alpha S\Delta t)^2 & -i\alpha\Delta t \\ -i\alpha S^2\Delta t(1-\frac{1}{4}(\alpha S\Delta t)^2) & 1+\frac{1}{2}\beta\Delta t-\frac{1}{2}(\alpha S\Delta t)^2\end{pmatrix}$$

$$= \begin{pmatrix} A & B \\ C & D\end{pmatrix} \qquad (4.3.7)$$

defining the functions A, B, C and D.

Information regarding the dispersion of the system can be found by solving the equation

$$\det(\underline{\underline{\Lambda}} - \lambda \underline{\underline{I}}) = 0 \qquad (4.3.8)$$

where $\lambda = \exp(-i\Omega\Delta t)$ is the eigenvalue of $\underline{\underline{\Lambda}}$. From this, the numerical stability criterion can be calculated by demanding that

$$\lambda\lambda^* \leq 1 \qquad (4.3.9)$$

where λ^* is the complex conjugate of λ. The eigenvalues of $\underline{\underline{\Lambda}}$ are the solutions of the simple quadratic equation

$$\lambda^2 + b\lambda + c = 0 \qquad (4.3.10)$$

where

$$b = -(A + D)$$

and

$$c = (AD - BC).$$

In solving (4.3.10) we need to consider two cases, depending on whether the discriminant is positive or negative.

Case I : $b^2 - 4c < 0$

For this case $\lambda \in \mathbb{C}$ and the criterion (4.3.9) reduces to

$$\lambda\lambda^* = c \leq 1$$

for stability. Hence

$$\frac{1 - \frac{1}{2}\eta K_\perp^2 \Delta t^2}{1 + \frac{1}{2}\eta K_\perp^2 \Delta t^2} \leq 1$$

which is trivially satisfied for all $K_\perp$ and $\Delta t \in \mathbb{R}$.

Case II : $b^2 - 4c \geq 0$

For this case, $\lambda \in \mathbb{R}$ and the criterion (4.3.9) becomes

$$1 + c \leq |b|$$

or

$$2 \geq |2 - (S\underline{K}.\underline{B}_o \Delta t)^2|$$

hence the result

$$\Delta t \leq 2/S(\underline{K}.\underline{B}_o) \qquad (4.3.11)$$

which is instantly recognisable as the slab analogue of the published stability criterion (4.2.7).

Since $\underline{B}_o$ is the axisymmetric component of the magnetic field, the criterion (4.3.11) when applied to the cylinder is valid for

circularly symmetric field structures only, i.e. for untorn configurations. As soon as the flux surfaces tear apart, the denominator of (4.3.11) should include the full magnetic field $\underline{B} = \underline{B}_o + \tilde{\underline{B}}$. This introduces a radial component into the equation which is dependent on the number of radial mesh points through the K_r term. Separating the axisymmetric components of the field from the non-linear components caused by the growth of the magnetic island :

$$\underline{K}.\underline{B} = K_r \tilde{B}_r + \frac{m}{r} \tilde{B}_\theta + (m - nq(r)) .$$

Now,

$$\tilde{B}_r = \frac{m}{r} \phi_{mn}(r)$$

and

$$\tilde{B}_\theta = - \frac{\partial \phi_{mn}}{\partial r} \sim \frac{\Delta \phi_{mn}}{\Delta r} \sim \Delta \phi_{mn} \, N_m / a$$

where N_m is the number of mesh points in the radial direction. Since ϕ is a smooth and continuous function, $\Delta\phi(r) << \phi(r)$ so that $\tilde{B}_r >> \tilde{B}_\theta$. So,

$$\underline{K}.\underline{B} \approx K_r \tilde{B}_r + (m - nq(r))$$

$$\sim m \frac{N_m}{r} \phi_{mn}(r) + \{m - nq(r)\} \qquad (4.3.12)$$

Since $(m - nq) \sim 0(1)$, equation (4.3.12) is dominated by the first term which is dependent on the number of radial mesh points (the Oak-

Ridge calculations have used $N_m \sim 200\text{-}300$).

The effect of the B_r term can be interpreted as an effective tilting of the magnetic flux surfaces with respect to the radial mesh. Initially, the untorn axisymmetric equilibrium has flux surfaces level with concentric surfaces of constant radius (i.e. y). As magnetic islands grow, the flux surfaces no longer remain aligned with the mesh, but tilt with respect to each other, see Fig.(4.1).

If the angle δ measures the inclination of the flux surfaces with respect to the (invariant) mesh and B is the strength of the perturbed field perpendicular to the z-direction, then

$$(\tilde{B}_r,\ \tilde{B}_\theta,\ B_z) \sim (B \sin\delta,\ B\cos\delta,\ B_z)$$

and so

$$\underline{K}.\underline{B} \approx (K_y \sin\delta + k_x \cos\delta)/q - n$$

$$\approx \left(\frac{\sin k_y \Delta y}{\Delta y} \sin\delta + m\cos\delta\right)/q - n$$

hence

$$(\underline{K}.\underline{B}) \approx (N_m \sin 2\theta \sin\delta + m\cos\delta)/q - n \qquad (4.3.13)$$

$$2\theta = k_y/N_m = \pi p/N_m$$

where p is an integer. Note, if $\delta = 0$ the unperturbed value of $\underline{K}.\underline{B}$ is retrieved.

By similar argument,

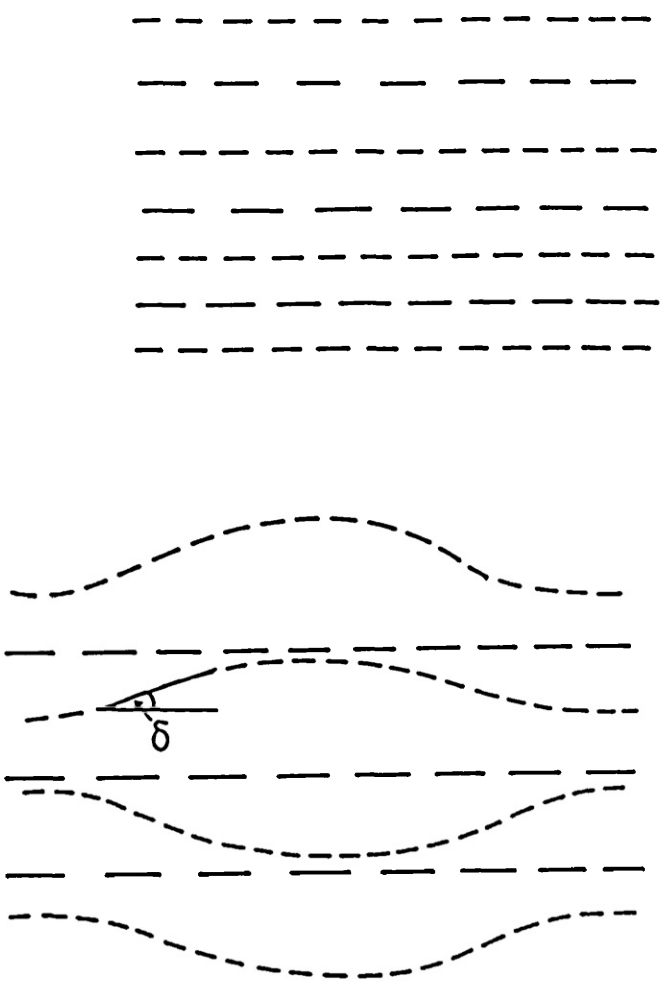

Fig.(4.1) Illustrating the effect of the flux surfaces (dotted lines) initially level with the mesh (hatched lines), tilting with respect to each other as the island forms.

$$\eta K_{\perp}^{2} = \eta(4 N_{m}^{2} \sin^{2}\theta + m^{2}) \qquad (4.3.14)$$

Thereby, the parametrisation of $\underline{K}.\underline{B}$ and $\eta K_{\perp}^{2}$ by k_y is by virtue of the parameter θ.

Define

$$g = S(\underline{K}.\underline{B})/2\Delta t$$

and

$$\alpha = \eta K_{\perp}^{2}$$

where g is a measure of the normalised inverse Alfvén time and α is a measure of the inverse resistive damping time. Clearly

$$g = g(S, \delta, \Delta t, N_m, \theta)$$

and

$$\alpha = \alpha(S, N_m, \theta)$$

so by plotting g against α for fixed values of S, N_m, and Δt whilst varying δ and θ gives a sequence of operating curves. If, for any value of θ, the curve in the g-α plane exceeds the stability limit g = 1, then the wave numbers characterised by those values of θ will be numerically unstable. See Fig.(4.2).

The first mode to exceed the stability boundary can be found by calculating the first mode k_c to touch the curve g = 1, i.e. when

$$\frac{dg}{d\alpha} = \frac{\partial g}{\partial K}\frac{\partial K}{\partial \alpha} = 0 \qquad (4.3.15).$$

Equation (4.3.15) is satisfied when

1) $\sin \delta = 0$ i.e. when there are no magnetic islands

2) $\cot 2\theta = 0$ i.e. when $k_c = \frac{1}{2}\pi N_m$.

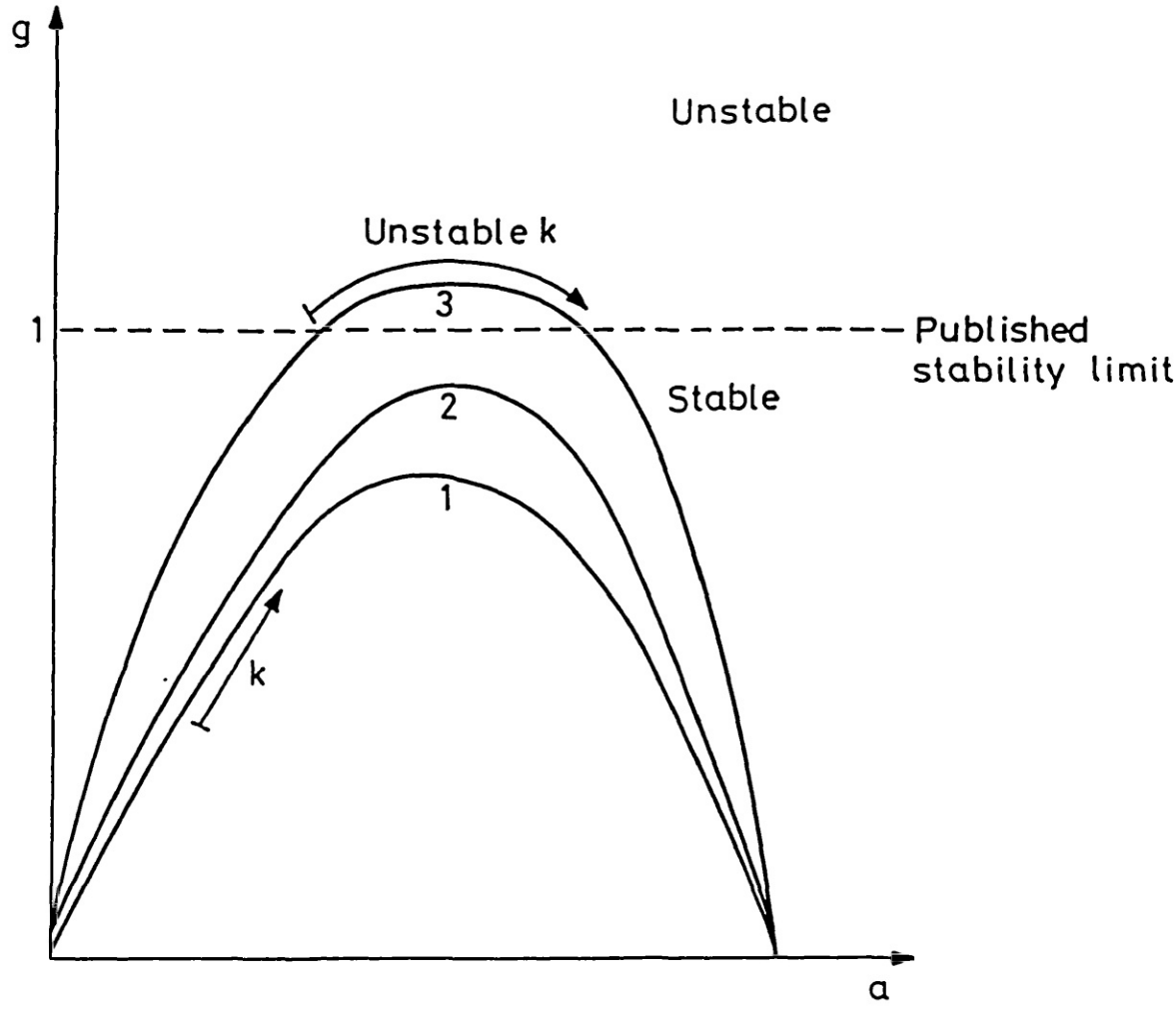

Fig.(4.2) Operating curves in the g-α plane, curves 1, 2 and 3 are for successively larger values of δ. For a critical angle, the curve touches the stability boundary g = 1. All K for which the curve exceeds g = 1 will be numerically unstable.

Therefore, an upper bound for the full stability criterion is

$$\tilde{g} = \frac{S}{2\Delta t}\left\{ \tfrac{1}{2}\pi N_m \max \left| m - \frac{\phi_{mn}(r)}{r} \right| + \max\,(m - nq(r)) \right\} \leq 1 \qquad (4.3.16).$$

Figure (4.3) shows how the stable values of Δt, normalised to the previously published result varies with magnetic island width, i.e. δ.

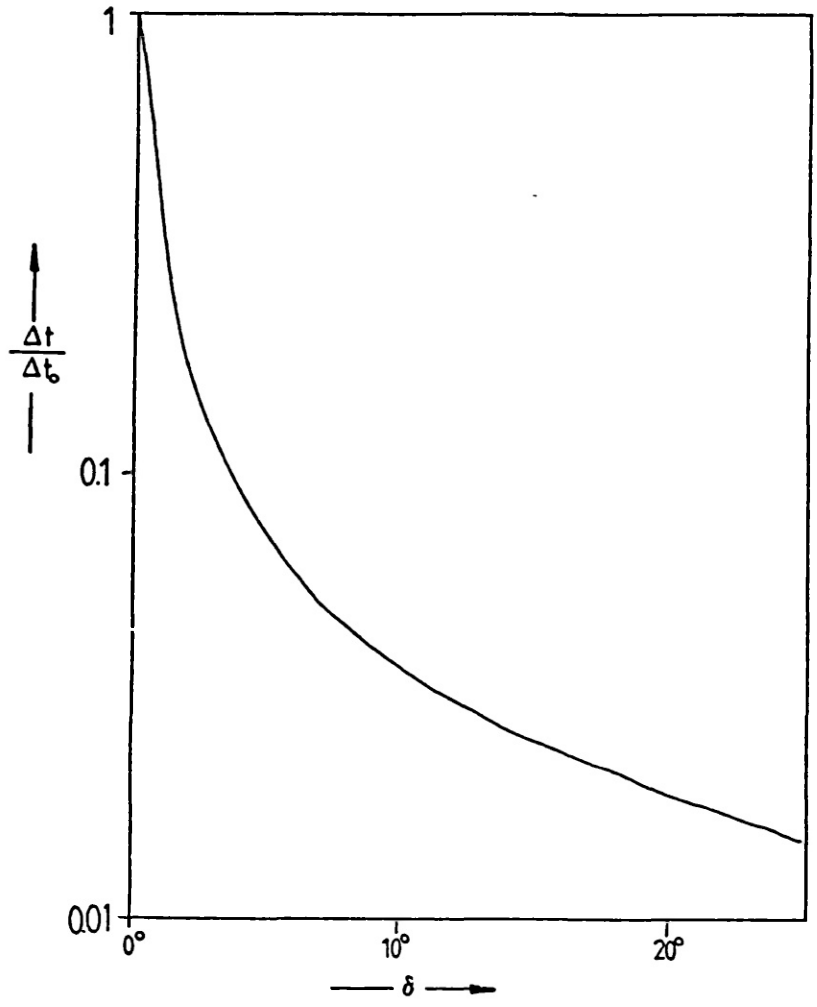

Fig.(4.3) Variation of stable timestep with island size for N_m = 300.

By plotting $\tilde{g}$ as a function of r, the local stability properties can be deduced. If $\tilde{g} > 1$ in an interval (r_1, r_2), then the radial modes for which $g(k) > 1$ will be numerically unstable in (r_1, r_2).

The numerical instability is unique for two reasons.

1) Only a finite number of modes are potentially susceptible to the instability.

2) The region where the modes are unstable is localised spatially to where $\tilde{g}(r) > 1$.

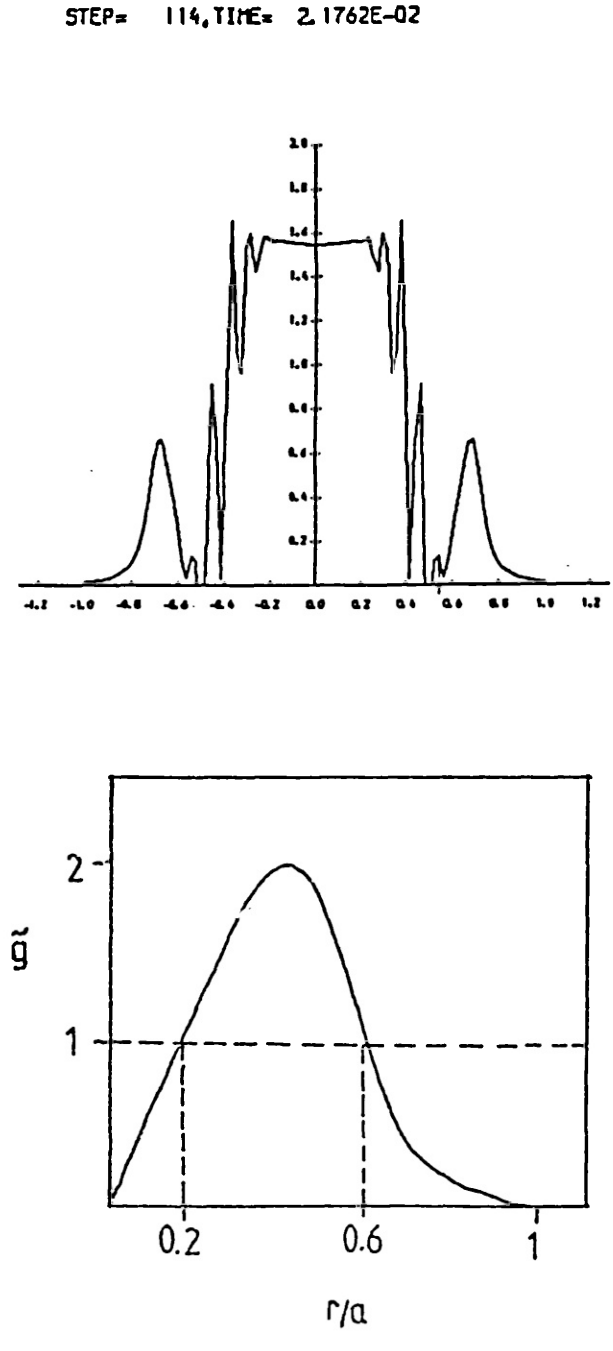

Fig.(4.4) *Showing the stability parameter $\tilde{g}(r)$. Note the instability grows roughly where $\tilde{g}(r) > 1$.*

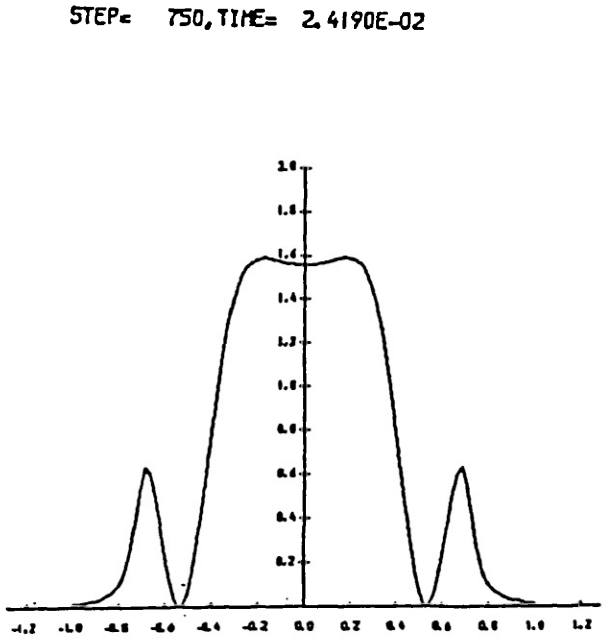

Fig.(4.5) *Current density and stability parameter after a further 450 timesteps, $\tilde{g} < 1$ throughout. Note that the current filaments have been damped away.*

Since $\phi_{mn}(r)/r$ peaks inside the resonant surface of the mode, we can infer that the numerical instabilities will grow within the rational surfaces. Furthermore, the instability would show initially on the current profile since j is the second derivative of ϕ. Figure (4.4) shows the current profile in the presence of a *single* tearing mode of helicity 2/1. This profile was obtained by running RSF for 114 timesteps with $\Delta t = 4/5\ \Delta t_{PUBLISHED}$. Below is plotted the stability parameter $\tilde{g}(r)$. Note that the region where the current filaments grow is roughly where $\tilde{g}(r) > 1$. The filaments are most certainly of numerical origin since a single mode is only able to interact with the 0/0 component of the flux.

Continuing RSF from the state depicted in Fig.(4.4), but with the criterion $\tilde{g} < 1$ imposed by reducing Δt gives, after a further 636 timesteps, the state shown in Fig.(4.5). Clearly the current filaments have been dissipated away. The timescale for the dissipation is the resistive time of the system.

4.4 CONCLUSIONS

In this chapter, the numerical stability properties of the RSF computer code have been briefly presented. The full details[35] have not been given since they are largely of computational interest and add nothing to the argument pursued in this thesis. We have given sufficient evidence to suggest that many of the current filaments could be produced by numerical instability rather than a real physical instability. Indeed the numerical instabilities occur in regions where physical instabilities might be expected to grow and therefore there is doubt concerning the validity of the Oak-Ridge calculations.

We saw in Chapter III that the quasi-linear calculation

suggested that the island overlap phase need not be a physical barrier and that the evolution can continue thereafter. The results of this chapter show that RSF is prone to numerical instability, albeit rather different from that usually encountered. Clearly, there is a need to re-examine the calculations performed with RSF. In the next chapter, we repeat the calculation of Chapter III, using RSF instead of TRINIO, and with the new stability criterion (4.3.16), i.e.

$$\tilde{g} \leq 1.$$

CHAPTER V

5.1 INTRODUCTION

In this chapter, the results of a full non-linear calculation using RSF are presented. The new stability criterion (4.3.16) forces the code to be run under for more stringent conditions than hitherto. This naturally makes the calculations more expensive. Therefore we are unable to include all the modes used in ref.(23), neither are we able to use the same value of magnetic Reynolds number. It must be emphasised however, that the 'non-linear' destabilisation mechanism was illustrated at $S = 10^4$, and it was claimed[23] that the time for the destabilisation was independent of S.

The results presented must therefore be treated as suggesting a trend rather than being a definitive answer to the problem.

We show that the results conform to those obtained by the quasi-linear theory calculation of Chapter III. The implciations of this are discussion in the conclusion.

5.2 RESULTS

The initial equilibrium profiles are the same as used in Chapter III, though no temperature profile is required since the version of RSF without an energy equation was the only one available for use.[36]

The parameters used for the calculation are as follows :

q-profile parametrisation

$$\lambda = 3.24$$

$$q(1) = 4.2$$

$$q(0) = 1.34 .$$

Number of radial mesh points

$$N_m = 100 .$$

Magnetic Reynolds number

$$S = 10^4 .$$

Helicities present

2/1, 3/2, 5/3, 1/1, 0/0 .

The initial perturbation to the system is primed from an analytic representation of the tearing mode eigenfunctions

$$\phi_{mn}(r) = \left(\frac{W_{mn}^I}{4}\right)^2 \frac{r^m(1-r)}{r_{mn}^m(1-r_{mn})} \frac{2}{1+\exp(10(-1+r/r_{mn}))} \frac{r_{mn}q'(r_{mn})}{q(r_{mn})^2} \qquad (5.2.1)$$

the free parameter being the initial island width W_{mn}^I. The values used for W_{mn}^I and the position of the resonant surfaces r_{mn} are listed below.

m/n	W_{mn}^{I}	r_{mn}/a
2/1	0.05	0.66
3/2	0.05	0.50
5/3	0.01	0.57
1/1	-	-

The size of the initial perturbation is not critical. Runs with different initial perturbations yielded similar results.

The boundary conditions used are the same as those of section 3.2 and ref.(23).

Figure (5.1) shows the initial current profile below which is plotted the perturbation to the current in the $\theta = 0$, $\zeta = 0$ plane.

Figure (5.2) shows the time evolution of the magnetic islands plotted at their respective positions within the plasma.

The similarity between Fig.(5.2) and Fig.(5.3) is quite remarkable. More importantly though, Fig.(5.2) should be compared with Fig.(2.1). The implementation of the stringent stability criterion $\tilde{g} < 1$ enables the code to continue past the strong coupling phase with none of the numerical difficulties that have been reported[29], nor any of the curious current filaments growing (apart from those which can be expected to grow).

Figure (5.3) illustrates the current density and perturbed current density at time $t \sim 2.7 \times 10^{-2}\ \tau_R$, when the islands cover 36% of the minor radius. The structures at $r = \pm 0.54a$ are caused by the 2/1 component of the flux, and is symmetric about the minor axis. The asymmetric structure at $r = 0.4a$ is due to the 3/2 component of

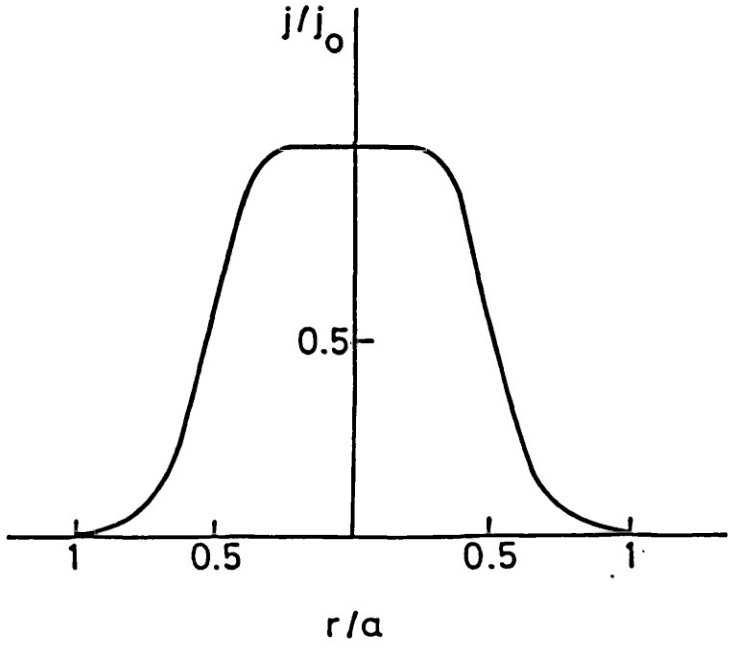

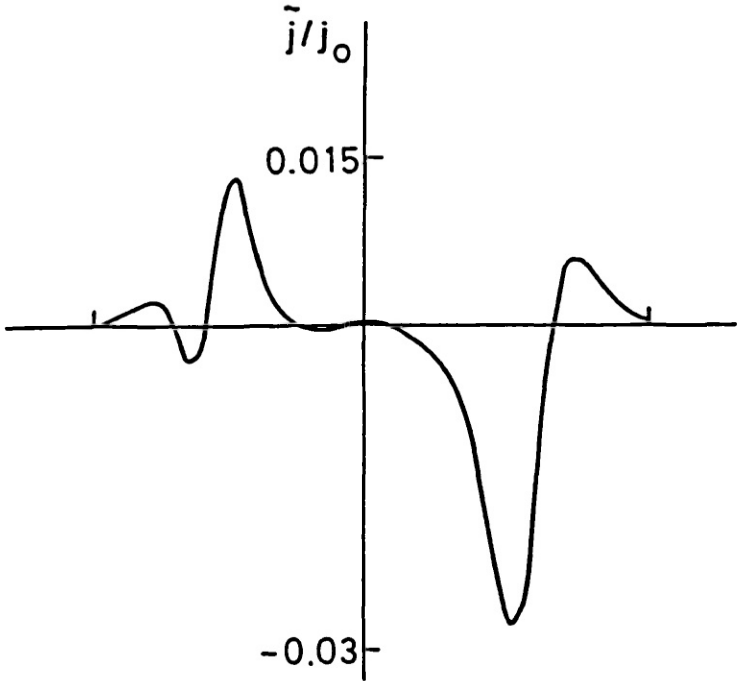

Fig.(5.1) Total current density and the perturbed current used to initialise the calculation.

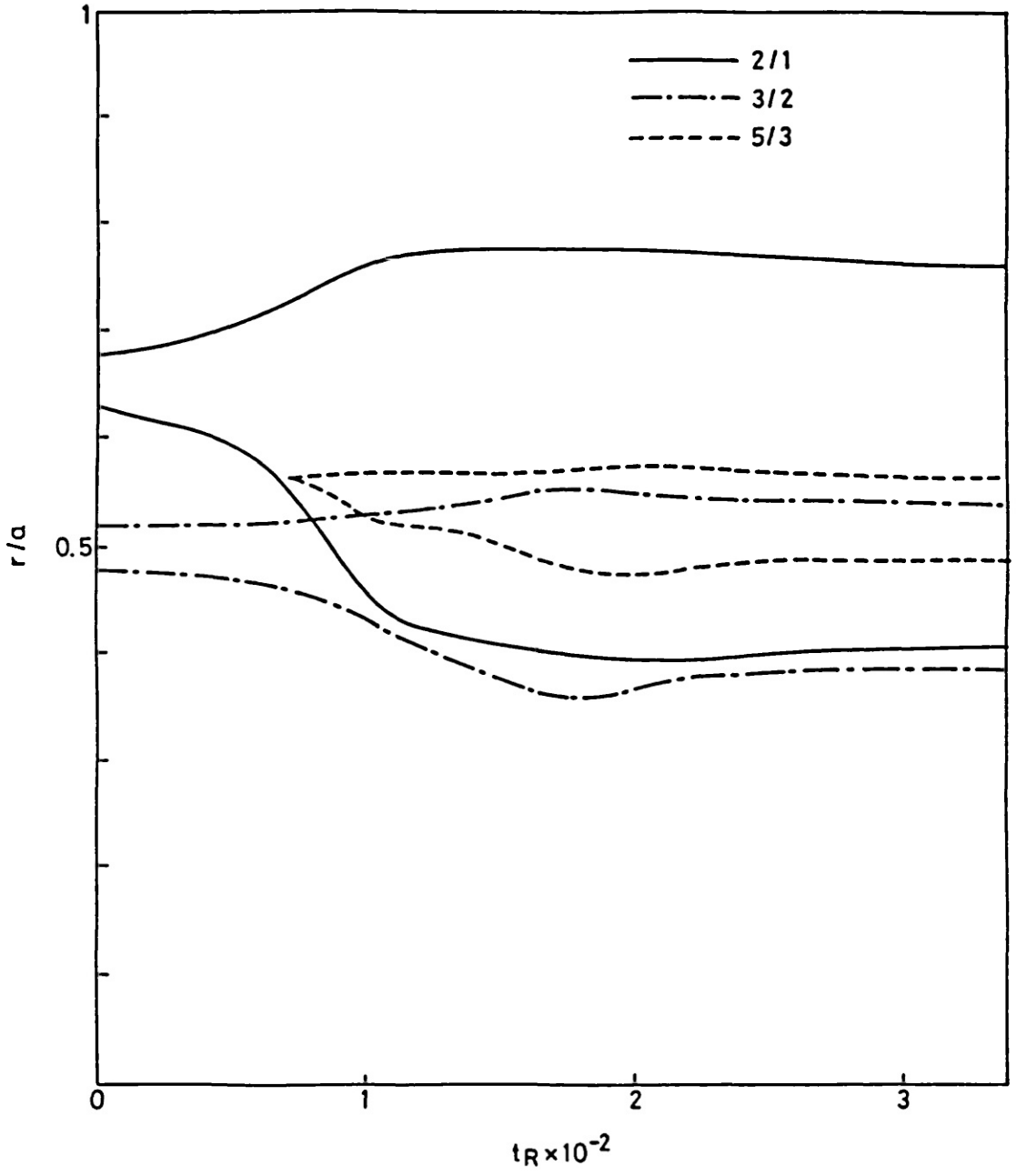

Fig.(5.2) Magnetic island widths of the 2/1, 3/2 and 5/3 helicities plotted as functions of time.

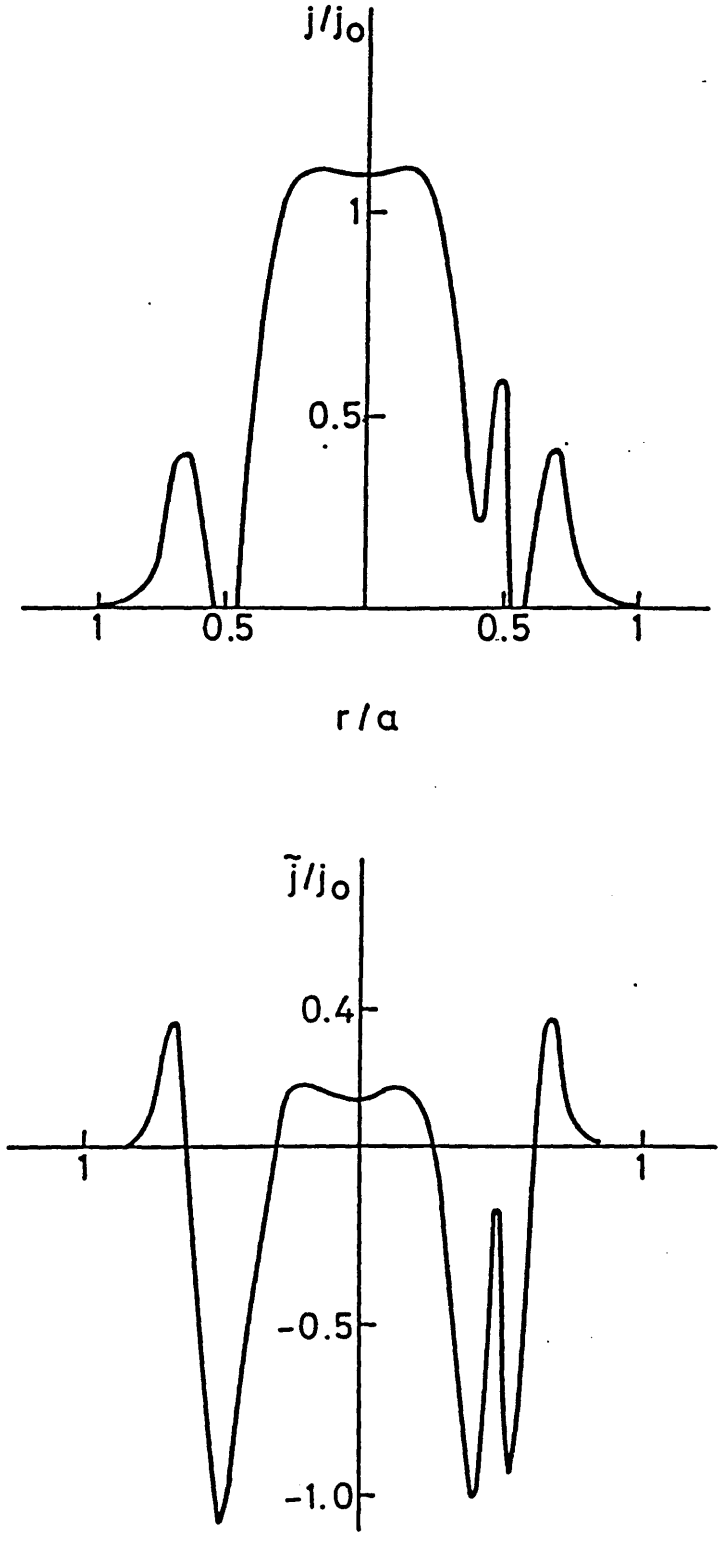

Fig.(5.3) *Current density and perturbed current density at time* $t = 2.7 \times 10^{-2} \tau_R$ *when the islands cover 36% of the minor radius.*

the flux. No other features on the current profile are apparent.

Many of the features in Fig.(2.1) can be seen in Fig.(5.2) despite the difference in magnetic Reynolds number and despite the difference in the number of modes used in the calculation. One slight difference is that the 5/3 mode grows once the 2/1 mode has touched the q = 5/3 surface. This does not necessarily imply that the 5/3 mode is driven unstable by non-linear effects alone. The stability equation (2.3.5) is 'contained' within the $(\nabla\phi\wedge\nabla j).\underline{\hat{z}}$ term in equation (2.2.2); hence the quasi-linear effect of the modification to the j_{oo} component of the current by the other modes is still present. The destabilisation of the 5/3 is likely to be caused by an amalgam of quasi-linear and non-linear effects. Note that the 5/3 persists once the islands have overlapped. The driving of this mode must be of non-linear origin.

The 'destabilisation' of the 3/2 mode is also present, though to a lesser degree than in ref.(23). This is illustrated in Fig.(5.4) which shows the growth rates as calculated from the magnetic energy E_{mn}^{M} of each mode, where :

$$\gamma_{mn}(t) = \frac{\partial \ell n}{\partial t} (E_{mn}^{M}(t)) \qquad (5.2.2)$$

and

$$E_{mn}^{M}(t) = \tfrac{1}{2}\int_{V} |\nabla\phi_{mn}|^{2}\, dV \ .$$

The destabilisation of the 3/2 mode occurs when the island touches the 2/1 island. Since no equation for the temperature is used in the version of RSF at our disposal, the peak in γ_{32} cannot

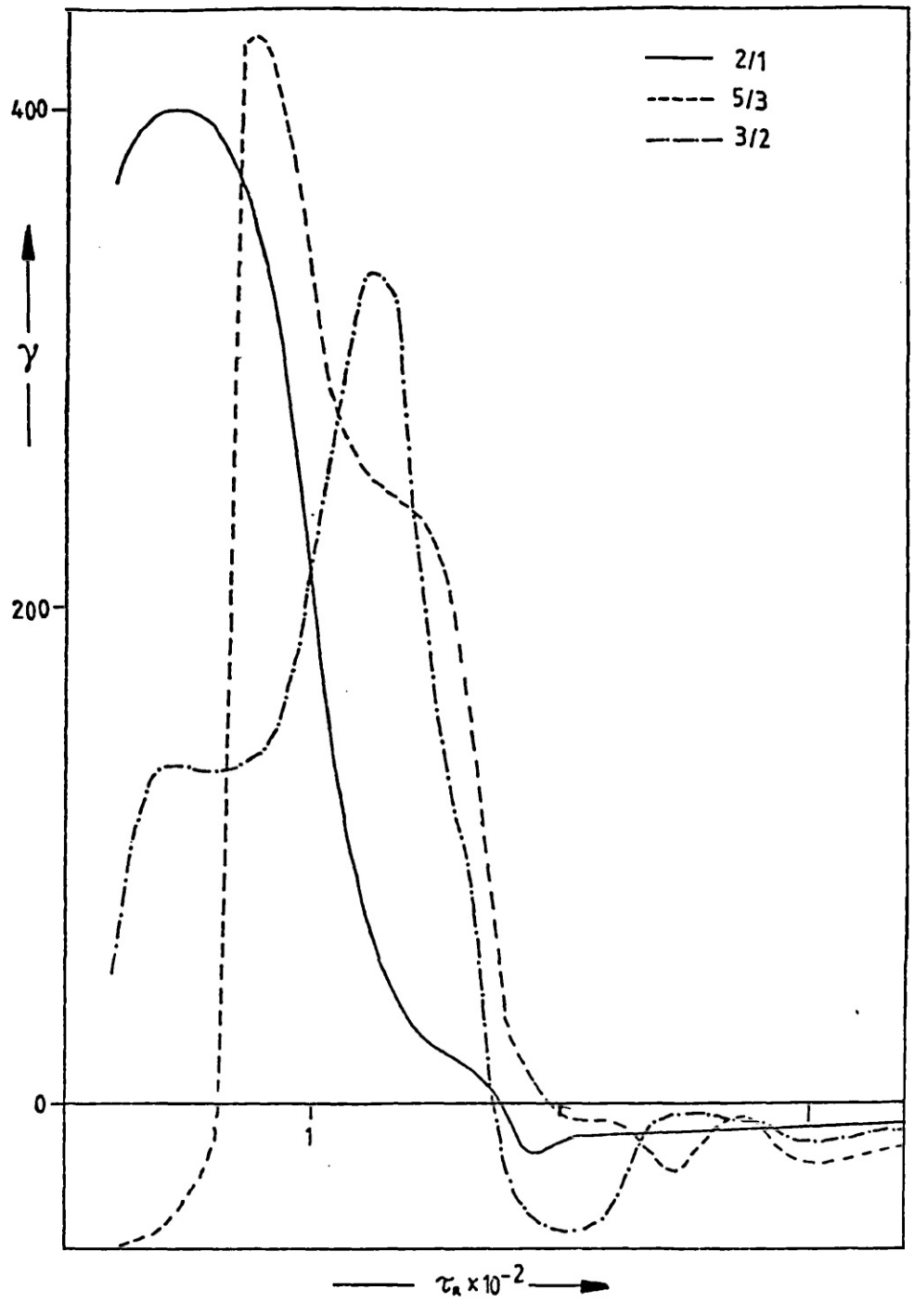

Fig.(5.4) Growth rate γ_{mn} calculated from the magnetic energy of each mode.

partially be attributed to the cooling of the island, as described in section 3.2. However, the quasi-linear effect, i.e. the deformation of the axisymmetric component of the current influencing the evolution, is still present. Again, the 'destabilisation' cannot be

exclusively ascribed to mode-coupling.

The state shown in Fig.(5.2) at time $t = 3 \times 10^{-2}\ \tau_R$ persists to long times since

$$\lim_{t\to\infty} \gamma_{mn}(t) = 0$$

The final state has overlapping magnetic islands covering 35% of the minor radius centred about $r = 0.57a$; a result almost identical with the TRINIO result!

The axisymmetric component of the current $j_{oo}(r)$ is shown in Fig.(5.5) at the time when the islands have saturated and a steady state exists (the final state is one with non-zero flow, the maximum velocity within the 2/1 vortex is $\sim 1/10\ V_A$). This component of the current is equivalent to that calculated by TRINIO. In section 1.6, it was shown that a torn plasma has a lower energy than an untorn plasma. The excess energy is shed by reduction of the destabilising $\underline{B}.\nabla j_z$ couple. This is achieved by reducing the magnitude of ∇j_z at the rational surface. This effect is clearly visible in Fig.(5.5), where the 2/1 island creates a plateau in $0.55a < r < 0.68a$. A less pronounced reduction of ∇j_z can be observed at $r \sim 0.45a$ and is due to the 3/2 island.

The convergence of the solution was tested by re-running the calculation with the first harmonic of each of the fundamentals inserted, i.e. the modes 2/1, 3/2, 5/3, 1/1, 4/2, 6/4, 10/6, 2/2, and 0/0. The evolution followed as before and the final island widths differed by < 3%.

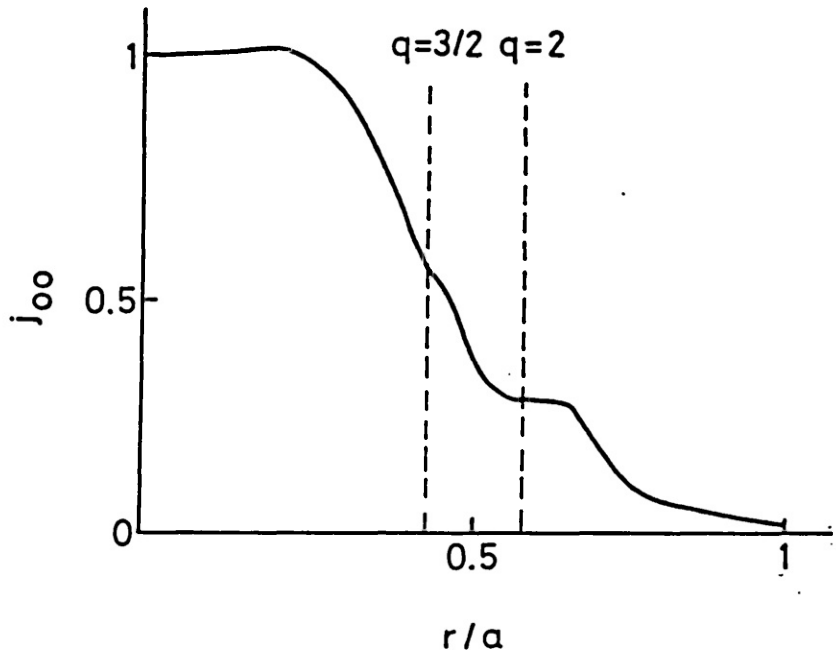

Fig.(5.5) Axisymmetric component of the current in the steady state.

5.3 DISCUSSION

In this chapter, the results of a non-linear calculations of the previously studied unstable equilibrium have been presented. The results exhibit almost identical behaviour to the quasi-linear results of Chapter III. Again, there is no evidence to suggest that a disruption has occurred. Indeed, the final steady, saturated island widths are identical.

There is clearly a need to repeat this calculation with more modes and at a higher value of S. However, tests examining the

stability of the initial and final equilibrium states show that the only modes which grow are the modes that have been used! The implication of this is that the only modes which are able to affect the dynamics are the non-linearly generated ones.

The non-linear interaction of a mode with helicity m_1/n_1 with another of helicity m_2/n_2 generates two modes with helicities

$$(m_1 + m_2) \; / \; (n_1 + n_2)$$

and

$$|m_1 - m_2| \; / \; |n_1 - n_2| \; .$$

This cascade mechanism necessarily restricts non-linear generated modes to be between the helicities of those modes initiating the cascade. This is illustrated in Fig.(5.6) which shows the position in m-n space of the modes generated by the ordering scheme of section 3.2.

Note that the modes lie between the 2/1 helicity and the 3/2 helicity. Hence, most of the non-linearly destabilised modes will be driven unstable in the spatial range

$$w \in (w_{32}^{IN}, w_{21}^{OUT})$$

where 'IN' and 'OUT' refer to the inner and outer separatrix of each island.

We conjecture that the inclusion of more modes will not necessarily lead to a greater covering of overlapping magnetic islands,

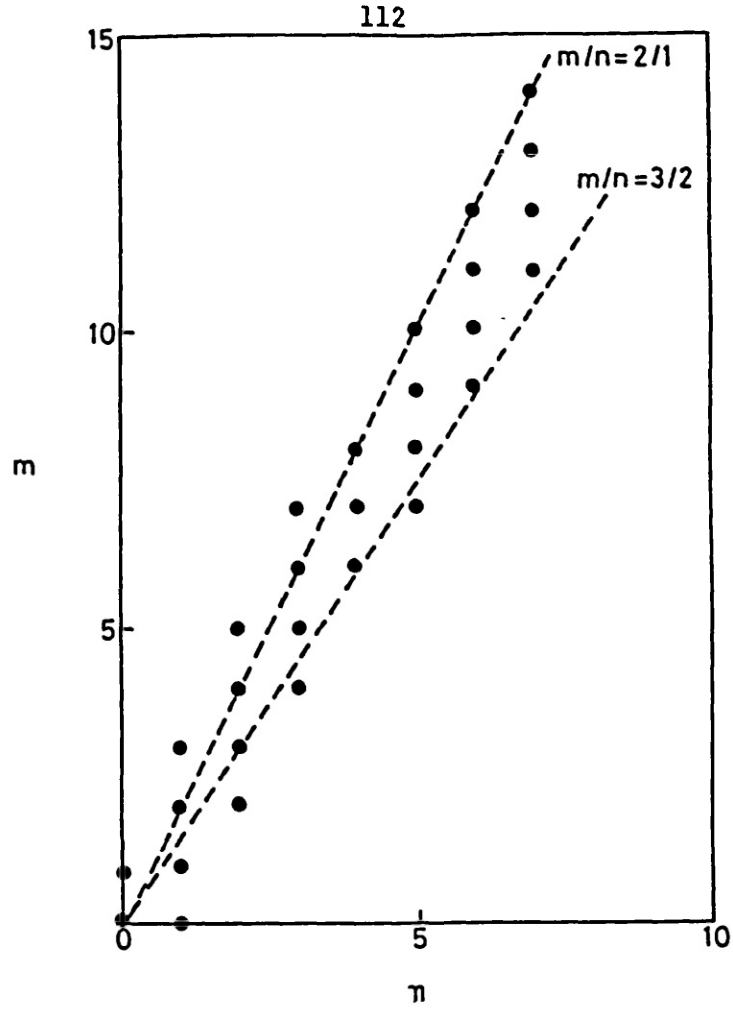

Fig.(5.6) Cascade of modes in m-n space. Note the modes lie between the m/n = 2/1 and 3/2 lines.

and that the final state will not be radically different to that shown in Fig.(5.2). The evolution to that final state may be quite different however, since there will be an exchange of energy between the different modes.

The other disparity between the calculation in this chapter and that in ref.(23) was the choice of S; our calculations being performed in a more resistive regime.

It is not entirely implausible that the plasma undergoes a phase transition between $S = 10^4$ and $S = 10^6$. If such a phase transition exists, it could be calculated by estimating when the anomalous diffusion time of magnetic field lines is less than the characteristic thermal diffusion time across the field lines. Such

a calculation would require detailed knowledge of the transport properties of the plasma, a subject which is poorly understood by contemporary theory.

Since the results of Chapter III are so similar to the results of this chapter and the model of Chapter III makes no assumptions about the size of S, we consider that $S = 10^4$ is an adequate value to assume. However, there is clearly a need to verify this, and such a calculation is planned for the future.

CHAPTER VI

6.1 INTRODUCTION

In this chapter we present the results of a calculation, in which the total plasma current is slowly increased in time. The motivation for performing such a calculation is to investigate how the changing profiles evolve the plasma from a saturated, equilibrium state to one which is disruptively unstable. It is envisaged that the current 'ramp' begins once the flat-top phase of the total current has been reached. In practice, such a ramp would be achieved by discharging the capacitor banks into the primary windings. Hence the current would not rise smoothly, but in a series of discrete jumps. However, for simplicity, we shall assume that the poloidal flux at the plasma edge increases linearly in time and therefore refrain from considering the plasma-circuit coupling.

We show that the current ramp triggers a sequence of minor disruptions of increasing severity and that the discharge is terminated by a major disruption. The major disruption is triggered by two separate events which delineates it from the minor disruptions. Finally, we compare these results with an experiment in which the current was ramped in time.

6.2 DISRUPTIONS DURING A CURRENT RAMP PHASE

Throughout this chapter we use the 1-D TRINIO computer code to

simulate the plasma behaviour. Though this will not include the coupling of modes, it will provide a broad indication of how the plasma state is changing, so the results and interpretations drawn must be treated accordingly.

As previously stated, the aim of this calculation is to see how the plasma evolves from an equilibrium state to a disruptively unstable one by means of slowly increasing the total current.

Previous calculations have all been performed using a constant current boundary condition

$$B_\theta(a,t) = \text{constant}.$$

The boundary condition which will give a simple, linear current ramp is

$$B_\theta(a,t+\Delta t) = B_\theta(a,t) + \frac{\partial b}{\partial t}\,\Delta t \qquad (6.2.1)$$

with $\partial b/\partial t$ = constant.

The current must rise at a slow enough rate to allow the plasma profile to adjust. If the current increases by ΔI in time τ and an island grows by Δw in time τ_w, then

$$\tau \gg \tau_w$$

which fixes the magnitude of $\partial b/\partial t$.

Let the increase in poloidal field in time τ be Δb, then the change in the safety factor $\Delta q(a)$ is

$$\Delta q(a) \approx - \frac{R\, q^2(a)}{a\, B_z} \Delta b \qquad (6.2.2).$$

Thus, q(a) decreases in time and so the resonant surfaces move towards the plasma edge.

The calculation is initiated from a non-linear equilibrium depicted in Figs.(6.1) and (6.2). A saturated m/n = 2/1 island of width 0.09a is situated about $r_{21} \approx 0.75a$. Also a m = 1 island of width 0.2a is present. The state is one in which Ohmic heating is balanced by thermal conduction losses; radiation losses are not considered.

The total plasma current is

$$I_p = \frac{2\pi a^2 B_z}{R\, \mu_o\, q(a)}$$

which for the DITE parameters used gives a value of 123.9 kA for q(a) = 3.125.

The current is increased at a rate

$$\frac{\partial I}{\partial t} \sim 7 \times 10^5 \text{ A s}^{-1}.$$

Applying the ramp for a period $\sim$ 50 ms, the fractional increase in the current is

$$\Delta I/I \sim 0.25$$

however, such a moderate increase of current causes the plasma to eventually disrupt.

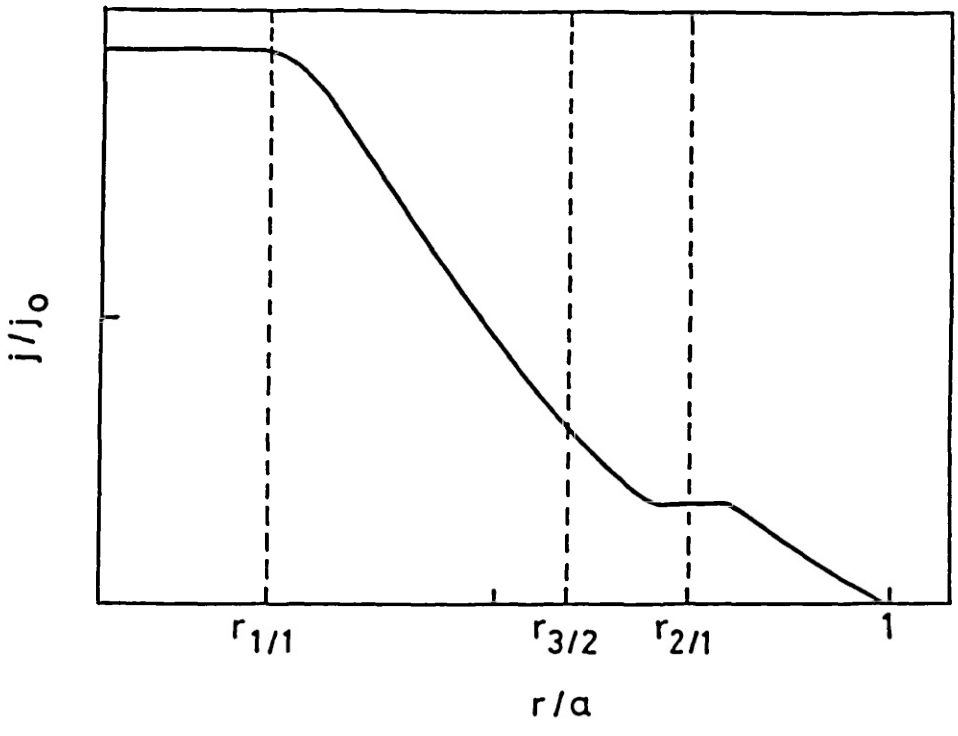

Fig.(6.1) *Saturated equilibrium current profile used to initialise the calculation.*

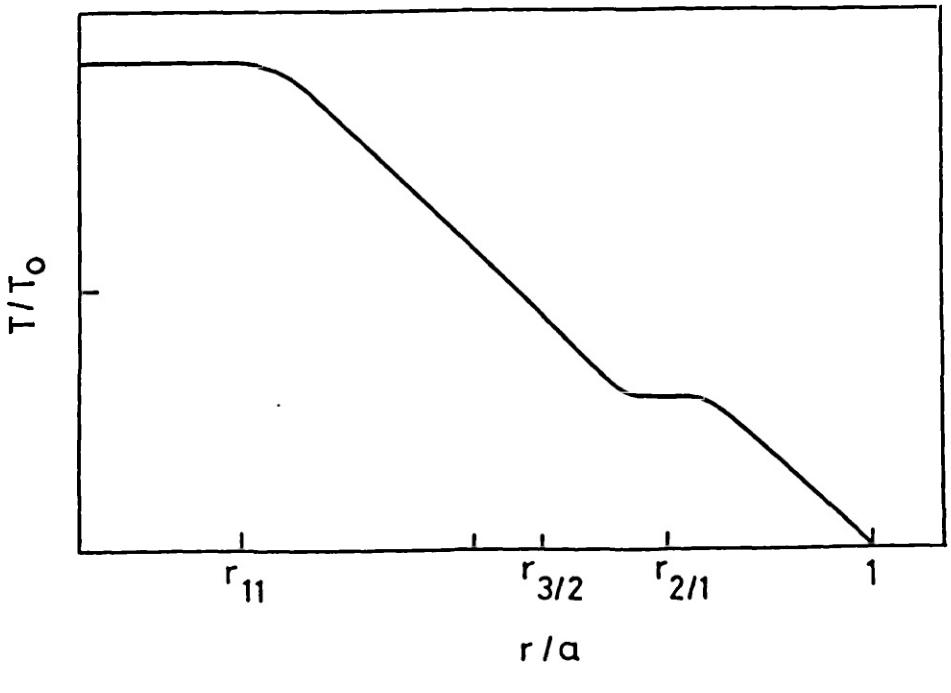

Fig.(6.2) *Equilibrium temperature profile, with Ohmic heating balanced by thermal conduction.*

Figure (6.3) shows the magnetic island widths of the 2/1, 3/2 and 1/1 modes, plotted at their respective radial positions as time progresses. Other modes, though present throughout remain close to marginal stability/instability and do not play a major role in the evolution. Plotted above is the central temperature as a function of time.

There are four distinct pulses of 2/1 and 3/2 activity and also four distinct pulses of enhanced m = 1 activity.

The time lag between the 2/1, 3/2 and 1/1 activity suggests an adaxial propagation of current density.

The following sequence of events describes the evolution from each burst of 2/1 activity to the fall in the axial temperature.

a) The Poynting flux directed into the plasma causes a rise in the plasma current density, which propagates inwards, steepening the current density gradient within the q = 2 surface.

b) The increased current gradient within the q = 2/1 surface destabilises the 2/1 island which grows and 'pumps' the current inwards on a timescale faster than the resistive diffusion time.

c) The current density gradient within the q = 3/2 surface increases and destabilises the 3/2 island which again pumps the current towards the axis.

d) The rise in current on the axis, together with the restriction of current due to the m = 1 island pushes the q = 1 surface outwards, transporting energy from the central core and causing the temperature to drop.

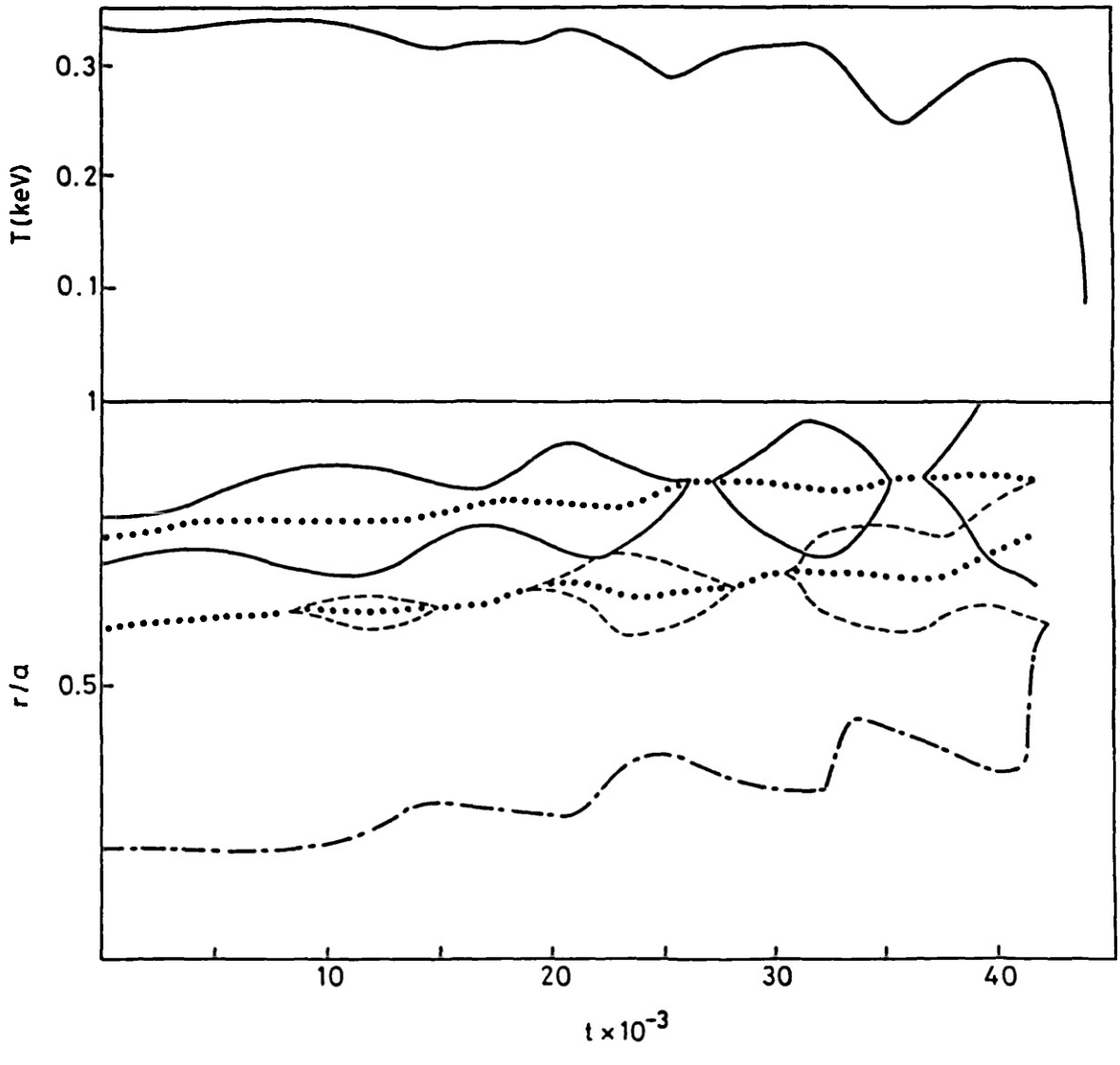

Fig.(6.3) *Island widths and central temperature plotted as functions of time.*

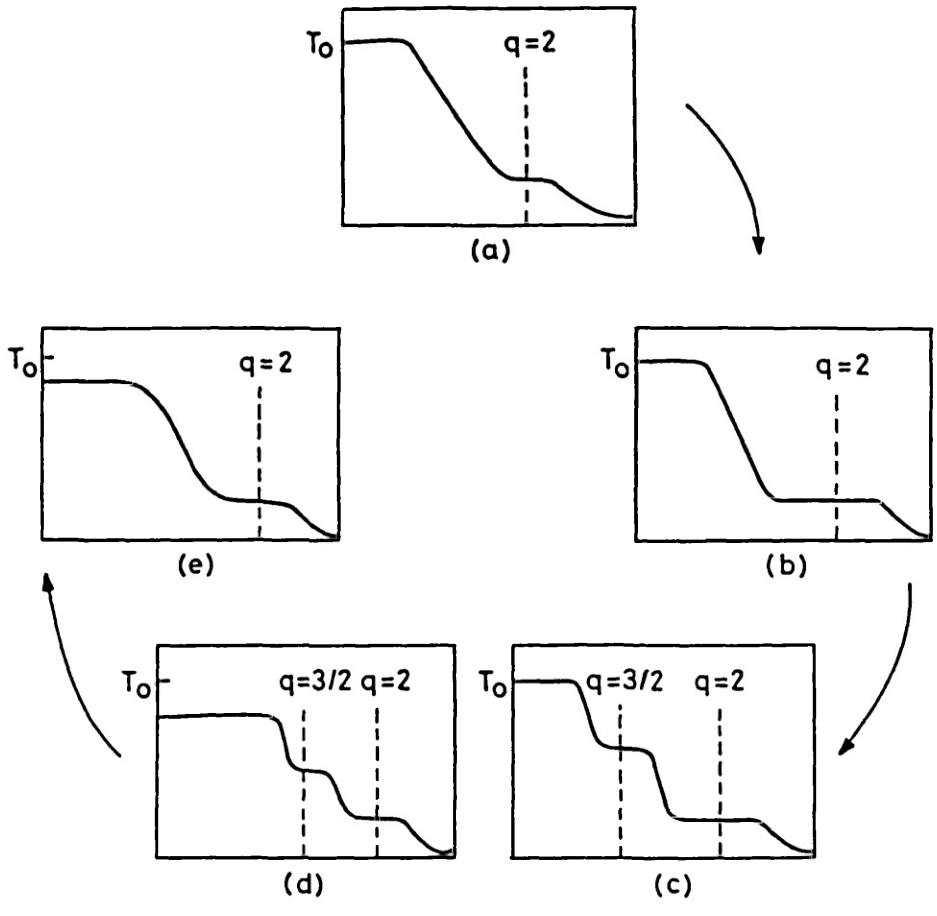

Fig.(6.4) *Sequence of events explained in points a) - e) in the text.*

e) The cooling of the central region lowers the current around the axis and thereby causes the q = 1 surface to contract, though its average position is at a greater radius than that prior to the disruption.

The sequence a) - e) is depicted schematically in Fig.(6.4).

Figure (6.5) shows the total plasma current and the current within the q = 2 and q = 3/2 surfaces. This clearly shows the pumping effect of the islands. The peak in the current at the q = 2 surface I(q=2) at time t = 18.75 ms is coincident with the minimum in the width of the 2/1 island. As the current gradient rises within the q = 2 surface, the island grows and pumps the current inwards on a timescale faster than the resistive diffusion time. The current I(q = 3/2) peaks at t = 2.5 ms after the peak in I(q=2). Hence, the 3/2 island grows for the same reason as before and pumps the current further inwards. At this time, I(q=2) begins to rise, and the process repeates. Note that the fluctuations of I(q=2) and I(q=3/2) are quite pronounced when compared with the monotonically increasing total plasma current.

The current is pumped towards the magnetic axis on a timescale faster than the characteristic resistive diffusion time. The time between subsequent peaks in I(q=2) and I(q=3/2) is $\sim$ 2.5 ms, whilst the resistive diffusion time is

$$\tau_R^{-1} \approx \frac{\eta(q=*)\ \left|B_\theta(q=2) - 2B_\theta(q=*) + B_\theta(q=3/2)\right|}{\mu_o\ B_\theta(q=*)\ \Delta r^2}$$

where '*' represents a surface between the q=2 and q=3/2 surfaces and $\Delta r = r_{21} - r_{32}$. Inserting values

$B_\theta(q=2) = 0.1297$ T

$B_\theta(q=*) = 0.1360$ T

$B_\theta(q=3/2) = 0.1372$ T

$\Delta r = 0.18a$

and

$T(q=*) = 0.138$ keV

gives

$\tau_R \sim 125$ ms.

The current penetrates some fifty times faster than if it were to diffuse resistively inwards.

The sequence a) - e) illustrates how the soft disruptions at times t = 15, 25 and 36 ms, occur. The circumstances causing the major disruption at t = 44 ms are however, different.

The major disruption is triggered by the 2/1 island intersecting the cold limiter at r = a. This occurs because the resonant surfaces move outwards due to the current rise.

Once the island touches the limiter, the island is rapidly cooled due to the enhanced thermal conductivity within the island region. Indeed, the cooling may, in reality, be even more rapid due to the influx of impurities from the limiter. Moreover, since the 3/2 island overlaps the 2/1, the temperature is flattened across the entire overlap region, of the order 35% of the minor radius. This has the effect of rapidly reducing the width of the current channel.

The inward displacement of the current, and the restriction of the current on axis due to the m = 1 instability forces the q = 1 surface outwards, and so the m = 1 island grows explosively. The m = 1 and m = 2 islands touch, thereby connecting field lines from

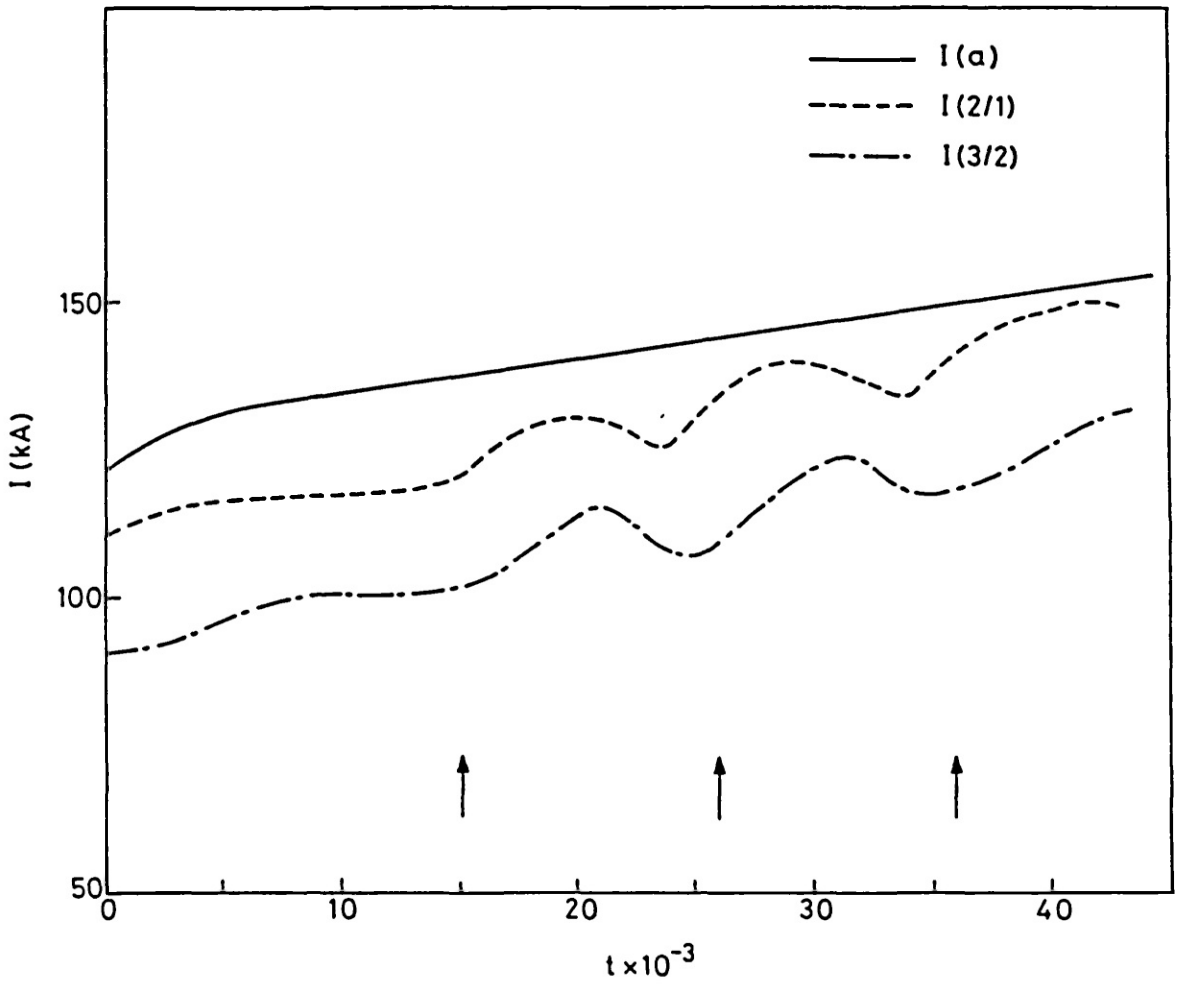

Fig.(6.5) Total plasma current I, I(q=2) and I(q=3/2) plotted as functions of time.

centre of the plasma to the edge. Thus a thermal 'short circuit' is created and confinement is lost across the entire minor radius.

6.3 DISCUSSION AND COMPARISON WITH EXPERIMENT

Results have been presented purporting to explain a sequence of minor disruptions during the slow current rise of a tokamak plasma. The events preceding the terminating major disruption are quite distinct from those events triggering the sequence of minor disruptions. As stated previously, all modes other than those shown in Figs.(6.3) and (6.5) remain close to marginal stability, being momentarily driven unstable as the current is pumped through the respective resonant surfaces.

The variation of the central temperature as a function of time is somewhat reminiscent of sawtooth oscillations. However, no confusion can be made between these variations and sawteeth, since the period between successive troughs is of order ten time a typical sawtooth time. Also the fractional change in the temperature, $\Delta T/T$ is greater than for a typical sawtooth oscillation.

An experiment in which the total plasma current was increased in a similar way to that described was performed in the PULSATOR tokamak.

Though the dimensions and plasma parameters of the PULSATOR tokamak are quite different from DITE, many of the salient features observed in the experiment can be ascribed to the model.

In the experiment, it was implied that the current profile for low-q discharges was flat in the central region, due to continued sawtooth activity (a modulation of m = 2 Mirnov oscillations by the m = 1 mode was seen). Also, measurements of impurities showed an

accumulation close to the magnetic axis. This aspect will be considered in Chapter VII. It was noted that during the slow current increase, many minor disruptions occur, especially in low-q discharges.

Once the disruption sequence begins, the central temperature falls continuously, unlike our simulation. However, this could be explained by an influx of impurities released from the limiter by the outward propagating heat pulse. This conjecture is supported by the observed rise in the electron number density.

Finally, the authors of ref.(37) describe a reasonably reliable method of controlling disruptions, known as the 'hammer method'. The fast growing m = 2 Mirnov oscillations were used as a precursor of the disruption. When observed, a high pulse was applied to the vertical magnetic field which displaced the plasma inwards. After a few milli-seconds, the plasma was allowed to expand freely to its original position, the disruption having been averted.

This could be interpreted in terms of the m = 2 island - limiter interaction triggering the disruption. If, when the 'hammer' is applied, the m = 2 island decays as in the minor disruption sequence, then when the plasma is allowed to expand freely, the island could be sufficiently small so as not to come into contact with the limiter. Clearly, the precise position of the limiters and the direction in which the plasma is shifted during the hammer are crucial factors.

CHAPTER VII

7.1 INTRODUCTION

The calculations which have categorically resulted in a major disruption, described both in this thesis and elsewhere[24,25], all have a common feature. The mutual feature is the presence of the m = 1 mode both prior to and during a disruption. However, it is stated in ref.(37) that disruptions have occurred without m = 1, Mirnov oscillations or soft X-ray sawtooth emissions having been detected.

In this chapter, it is shown by means of a calculation similar to that described in Chapter VI, that such disruptions can be explained within the context of the plasma current restriction model. Indeed the results broaden the scope of the model.

7.2 RESULTS

In ref.(37) it is stated that a disruption occurs without the m = 1 mode being present, however, high-Z impurity ions residing close to the magnetic axis were detected. We shall see that inserting a distribution of ions, strongly peaked about r = 0 causes the plasma to become more resistive, thereby restricting the amount of current able to flow close to the axis. Hence the impurities perform precisely the same function as does the m = 1 island.

The results of this chapter must be treated as illustrating rather than proving a point in a rigorous and self consistent fashion.

A full calculation would require modelling the radiative processes of the ion species and a full transport calculation. To perform this would probably involve making many ad hoc assumptions regarding the transport coefficients. We therefore will not consider the details of how the ions cross magnetic surfaces to get to the magnetic axis, but rather assume a distribution a priori.

We assume that the number density of the impurity ions is a simple Gaussian, centred about r = 0 :

$$n(r) = n_o \exp(-r^2/c^2) \qquad (7.2.1)$$

though the exact functional form is unimportant. The experimental evidence requires the distribution to be strongly peaked on axis, and (7.2.1) suffices in this respect for a sufficiently small choice of the parameter c. Furthermore, we assume the radiation loss function is given by

$$\mathcal{L}(T,r,n) = C\, n(r) \qquad (7.2.2).$$

It is considered that this is a particularly neutral choice of loss function, containing no dependence on temperature and depending linearly on the number density only.

The calculation is initialised from the profiles shown in Fig.(7.1). This is a saturated, radiative, resistive equilibrium with Ohmic heating, thermal conduction and radiation losses in balance, i.e. :

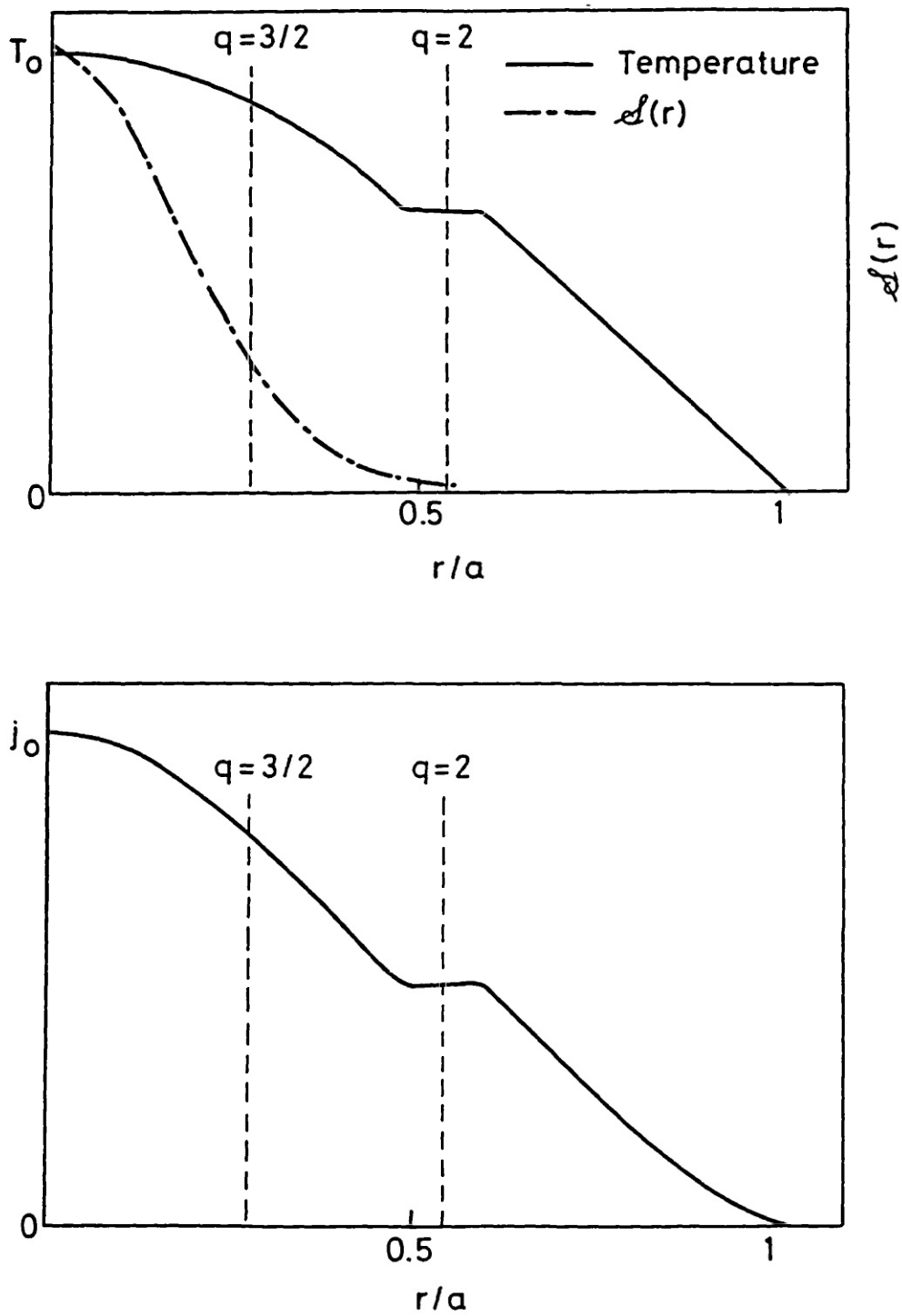

Fig.(7.1) *Non-linear equilibrium temperature and current density profiles. The form of the radiation loss function is also shown.*

$$j_z(r)E_z(r) + \frac{1}{r}\frac{\partial}{\partial r}\left(rK\frac{\partial T(r)}{\partial r}\right) - \mathcal{L}(r) = 0 \qquad (7.2.3)$$

where $E_z(r)$ = constant.

The values of q(o) and q(a) at the start of the calculation are 1.336 and 3.782 respectively. The 2/1 and 3/2 rational surfaces are located at 0.55a and 0.27a respectively. The initial value of the temperature on axis is 0.265 keV.

In order to evolve the plasma from the equilibrium depicted in Fig.(7.1) to a disrupted state, we apply the boundary condition (6.2.1) and ramp the current in time.

The stability properties of the 2/1 and 3/2 modes are calculated, all other modes being close to marginal stability throughout. A constant monitor of the 1/1 mode is maintained.

Fig.(7.2) shows the resulting magnetic island widths plotted as functions of time, together with the central temperature. Similar behaviour to that depicted in Fig.(6.3) is evident, though the 3/2 mode is marginally stable for 35 ms from the start. This is chiefly because the q = 3/2 surface is comparatively close to the minor axis, therefore the stabilising current gradient in the interval $(r_{32},a]$ dominates the destabilising current gradient in (o,r_{32}).

Many of the features in Fig.(7.2) are similar to those in Fig.(6.3). Again, the magnetic islands act as 'pumps', pushing the current adaxially, faster than if it were to diffuse inwards. The 3/2 island is significantly destabilised by the action of the 2/1 island at time t ≈ 31 ms. At the same instant there is a slight rise in the central temperature due to the current increasing

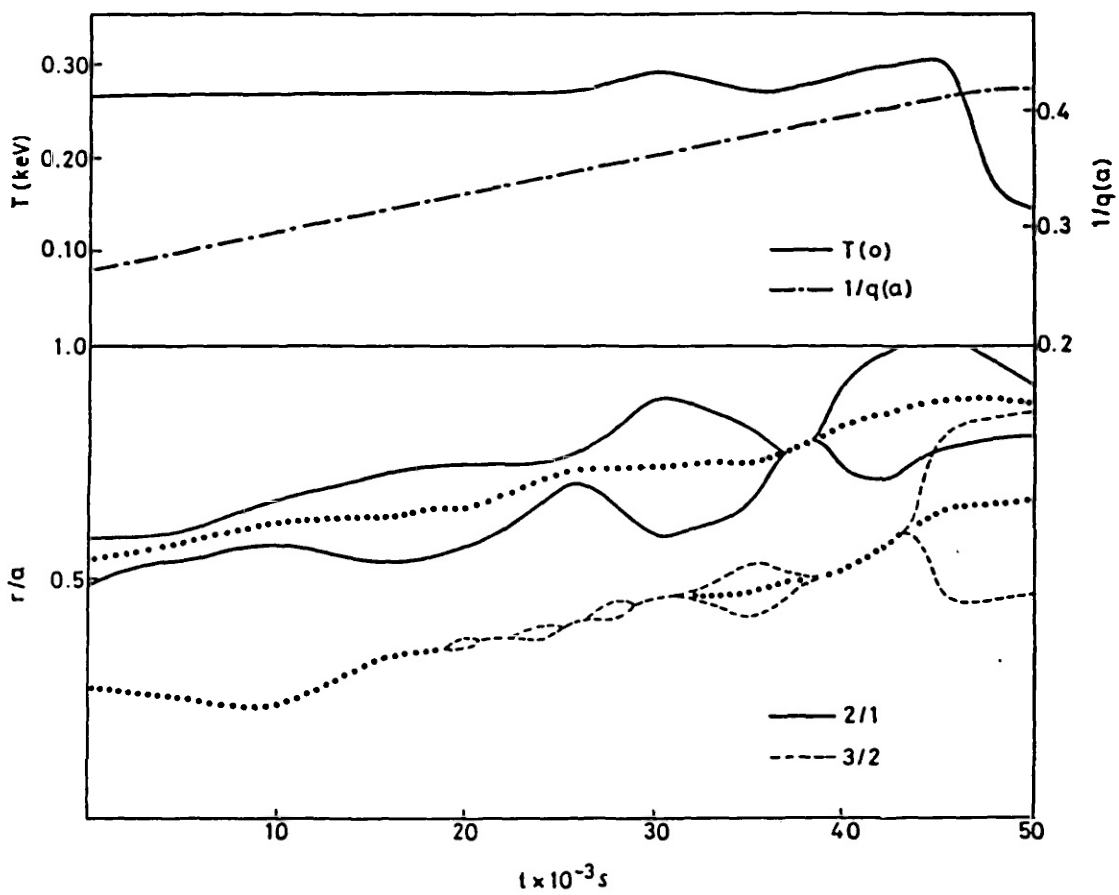

Fig.(7.2) *Magnetic island widths, central temperature and 1/q(a) as functions of time during the current ramp.*

and therefore raising the rate of Ohmic heating.

Since the rate at which the impurities radiate is a constant, a period of time must elapse in order to restore the energy balance condition (7.2.3). For this reason, the impurities restrict the current less severely than the m = 1 mode. The restriction of current by the m = 1 gives a particularly hard upper limit on the amount of current able to flow.

The destabilisation of the 3/2 island at time t ≈ 43 ms is caused for two reasons :

a) The intersection of the 2/1 island with the limiter contracts the current channel and removes the stabilising effect of the current gradients in $(r_{32},a]$.

b) The flattening of the current profile on axis due to the impurities steepens the destabilising current gradient in (o,r_{32}).

The combination of these two effects rapidly destabilises the 3/2 mode. The connection of the two islands removes the insulating magnetic surfaces from 55% of the minor radius. The central temperature falls from time t ≈ 43 ms onwards.

During the entire calculation, q(o) is a monotonically decreasing function of time, though the rate of fall is less than if the impurities were absent. At the time of the disruption, the value of q(o) is 1.07 and q > q(o) everywhere, hence both sawteeth and m = 1 Mirnov oscillations would not be detected experimentally.

The plasma actually recovers from this disruption, the central temperature recovering to a value close to that governed by the requirement of energy balance. It must therefore be interpreted as a

minor disruption.

In the following cycle (not shown), $q(o) < 1$ and so the $m = 1$ mode is destabilised. Since the current profile is flat at the axis and the shear is small, the $m = 1$ island can rapidly grow and connect with the other islands across the entire minor radius. This causes a major disruption similar to that described in Chapter VI, though clearly the events prior to the disruption are rather different.

The current and temperature profiles at the time of the minor disruption ($t \approx 45$ ms) are illustrated in Fig.(7.3).

7.3 SUMMARY

In this chapter, the results of a calculation, where the effects of impurities residing close to the magnetic axis, have been presented. As previously stated, the calculation illustrates a principle rather than describes the details of a particular experiment and must therefore be treated within that context.

Applying a Poynting flux at the wall and thereby ramping the total current, the plasma state is evolved. Behaviour similar to that described in Chapter VI is observed.

The important result of the calculation is that a disruption is able to occur without the presence of an $m = 1$ island within the plasma. The impurities serve the same function as the $m = 1$ island, restricting the amount of current able to flow and thereby steepening the current gradient within the 2/1 resonant surface. This broadens the conditions under which disruptions can be explained within the scope of the quasi-linear model.

The common feature of all the calculations which have resulted in a major disruption is the connection across the entire minor radius

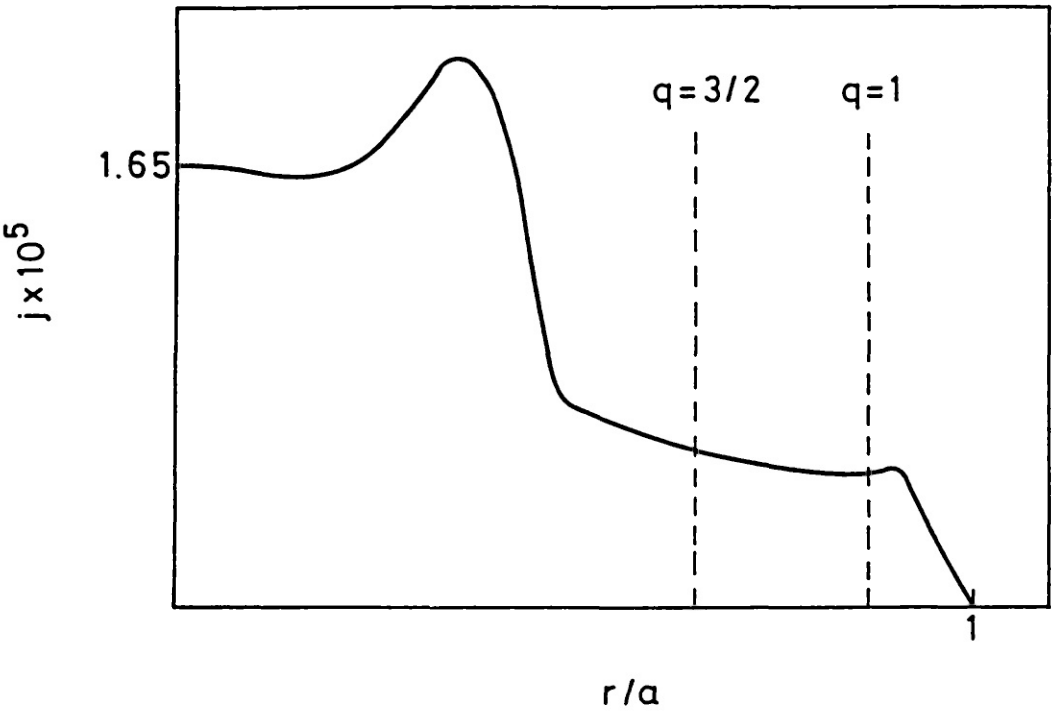

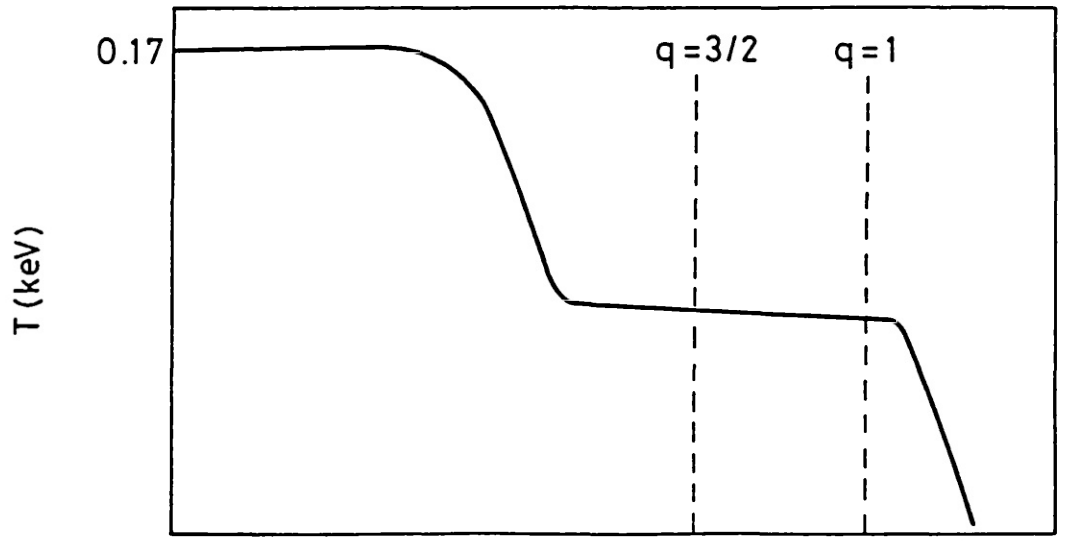

Fig.(7.3) *Current and temperature profiles at the time of the soft disruption, t ∿ 45 ms.*

of magnetic islands. The disruption illustrated in Fig.(7.2) at $t \approx 45$ ms was described as being 'minor' albeit a particularly severe minor disruption. The classification 'minor' was used purely because the plasma was able to recover. It is debatable whether, under experimental conditions, the plasma would be able to recover. The influx of edge impurities could contract the current channel and drive a hard disruption similar to that described in section 6.2.

CHAPTER VIII

8.1 SUMMARY AND CONCLUSIONS

In this thesis, we have considered various aspects appertaining to disruptions in tokamaks.

In Chapter I, by way of an introduction, the experimental signatures, precursors and effects of disruptions were briefly discussed. Experiment indicates that the theory of resistive MHD is an adequate tool to explain the main features of the disruption. A brief review of resistive MHD theory was given and it was shown that the most important resistive mode in tokamaks, the tearing mode, must be treated non-linearly.

In Chapter II, a review of two theories of the disruption was given. The two models were discussed and contrasted. Three criticisms of the mode-coupling model were raised and the line of argument subsequently pursued in this thesis was in investigating, clarifying and hopefully resolving some or all of those criticisms.

In Chapter III, the results of a quasi-linear calculation using the TRINIO computer code were presented. The motivation for such a calculation was to assess the importance of mode-coupling effects. It was found that the quasi-linear evolution was very similar to the fully coupled evolution with the important proviso that there was no evidence of a disruption having occurred. The effects of a free boundary was discussed. The wall on the plasma has a stabilising effect and it was argued that future calculations

should be performed with a free boundary.

In Chapter IV the numerical stability of RSF was examined. It was shown that the code is prone to a novel numerical instability on account of its hybrid spectral/finite-difference formulation. In particular it was shown that the instability manifests itself by the growth of finescale oscillations on the toroidal current density profile. Since similar oscillations were seen in the published RSF results, it was considered that there was a need to perform a recalculation with a more stringent stability condition employed.

In Chapter V, the result of this calculation was presented, albeit with a smaller value of S and fewer modes. The details showed very similar behaviour to the quasi-linear calculation of Chapter III. Again no evidence of a disruption was seen to occur which supports the view that the evolution is quasi-linear rather than non-linear. We conclude by recognising the need for a calculation with more modes, performed at higher S.

In Chapter VI, a calculation showing how the plasma evolves from a marginal state to a disruptive one was described. A sequence of minor disruptions terminated by a major disruption are observed to occur. It was shown that the magnetic islands act like 'pumps', forcing the current towards the axis on a timescale faster than if it were to diffuse inwards. The conditions occurring prior to major and minor disruptions were delinated and the results compared with those observed in experiment.

In Chapter VII, the concept of the $m = 1$ mode restricting the current flow on axis being instrumental in triggering the disruption was broadened to when there was no $q = 1$ surface in the plasma. It was suggested that the results could explain those disruptions where

neither sawteeth or m = 1 Mirnov oscillations are observed.

All our results support the conjecture that the following elements are required in order to cause a major disruption.

1) *A large magnetic island intersecting the limiter or cold plasma mantle*

   Present tokamaks operate at high currents, implying that q(a) is low, $q(a) \lesssim 3$. The obvious candidate for this mode is the m/n = 2/1.

2) *An intermediate large magnetic island in the central region*

   The presence of such an island, resonant between the q = 1 and q = 2 surfaces, ensures a thermal short circuit across the entire minor radius, though this condition is not strictly necessary.

3) *A method of restricting the amount of current flowing about the magnetic axis*

   It has been shown that the m = 1 island and impurities have equivalent effects.

The three elements above are able to explain disruptions without appealing to the effects of mode-coupling.

8.2 OUTSTANDING PROBLEMS IN THE STUDY OF TOKAMAK DISRUPTIONS

In this thesis we have examined a few aspects of a large and particularly rich field in plasma physics research. We have concentrated upon two theories of the disruption (one admittedly being the 'consensus view') and our findings must be contrasted with other

theories and with experiment.

The immediate future work must resolve the questions raised at the end of Chapter V, namely, does the inclusion of many other modes and a larger value of magnetic Reynolds number substantially affect the previous results? The boundary conditions must also be changed to relax the constraint of the plasma surface also being a flux surface.

It would be desirable to find an analytical explanation for the form of $\Delta^*(w)$ close to disruptive conditions. At present, the form of Δ^* can be inferred from numerical calculations alone.

All the calculations described have been performed in periodic cylindrical geometry with ordering appropriate for small aspect-ratio tokamaks. This precludes direct applicability of the results to the new generation machines. In machines like JET and the 'BIG-DEE' (DOUBLET III upgrade), the shaped cross-sections and tight aspect-ratio allow toroidal coupling effects to become important. This may have important effects on the confinement properties of the plasma. Furthermore, the new machines are designed to operate at large values of β. The Shafranov shift associated with high-β effects introduces an important asymmetry into the system which we have neglected. All of these effects must be investigated in the future if the disruptive instability is to be avoided in tokamak fusion devices.

REFERENCES

1. S. von Goeler, W. Stodiek, N. Sauthoff, Phys.Rev. Letters, 33, 1201, (1974).

2. G. Bateman, MHD Instabilities, MIT Press, pp.11-4.

3. B.B. Kadomtsev, 'Behaviour of Disruptions in Tokamaks', IAEA Proceedings, Aachen (1983).

4. I.H. Huchinson, Phys.Rev. Letters, 37, 338, (1976).

5. T.J.M. Boyd, J.J. Sanderson, Plasma Dynamics, Nelson, pp.60-63.

6. S. Chandrasekah, Hydrodynamic and Hydromagnetic Stability, Oxford Clarendon Press, Ch.10.

7. F. Cap, Handbook on Plasma Instabilities, Vol.I, Academic Press, pp.310-311.

8. J.A. Wesson, Nuclear Fusion, 18, 87, (1978).

9. J.W. Dungey, Cosmic Electrodynamics, Cambridge University Press, pp.98-102.

10. H.P. Furth, J. Killeen, M.N. Rosenbluth, Phys.Fluids, 6, 459, (1963).

11. T.J.M. Boyd, J.J. Sanderson, Plasma Dynamics, Nelson, pp.50-51.

12. H.P. Furth, Propagation and Instabilities in Plasmas, Stanford University Press, pp.87-102.

13. J.A. Wesson, Plasma Physics and Nuclear Fusion Research, Academic Press, pp.223-225.

14. H.R. Strauss, Phys. Fluids, 19, 134, (1976).

15. P.H. Rutherford, Phys. Fluids, 16, 1903, (1973).

16. R.B. White, D.A. Monticello, M.N. Rosenbluth, B.V. Waddell, Phys. Fluids, 20, 800, (1977).

17. D. Biskamp, H. Welter, Proceedings of IAEA Conference, Baltimore, (1982).

18. M. Cotsaftis, Proceedings of IAEA Conference, Baltimore, (1982).

19. L. Woods, J. Plasma Physics, 29, 143, (1983).

20. B.V. Waddell, M.N. Rosenbluth, D.A. Monticello, R.B. White, Nuclear Fusion, 16, 528, (1976).

21. B.V. Waddell, B. Carreras,H.R. Hicks, J.A. Holmes, Phys. Fluids, 22, 896, (1979).

22. H.R. Hicks, B. Carreras, J.A. Holmes, D.K. Lee, B.V. Waddell, J. Comput. Phys., 44, 44, (1981).

23. B. Carreras, H.R. Hicks, J.A. Holmes, B.V. Waddell, Phys. Fluids, 23, 1811, (1980).

24. A. Sykes, J.A. Wesson, Proceedings of IAEA Conference, Brussels (1980).

25. M.F. Turner, J.A. Wesson, Nuclear Fusion, 22, 1069, (1982).

26. B.B. Kadomtsev, Fiz. Plasmy, 1, 710, (1975).

27. A. Sykes, J.A. Wesson, Phys. Rev. Lett., 37, 140, (1976).

28. J.A. Wesson, A. Sykes, M.F. Turner, Culham Laboratory Report CLM R233 (1982).

29. H.R. Hicks, Private communication.

30. M.F. Turner, J.A. Wesson, S. Johns, Culham Laboratory Report, PLN 83/1, (1983).

31. F. Alladio, Culham Laboratory, DITE Memo 260, (1979).

32. J.W. Eastwood, K.I. Hopcraft, Culham Laboratory Report, CLMP 709 (submitted to Journal of Computational Physics).

33. D. Potter, Computational Physics, Wiley and Sons.

34. D. Potter, Computational Physics, Wiley and Sons.

35. J.W. Eastwood, K.I. Hopcraft (to be submitted to Journal of Computational Physics).

36. H.R. Hicks, Private communication.

37. F. Karger et al, Proceedings of IAEA Symposium on Current Disruption in Toroidal Devices, Garching (1979).